Order Number 9024650

# Lanthanide trifluoride thin films: Structure, composition, and optical properties

Lingg, Linda Jeanne, Ph.D.

The University of Arizona, 1990

U·M·I
300 N. Zeeb Rd.
Ann Arbor, MI 48106

# LANTHANIDE TRIFLUORIDE THIN FILMS: STRUCTURE, COMPOSITION, AND OPTICAL PROPERTIES

by

Linda Jeanne Lingg

---

A Dissertation Submitted to the Faculty of the

COMMITTEE ON OPTICAL SCIENCES (GRADUATE)

In Partial Fulfillment of the Requirements
For the Degree of

DOCTOR OF PHILOSOPHY

In the Graduate College

THE UNIVERSITY OF ARIZONA

1 9 9 0

THE UNIVERSITY OF ARIZONA
GRADUATE COLLEGE

As members of the Final Examination Committee, we certify that we have read the dissertation prepared by Linda Jeanne Lingg

entitled Lanthanide Trifluoride Thin Films: Structure, Composition, and Optical Properties

and recommend that it be accepted as fulfilling the dissertation requirement for the Degree of Doctor of Philosophy.

| | |
|---|---|
| H. A. Macleod | 7/10/89 Date |
| B. O. Seraphin | 4/19/90 Date |
| John C. Lewis | 4/20/90 Date |
| | Date |
| | Date |

Final approval and acceptance of this dissertation is contingent upon the candidate's submission of the final copy of the dissertation to the Graduate College.

I hereby certify that I have read this dissertation prepared under my direction and recommend that it be accepted as fulfilling the dissertation requirement.

| | |
|---|---|
| H. A. Macleod | 7/10/89 |
| Dissertation Director | Date |

## STATEMENT BY AUTHOR

This dissertation has been submitted in partial fulfillment of requirements for an advanced degree at the University of Arizona and is deposited in the University Library to be made available to borrowers under rules of the Library.

Brief quotations from this dissertation are allowable without special permission, provided that accurate acknowledgment of source is made. Requests for permission for extended quotation from or reproduction of this manuscript in whole or in part may be granted by the head of the major department or the Dean of the Graduate College when in his or her judgment the proposed use of the material is in the interests of scholarship. In all other instances, however, permission must be obtained from the author.

SIGNED: 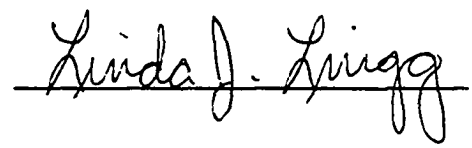

This dissertation is dedicated to my parents,

William Joseph Lingg and Jeanne Rohana Lingg,

and my sister, Carole Adele Lingg.

# ACKNOWLEDGEMENTS

Without the patience and encouragement of a number of people, this research and my graduate work could never have been completed. I am proud to have had Angus Macleod as my advisor. He created a positive environment where we as graduate students were allowed the facilities and freedom to pursue our ideas and research interests. I especially appreciate his effort in the 9 am study sessions and the financial support I received every semester and summer. Talking with Bernie Seraphin and learning some of his conceptual approach to physics was crucial to my understanding and interpretation of these experimental results. His stories about his early days in physics were particularly inspiring when things were not going as smoothly or as quickly as I wanted. The RBS measurements and tutorials on backscattering spectrometry provided by John Leavitt, as well as our discussions about the experimental data, were an essential part of this work. I am grateful for his longstanding encouragement and tolerance of my habit of always handing things in at the last minute.

It was a pleasure to work with the various members of the Thin Films Group and I learned a great deal from them. Bertrand Bovard's collaboration, thoughtful management, and camaraderie were priceless. It was also my good fortune to share the 760 with Chang Kwon Hwangbo who provided the FTIR measurements reported here. I am grateful to Jim Targove for a timely rescue from the cubicles. I always enjoyed an opportunity to work with Ross Potoff and will fondly remember overhauling the 760. Shahida Rana performed some of the optical transmittance measurements reported here. The cheerful and enthusiastic atmosphere which she brings to the measurements lab made me look forward to working there. Anna McKew's help with word processing was very much appreciated as well as our breakfasts at the real Bentley's. Robert Sargent maintained the personal computer system in our lab to the benefit of the rest of the students. Karl Chao's generous loan of his thesis formatting in ps made it possible for me to get a draft to the graduate college three weeks before my defense. Brenda Perry was instrumental in getting the final draft to the graduate college

I would like to thank Prof. L. C. McIntyre, Peter Stoss, Don Ashbaugh, Jeff Oder, and Bijan Dezfouly-Arjomandy of the University of Arizona Physics Department who performed the RBS measurements. Prof. Leroy Eyring of Arizona State University was kind enough to spend some time with me for several extremely informative discussions about the lanthanides. I would also like to acknowledge Wes Bilodeau of the University of Arizona Geosciences Department for x-ray diffractometer training and Dave Thiessen and John Bousman of the Jet Propulsion Laboratory for VUV measurements. The friendship of Andy DiRienzo and Carolina Van Stone was indirectly quite important in completing this work.

It is not possible to express how much the true support of Wayne Bennett and his understanding, loyalty and clear thought have meant to me. I think he will be celebrating with even more enthusiasm than I now that school is out.

Funding for this work was provided by the Jet Propulsion Laboratory and the Air Force Office of Scientific Research.

# TABLE OF CONTENTS

# LIST OF ILLUSTRATIONS

## LIST OF ILLUSTRATIONS - Continued

# LIST OF TABLES

# ABSTRACT

This study characterizes thin films of eleven lanthanide trifluorides which are potentially very useful for optical applications. The natural and controlled transparency and real refractive index of single layers of these fluorides are examined, accompanied by studies of composition and crystal structure of the films which are made by conventional, high temperature, and ion-assisted thermal evaporation. Additionally, since these particular fluoride compounds provide an excellent opportunity for doing so, the mechanisms active in film modification through high temperature and ion-assisted thermal evaporation are explored.

# CHAPTER 1

# INTRODUCTION

This dissertation is a study of the physical properties of thin film lanthanide trifluorides ($LnF_3$) with emphasis on their optical properties. As an introduction, I will describe the bulk properties of the $LnF_3$ group and why they are good potential candidates for optical interference filter applications. Then I will briefly describe the methods we used to grow $LnF_3$ thin films and indicate deviations we expect from ideal bulk-like structural properties. This will be followed by an explanation of the cyclic nature of thin film experimental work between deposition processes, resulting films, and characterization methods.

## Bulk Properties

The lanthanide series begins with cerium (Z=58) and ends with lutetium (Z=71) and is characterized by each consecutive electron filling a level in the 4f shell. More specifically, lanthanum has the electron configuration $[Xe]4f^05d^16s^2$ with no 4f electrons and one 5d electron. In cerium, the 5d drops down to the 4f shell and the configuration is $[Xe]4f^25d^06s^2$. The 4f shell fills one by one until another irregularity arises at gadolinium (Z=64). Gadolinium has $[Xe]4f^75d^16s^2$ instead of $[Xe]4f^85d^06s^2$ but terbium, similar to cerium, has the configuration $[Xe]4f^95d^06s^2$. Again the 4f shell fills regularly being filled at ytterbium (Z=70) and lutetium has

the configuration $[Xe]4f^{14}5d^{1}6s^{2}$. The spins fill, as usual, all in one direction and then all in the other direction. The atoms lose $6s^2$ and either $5d^1$ or $4f^1$ to become triply ionized which is the most stable charged state for all the series. In addition, there exist the following less stable ionic states: $Ce^{4+}$, $Pr^{4+}$, $Sm^{2+}$, $Eu^{2+}$, $Tb^{4+}$, $Tm^{2+}$, $Yb^{2+}$ (Cotton and Wilkinson 1976).

The series is famous for the fact that as atomic number increases, ionic radius decreases, an effect known as the lanthanide contraction. It occurs due to the imperfect shielding of one electron by another in the same subshell. "As we proceed from La to Lu, the nuclear charge and the number of 4f electrons increase by one at each step. The shielding of one 4f electron by another is very imperfect (much more so than with d electrons) owing to the shapes of the orbitals, so that at each increase the effective nuclear charge experienced by each 4f electron increases, thus causing a reduction in size of the entire $4f^n$ shell. The accumulation of these successive contractions is the total lanthanide contraction" (Cotton and Wilkinson 1976, page 212). This phenomenon leads to the heavier lanthanides having some of the smallest ionic radii in the periodic table, for example, La ionic radius = 1.04 $\mathring{A}$ and Lu ionic radius = 0.91 $\mathring{A}$ (Kittel 1988).

Some of the lanthanide compound properties show little dependence on the ligands (Cotton and Wilkinson 1976), however, for our interests the ligand is quite important. Fluorine (Z=9) has the electron configuration $1s^22s^22p^5$. Due to the fact that it needs only one electron to fill the outer shell, it becomes an extremely reactive $1^-$ ion. It is the smallest of the halogens (ionic radius = 1.33 $\mathring{A}$).

$Ln^{3+}$ have electronegativities ranging from 1.10 to 1.27 and the electronegativity of $F^{1-}$ is 3.98. This combination results in very strong ionic bonding where the three electrons from a Ln atom are completely transferred to the fluorine. In a

solid, this extends to the lattice and the $LnF_3$ form a structure with extremely deep potential wells, where the electrons are localized. This strong localization is characteristic of an insulator with a very wide band gap. The character of the (empty) conduction band for these compounds comes from the Ln 5d-6s atomic levels and the character of the valence band (filled) from the F 2p levels (Wertheim 1972).

The number of 4f electrons is the only non-nuclear feature differentiating the lanthanide trifluorides and as stated earlier, the 4f electrons are essentially "hidden". As a result, their chemical properties are extremely similar, as are their optical, mechanical, and thermal properties. Only relatively recently have chemists been able to separate the members of the series from one another (Cotton and Wilkinson 1976, Wells 1962).

Observation of the standard optimum properties of a material usually requires that the measurements be made on a single crystal bulk sample. Although there are plenty of applications for single crystals, there are many more that require the material to adopt a specific shape or be of a designated optical thickness. This particular study was executed with the eventual application of optical interference coatings in mind. Interference filters consist of a stack of alternating high and low index layers of materials. The layers are thin enough to cause interference within themselves. They rely on sharp, smooth interfaces between layers and homogeneous index throughout a layer for optimum performance (Macleod 1987). There are many reasons why $LnF_3$ thin films are strong candidates for interference filters. Notably the excellent transmittance over the extended optical spectrum and an index of refraction (n average = 1.55) which is high for a VUV filter and low for an infrared filter. As is characteristic of the fluorides, they have a relatively low melting point among insulators such as oxides, nitrides and carbides, making them easy to handle.

In addition, they have a higher packing density at room temperature than many other fluorides and are known for their high laser damage thresholds. Unlike many fluorides, they are not radioactive, poisonous, or hygroscopic (Pulker 1984).

## Growth Techniques

Physical vapor deposition (PVD) is normally used for the deposition of optical thin film coatings. In the most common technique, thermal evaporation, the material to be deposited, the evaporant, is heated to a temperature at which it vaporizes. The vapor then condenses as a solid film on the substrates which are at temperatures below the melting point of the evaporant. This rapid quenching can give a structure different from a bulk-like sample formed by an equilibrium process, since the ordering time can be small relative to the quenching time. These structural differences may lead to differences in the electrical, optical, mechanical, and thermal properties. We characterized the lanthanide trifluorides as thin film materials based on their properties as deposited with thermal evaporation.

Modifications are sometimes necessary to remedy the problems caused by the deposition process itself. The simplest modification of the thermal evaporation process is heating the deposition chamber, including the substrate. This drives the process of condensation from the vapor phase more toward equilibrium and therefore allows more ordering of the condensate. Films deposited at higher temperatures have higher packing densities and better adhesion than their counterparts deposited at room temperature. A decrease in porosity moves the optical properties of the material closer to its bulk values and increases resistance of the thin film to moisture damage. The drawbacks are that certain substrates cannot stand the heat involved and that the heating and cooling processes are fairly slow. We used this

technique to sucessfully modify thin film properties as described in chapters four and six.

Another technique we used to adjust physical properties of deposited films was ion bombardment during growth (Martin 1986, Allen 1982). Since the evaporant has very low energy and hence low surface mobility, workers conclude that the microstructure problems would be eased if the surface mobility were increased by adding some momentum or energy to the evaporant. This is done by collisions between energetic ions and both evaporant and condensate. This method has been reported to have the same benefits as heating the substrate but without the drawbacks. Ion assisted deposition (IAD) does, however, have disadvantages of its own. Inclusion of the bombarding species and preferential resputtering of condensed atoms are the most serious. In chapter five we describe the affects of IAD on resulting $LnF_3$ thin film structure and properties. In particular we focused our investigation on $SmF_3$ to illucidate IAD mechanisms responsible for observed structural changes.

There are other variations of the thermal evaporation process such as reactive evaporation, ion plating, laser evaporation and molecular beam and atomic layer epitaxy. IAD is particularly important because it separates out one process important in many of these other procedures, ion bombardment of the growing film. In IAD the ion beam can be much better characterized than in the other techniques and, hence, fundamental results can be more readily obtained. These results are relevant to the other bombarding techniques. Furthermore, there are other deposition processes such as the many kinds of sputtering and chemical vapor deposition. Each technique has its own particular strengths and weaknesses. We will not digress to a comparison of these various techniques since this is covered extensively elsewhere (Pulker 1984).

Coating Characteristics

We know the bulk $LnF_3$ properties, why they are interesting for optical coatings, and how to make thin films. We can now begin to discuss the problems inherent in vacuum deposition in general, in thermal evaporation processes, and in the use of thermal evaporation with the lanthanide trifluorides. We must describe these in order to make the purpose of the dissertation and the methods and experiments therein clear.

High purity starting material for thermal evaporation is often difficult to obtain and thus expensive. All $LnF_3$ starting materials have residual oxygen, carbon, and heavy metals from the synthesis and separation processes. The boat from which the material is evaporated becomes extremely hot during the process and atoms of the boat and impurities from within it can become part of the evaporant (Glode 1987). The vacuum chamber is another source of impurities. There will be residual gases which become part of the film by condensing from the chamber atmosphere onto the substrate along with the evaporant. These are the most common types of impurities intrinsic to the thermal evaporation process and they can have varying degrees of influence on the optical properties of the thin films.

Optical thin-film coatings also possess a columnar microstructure. In the vacuum evaporated films that make up the vast majority of optical coatings, this microstructure is particularly pronounced and has profound effects on film properties. It includes considerable void volume between the columns and surface area around them. This increases the area and volume available for the accumulation of contaminants and has serious consequences for stability, optical, mechanical, and chemical.

In addition to impurities, the composition of the primary film material can be

a problem. Sometimes molecules will partially or completely dissociate in the evaporation process (Pulker 1984). This leaves, for instance, $LnF_2$ molecules instead of $LnF_3$ molecules. Sometimes the impurities described above are merely interstitial but very often they actually bond within the film material and form a new compound, LnOF, for instance. This clearly demonstrates the need for a chemical analysis tool. We used Rutherford Backscattering Spectrometry as described in chapter three.

Recall that thin-film coatings are characterized by the presence of materials with one exceedingly small dimension and with interfaces that are of prime importance in determining the overall properties. The surface/volume ratio of such thin-film materials is very large compared with bulk materials and that in itself causes problems. The fact that a material would rather be surrounded by itself (low surface energy) than not (high surface energy) results in stress, one cause of mechanical failure.

The interface between substrate and film system is another source of weakness. Because of the short range of the forces involved in film adhesion the character of the outermost molecular layer of substrate material is critical. The nature of the polishing and coating operations renders adequate control of the nature of the surface virtually impossible. The open microstructure permits entry of surface-energy-reducing contaminants that degrade the interface still further. This demonstrates the need for inspection of adhesion and mechanical stress in these films.

The lack of ordering time discussed earlier has a profound effect on the crystal structure thin films. Instead of adopting the low temperature phase that one would expect, films are often quenched into the high temperature phase or into a form with no visible long range order at all. The optical properties of some materials are profoundly effected by this and others not at all. We used x-ray diffracto-

metry to determine the resulting structures of our deposited films.

The rough microstructure described above gives rise to another important effect. When a film is moved from the vacuum into some atmosphere and exposed to moisture, air, and possibly other corrosive elements, its character may change. Water (n=1.33) in the voids instead of vacuum (n=1.0) will raise the index of the outer layers of the film (Macleod 1985). There are applications for coatings in fluorine or other corrosive environments and in space and radiation environments as well as on mirrors which are likely to be irradiated by high power lasers. The most important characterization technique for optical studies is spectrophotometry. Transmittance and reflectance measurements alone can give enough information to calculate index of refraction, extinction coefficient, and thickness of a homogeneous, nonabsorbing thin film.

From the above discussion, we see that a thin film of a material is usually quite different from a simple slice of bulk material. Assuming that the two are equivalent can lead to gross errors in interpreting optical properties of materials and to seemingly unreproducible results. It is therefore absolutely necessary for any kind of understanding of film properties that they should be well characterized. Studying materials in thin film form becomes cyclic, interchanging materials, processes, and film properties with one of the three being the variable and the other two being indicators of the effects of variable change. The characterization techniques are obviously crucial to fully appreciate the complexity of recording thin film optical properties.

# CHAPTER 2

## PHYSICAL PROPERTIES OF THE LANTHANIDE TRIFLUORIDES

In this chapter I will explain how the chemical and atomic properties of the $LnF_3$ which were mentioned in chapter one determine their solid state optical and structural properties. We chose the $LnF_3$ for their optical properties, in particular their large band gaps, since our original application was UV interference filters. To aid interpretation of our observations on the thin film optical properties of this series of compounds and to explain the significance of stoichiometric studies, I will begin this chapter by discussing the origin of the band gap and explaining why the band gaps of the $LnF_3$ are so wide. I will then explain the influence of physical structure and composition on the optical properties and consequently the requirement that we measure composition and structure for our samples. Finally, to help correlate thin film to bulk structure for the $LnF_3$ as a series, I have included a brief review of the known thermochemical and structural data on the bulk $LnF_3$.

### Origin of the Band Gap

Consider those outer electrons of an atom which are free to move inside a solid composed of the atoms. In the simple treatment of a free electron gas a given electron experiences no forces from the other electrons or the ionic cores. Instead, this electron is free to move without perturbations within the confines of the solid.

The edge of the solid acts as a potential barrier preventing the electron from escaping the solid. The Schrodinger equation applied to this electron yields a travelling wave solution exp(ikx) in one dimension. The values kx occur in a discrete series imposed by the length, L, of the solid in the x direction, $k_n=\left[\frac{\pi n}{L}\right]$ where n=±1, ±2, ±3. The relation between energy and wave vector is $E=\frac{\hbar^2k^2}{2m}$, where m is the free electron mass. Pauli exclusion prevents more than 2 electrons (with opposite spins) from occupying any one of these states exp(iknx).

In what follows we will see how energy gaps develop in this parabolic E(k) at the Brillouin zone boundary. Following Bloch we consider the perturbation produced on the electron wave functions by the ionic cores. He expanded the periodic ionic core potential V(r) as a Fourier series and solved the Schrödinger equation for the eigenstates. He found that the electron states far from the Brillouin zone boundary were in essentially travelling free electron states. But the wave functions of those states close to the Brillouin zone boundary were strongly modified, and the states at the boundary were standing waves. I will forego Bloch's more rigorous mathematical presentation in favor of the semiquantitative analysis shown below, which will supply physical insight into the origin and magnitude of the band gap.

Consider the free electrons of wavelength λ, normally incident on atomic planes of interplanar separation a. Just like the diffraction of x-rays, these matter waves will be diffracted if the Bragg condition is obeyed. For $\theta=90^0$ the Bragg condition is $n\lambda=2a$ or $k=\frac{\pi n}{a}$, i.e., once the electron has a wave vector which extends to a Brillouin zone boundary, the state exp(ikx) will be diffracted into exp(-ikx). But this new wave vector will be diffracted back into exp(-ikx). As Bloch predicted, the only time-independent solutions are the standing waves $\cos\left[\frac{\pi x}{a}\right]$ and $\sin\left[\frac{\pi x}{a}\right]$. This is the origin of the band gap. The probability density, $|\Psi|^2$, yields that the

travelling wave $\exp\left[\frac{i\pi x}{a}\right]$ has an equal probability of being anywhere in the solid whereas the standing waves pile-up the electron density either over the positive cores, $\cos^2\left[\frac{\pi x}{a}\right]$ or between the positive cores $\sin^2\left[\frac{\pi x}{a}\right]$. The energy of the cosine solution is smaller than that of the sine solution due to the coulomb potential energy of the electron in the field of the positive cores. In one dimension, representing the periodic potential of the ion cores by its first Fourier component $U(x) = U\cos\left[\frac{2\pi x}{a}\right]$ we evaluate the energy difference between the two standing waves as

$$Eg = 2U\int_0^1 dx\,\cos\left[\frac{2\pi x}{a}\right]\left\{\cos^2\left[\frac{\pi x}{a}\right] - \sin^2\left[\frac{\pi x}{a}\right]\right\} = U.$$

The gap in energy is equal to the amplitude of the Fourier component of the crystal potential. So the question of why this gap is large for the $LnF_3$ resolves to why U is large for these compounds, i.e., why the potential wells are so deep.

Strong electronegativity of the fluorine atoms efficiently pulls electrons away from the Ln's. (This indicates the significance of keeping fluorine in the structure and preventing less electronegative ions like oxygen from entering.) Electronegativity is defined as the ability of an atom in a molecule to attract an electron to itself. The Allred-Rochow value for fluorine is 4.10 which is the highest of any element. The lanthanides range from 1.14 to 1.06 (in no particular order) and these are relatively low values. The electronegativity difference between the anion and cation averages 2.94. Such a high value indicates a high degree of charge transfer, i.e., each of the $6s^2$ electrons and either the 5d or a 4f electron are transferred almost completely to fluorine 2p orbitals. This almost complete charge transfer between the Ln and F atoms in solid $LnF_3$ demonstrates the strongly ionic nature of these materi-

als.

Furthermore, fluorine is the smallest of the halogens and the lanthanides also have relatively small ionic radii, as mentioned in chapter one. This means we have a large charge localized over a relatively small volume of the lanthanide or fluorine ions. Consequently, the $LnF_3$ structure has a very high charge per unit volume alternating in sign from positive (rare earth ion) to negative (fluorine ion). This is the reason for existance of deep potential wells in $LnF_3$ and, as per our discussion, is responsible for the observed large band gap. Recall that within the $LnF_3$ series the ionic radius decreases as the atomic number increases. This should result in a band gap which becomes wider as atomic number increases. In contrast, the shallow, smeared-out potential wells of a nitride or chalcogenide give a small band gap (Kittel 1976).

Optical Properties

The electronic structure of the $LnF_3$, as with all materials, determines the optical properties assuming the ideal single crystal case (Black and Wales 1968). For instance, the band gap is observed in the form of a sudden and locally permanent decrease in transmittance and reflectance known as the fundamental absorption edge. Materials such as the $LnF_3$ with large band gaps are transparent materials and have fundamental absorption edges in the VUV. For the $LnF_3$, the edge is located around $E = 10$ eV or $\lambda = 1216$ Å. Considering the lanthanide contraction and our explanation of the band gap, the fundamental absorption edge should move further into the VUV as the atomic number of the Ln increases. For the $LnF_3$ with unfilled shells, that is all except $LnF_3$ [Ln=La,Gd,Lu], there are atomic transitions occuring right around or superimposed on the absorption edge. These make it diffi-

cult to tell exactly where the edge is in many cases. But the rule should hold for $LaF_3$, $GdF_3$, and $LuF_3$. It is difficult to find published optical data for the $LnF_3$ in the VUV but through our own work, as shown in chapter six, we have verified this prediction. (In addition to these general limits to the transparency of the $LnF_3$, there are other less important mechanisms which would bring the absorption edge closer to the visible, such as the presence of Frenkel excitons or valence band plasmons (Kato 1960).) In the UV, VIS, and NIR the $LnF_3$ are transparent (Heaps 1976) but throughout the transparent region sharp electron transitions between atomic levels will cause absorption, such as the 4f to 4f transitions in the NIR. In the mid-IR, around 500 $cm^{-1}$, optical phonons begin to cause absorption again (Rast et al 1968 and Lowndes et al 1969). The onset of these can also be correlated to the lanthanide contraction. The heavier the atom, the farther into the IR the lattice vibrations begin. Compared to other fluorides and insulating materials, the $LnF_3$ have an extremely wide region of high transmission from approximately 1000 $\mathring{A}$ to 20 $\mu$m due to their unique electronic structure.

As we will see in the next chapter, our lanthanide trifluoride samples are not in single crystal form and may be composed of elements other than just the Ln and F intended. Instead they are thin films in some combination of stable and metastable phases on a substrate. The models above are obscured when the sample is not of the prescribed single crystal form or the assumed composition. The electric field inside the material is not as uniform, so the basic electrical and optical properties still hold but values of transition energy are slightly different from the predicted ones. This will change the refractive index and shift absorption bands slightly, since they are a result of the electric field inside the material. The change from bulk single crystal to bulk glass usually leaves desired insulator or dielectric proper-

ties intact. Another effect of that structure change is to eliminate birefringence, which is an improvement for some applications. A polycrystalline type structure can scatter infrared radiation and can alter mechanical properties such as stress and adhesion enormously. The rapid quenching and high condensation rates of the thermal evaporation process give the added problem of voids and extra contaminants. Oxygen can bring the band edge down in energy as discussed in the previous section. There is also the phenomenon of water adsorption which becomes much more important for coatings as observed by Macleod and Ogura. When a film is removed from the vacuum, the ambient atmosphere will fill up voids and pores thereby changing the effective optical constants and the mechanical properties of the material. All of these facts taken together require that we develop a strong interest in structure and composition.

Bulk Structure

By looking at figure 2.1, the equilibrium phase diagram for the series of bulk lanthanide trifluorides, we can tell what structures to expect. In the paragraphs below we discuss this phase diagram extensively to prepare us for the interpretations of our thin film data presented in chapter four.

One of the most interesting properties of the lanthanide trifluorides is their polymorphism. They can be divided into four catagories according to the crystal structure at various temperatures. The $LnF_3$ [Ln=La-Nd] have the tysonite structure with the space group $P\bar{3}c1$ at low temperatures. "In this structure there are hexagonal nets of $La^{3+}$ and $F^-$ ions with F ions on each side of the layer giving La five equidistant nearest neighbours, at the apices of a trigonal bipyramid. Since the next nearest neighbours of La are six more F at the apices of a trigonal prism, at a

slightly greater distance (2.70 Å compared with 2.36 Å, the shorter La–F distance), it is probably preferable to regard this structure as one representing a transition between c.n. 5 and some higher value (5(+6)), rather than as a layer structure containing 5-coordinated $M^{3+}$ ions." (Wells 1962 page 99) There is a second order phase transition around 1400°C when they assume the P63/mmc form of the hexagonal tysonite structure. Promethium is synthetically prepared so there is a lack of data for that material. The $LnF_3$ [Ln=Sm-Gd] have the orthorhombic structure, space group Pnma, at low temperatures. In this (orthorhombic) structure Y is surrounded by six F at the corners of a trigonal prism and three F beyond the midpoints of the lateral faces, but of these neighbours eight are at ≅2.3 Å and the ninth at 2.6 Å so that here the c.n. is 8(+1). This is the more reasonable in view of the fact that $Y^{3+}$, which is smaller than $La^{3+}$, has a rather high coordination number in $YF_3$." (Wells 1962, page 341) They go through a first order phase transition to the (larger volume) tysonite $P\bar{3}c1$ structure at high temperatures. $LnF_3$ [Ln=Tb-Ho] are monomorphic and have the orthorhombic Pnma structure. For $LnF_3$ [Ln=Er-Lu], the low temperature form is Pnma and a first order phase transition to the hexagonal yttrium fluoride $P\bar{3}m1$ structure occurs around 1200°C.

The first-order solid-solid phase transition between orthorhombic and hexagonal tysonite is a displacive transition (Sobolev 1976). Displacive transitions correspond to a change in the secondary coordination by a distortion of the structure without breaking bonds or changing the numbers of nearest neighbors. These transformations are rapid and occur at a definite temperature by merely displacing atoms from their previous positions. The structural energy of the system is lower in the low temperature form which is more compact than the high temperature, more symmetric form. There is no activation energy barrier to this type of transition (Kingery

1976).

The first-order solid-solid phase transition between orthorhombic and hexagonal $YF_3$ is a reconstructive transition (Sobolev 1976). Reconstructive transitions involve a substantial change in the secondary coordination, requiring that interatomic bonds be broken and a new structure reconstructed. To break and reform bonds requires greater energy and so these transformations occur slowly. The energy required for this breaking up of the structure is recovered when the new structure is formed (Kingery 1976).

For compounds with such similar properties, one might ask why the structure varies so much, or even, why does a compound have the particular structure it has. The theory of Goldschmidt says that the radius ratio of the atoms in a diatomic compound can be of significance in determining the choice among alternative structures for the compound (Pauling 1960). The radius ratio of the two ions in a compound determines the number of anion nearest neighbors a cation can have. Crystal structure is the result of this nearest neighbor limit or coordination number. Compounds are catagorized by their ratio and this determines which crystal structure they can have. Furthermore, the point at which one structure becomes unstable and another stable is marked by a critical radius. For a crystal to have a particular structure it must meet the radius ratio criterion. The theory goes quite far in terms of proving the influence of ratio on boiling point, melting point, and crystal energy by applying what is known as the radius ratio correction factor to the cohesive energy of a crystal (Kingery 1960, Pauling 1960).

The progression of radius ratio determining coordination number and coordination number determining structure holds for such highly symmetric compounds as the alkali halides but is less accurate for triatomic molecules such as $MgF_2$. Finally,

it is not recommended to apply it to "crystals in which the environment of an atom is less regular (e.g. $LaF_3$). We have listed only the most symmetrical coordination groups (NaF, KBr). Less symmetrical coordination polyhedra are found in some crystals, and to these the radius ratio criterion cannot usefully be applied. This is true for the $LaF_3$ structure, for example. The five nearest neighbors of a metal ion are arranged at the apices of a trigonal bipyramid, but there are six more neighbors not much more distant from the metal ion. In such cases the definition of coordination number of equidistant nearest neighbors is unsatisfactory, and a definition based on the polyhedral domain of an atom of ions is more realistic. In the $LaF_3$ structure the (5+6) coordination then becomes 11-coordination, more in line with the high coordination numbers of $La^{+3}$ in other salts (e.g. 9 in $LaCl_3$ and $La(OH)_3$)." (Wells 1962)

Although the radius ratio criterion cannot be applied to the $LnF_3$ in an absolute sense, it can be applied in a relative sense. The concept that structures systematically change with ionic radius is crucial to understanding the progression of structures taken by the $LnF_3$. By looking at specific sections of figure 2.1, one can see the gradual influence of the lanthanide contraction. According to Sobolev, it can be looked at as a decrease in the coordinating ability of the cation, the effective coordination number going from 11 for $LaF_3$ to 9 for $LuF_3$ (Wells 1962). Take for instance one structure sensitive region of the diagram from $SmF_3$ to $GdF_3$. Consider that as the temperature is increased the lattice will expand, this means that the volume of the $LnF_3$ increases. The more separated the ions are from one another, the more likely these compounds are to adopt the hexagonal structure. (The volume of the primitive cell is larger for the hexagonal tysonite structure than for the orthorhombic structure.) As the series progresses from Sm to Gd, having smaller ionic radii, the compounds can stay in the orthorhombic structure at higher tempera-

tures. They require more heating to achieve the threshold volume that triggers the displacive transition from orthorhombic to tysonite hexagonal. The heavier lanthanides show similar behavior in the transition from the orthorhombic to the $YF_3$ hexagonal structure for $LnF_3$ [Ln=Er-Lu]. This transition is reconstructive, however, and so always takes place at higher temperatures since it must overcome the activation energy barrier (Sobolev et al. 1976). The smaller the cation the more stable the hexagonal phase becomes.

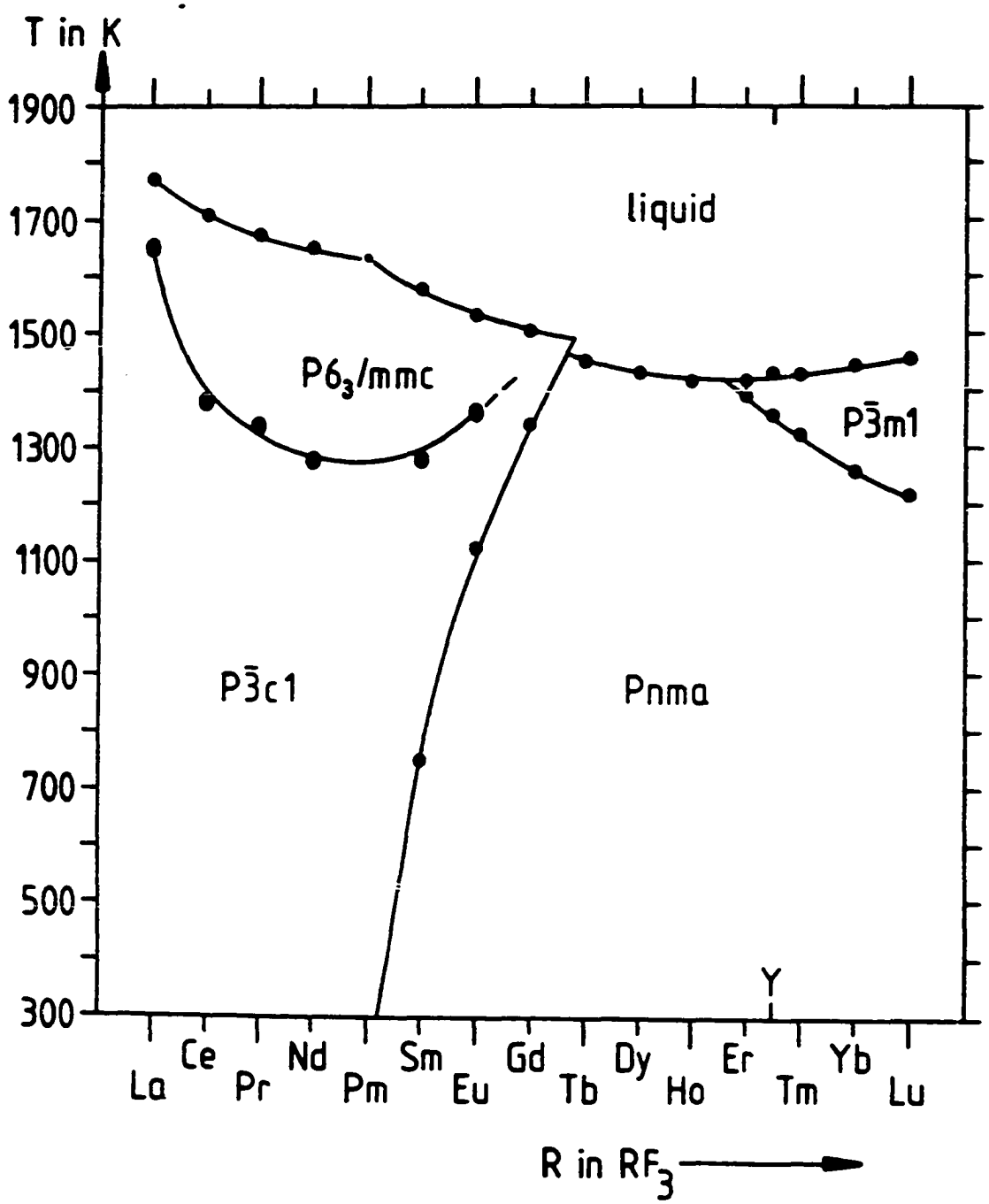


Figure 2.1 Bulk equilibrium phase diagram (after Greis 1985).

# CHAPTER 3

# EXPERIMENTAL METHODS

## Deposition Techniques

All of this work used a Balzers 760 BAK box coater of dimensions 1000 x 900 x 900 mm. Vacuum is achieved by means of a single stage rotary vane pump and Roots blower which rough the system down to $5x10^{-2}$ mbar and then by a cryopump which goes to pressures as low as $2x10^{-7}$ mbar. Most of this work was performed in the high $10^{-7}$ mbar range.

The system is equipped with two electron-beam thermal sources and two resistive thermal sources. A quartz crystal mounted in the center of the chamber 24" above the sources is used for thickness monitoring. Four tungsten lamps used as heaters are mounted some 3" above the substrate table and bake-out took the temperature to 70°C before an ambient temperature run, 120°C before a 100°C run, and 220°C before a 200°C run. Temperature is measured by a thermocouple mounted on baffles in the rear of the chamber just below substrate level. A mass spectrometer is mounted behind baffles three feet away from the sources.

Sets of substrates are positioned 90° apart on a rotatable table 22.5" above the sources. Masks placed below this table permit deposition onto one of the substrate sets at a time. For this work the table was not rotated during deposition but only between depositions in order to expose a new set to the source beam. Both manual

and microprocessor control options exist. Our initial premelt was always done manually and microprocessor control was used during a deposition for premelt, rate control, shutter control, timing, etc. Table 3.1 gives evaporation details. All permutations of available boat material and $LnF_3$ compound were not tested but instead the first combination which worked for a given compound was used.

We carried out ion-assisted deposition using a 3 cm Kaufmann hot-cathode ion source and an ID-2500 Ion Beam Drive manufactured by Commonwealth Scientific Corporation. Working gas was introduced into the ion gun via a needle valve. Regular welding grade argon gas was used for most of this work although some experiments were done with nitrogen, oxygen and krypton. The ion gun was run at a pressure which gave a total chamber pressure of $8x10^{-5}$ mbar. A tungsten filament was used with a Ni grid for low energy operation (50-200 eV) and with two carbon grids for high energy operation (250-1200 eV). The grids extract ions from a discharge at reasonably low pressure within the body of the gun. Because the discharge is maintained by electrons from a hot filament with long paths in crossed electric and magnetic fields, the energy of extracted ions is very well defined. We aimed the ion beam at $15^0$ to the substrate normal and the top of the gun was 14" from the substrate in deposition position. The beam typically has a width of 4 cm at the substrate table level with an incident energy of 500 eV and current density of 20 $\mu A/cm^2$. A Faraday cup was rotated in front of the substrates before and after deposition to measure current reaching the substrate. It consisted of an aluminum plate with a small hole in it. The hole is covered by copper cup which itself is surrounded by another copper cup at ground potential. Neutralizing electrons, also produced by the gun, were repeled by a 45 v bias before the beam current was read by a multimeter.

Table 3.1. Evaporation Details for Lanthanide Trifluorides.

| $LnF_3$ | VENDOR & FORM | PURITY | PRICE per gram | BOAT (5 mil canoe) | RATE Å/sec | MELT COMMENTS |
|---|---|---|---|---|---|---|
| $PrF_3$ | Cerac 3-6mm fused $^1/_8$-$^1/_4$" pieces | 99.9 vac. dep. grade | $1.60 | W (no Mo,Ta) | 6 | bright green smooth melt large, shiny grains |
| $SmF_3$ | " | " | $1.62 | Mo | 6 | pale yellow uneven melt small, dull grains |
| $EuF_3$ | " | " | $16.00 | Pt sheet 2 mil (no Mo,Ta) | 4 | light brown smooth melt large, shiny grains |
| $GdF_3$ | " | " | $1.70 | Mo | 6 | white, grey uneven melt small, shiny grains |
| $TbF_3$ | " | " | $7.50 | Ta | 4 | white, grey smooth melt small, shiny grains |
| $DyF_3$ | " | " | $1.60 | Ta | 6 | dark grey smooth melt small, shiny grains |
| $HoF_3$ | " | " | $2.30 | Ta | 6 | pink smooth melt large, shiny grains |
| $ErF_3$ | " | " | $1.90 | Ta | 6 | pink smooth melt large, dull grains |
| $TmF_3$ | " | " | $18.30 | Mo | 6 | white, grey smooth melt large, dull grains |
| $YbF_3$ | " | " | $2.40 | Mo (no Ta) | 3 | tan smooth melt large, dull grains |
| $LuF_3$ | " | " | $37.00 | Mo | 6 | white |
| | Aesar crystalline lump | 99.99 elec.grade low oxy | $45.00 | Mo | 6 | whiter smooth melt large, dull grains |

Pre- and Post-Deposition Procedures

Several characterization techniques are employed in this work, each of which optimally requires a different substrate and hence a different method of cleaning.

Grade B Spectrasil 1" x 1" x $^1/_{16}$" substrates from Thermal American Fused Quartz Co. were used for optical measurements in the UV, VIS, NIR, for XRD, for annealing studies, and for resistivity measurements. They were chosen for their high and consistent optical transmittance from about 240 nm to 1000 nm and because their optical constants are well defined (Targove 1987). These substrates were cleaned using the following technique : 20 min in chromerge bath at 60°C, scrub using cotton, deionized water, and liquid soap, 20 min in high frequency ultrasonic cleaner filled with deionized water at 80°C, 20 min in low frequency ultrasonic cleaner filled with deionized water at 80°C, 20 min in high frequency ultrasonic cleaner filled with room temperature deionized water, blow dry with compressed $N_2$, store in ventilation protected pass-through until needed for use in coating chamber. The final step was a 60 sec argon ion sputter clean immediately prior to deposition.

For VUV transmittance and reflectance measurements, LiF and $MgF_2$ circular substrates $^1/_2$" in diameter and 2 mm thick were used. These materials were chosen for their relatively low absorption in the VUV. The first set of films were deposited onto LiF substrates which are known to be hygroscopic and very difficult to polish. There were sleeks on the polished substrates and they were abandoned in favor of $MgF_2$. All LiF and early $MgF_2$ were obtained from Harshaw. Later $MgF_2$ were obtained from Optovac. All of the Optovac substrates were scribed before coating for identification and measured for transmittance, since it can vary by as much as 20% at Lyman alpha ($\lambda$ = 1216 Å). The reflectances were found to be

very close so an average before coating value was obtained from about 10 substrates. Drag wiping with acetone did not seem to effect the film performance so it was stopped and the standard cleaning procedure was reduced to dusting with compressed $N_2$ or Dust-Off and 10 sec ion sputter immediately prior to deposition. A recommended procedure for cleaning $MgF_2$ was discovered after the fact and is as follows : degrease cotton or gauze completely by boiling in sodium hydroxide for at least 4 hrs, desiccate the cotton or gauze and remove fluff, mix 3 parts of ethyl ether and 1 part of ethyl alcohol to make cleaning solvent, moisten the cotton or gauze with the above cleaning solvent and wipe the window outward from the center (Hamamatsu 1987).

Films for RBS measurements were deposited on graphite substrates. 2" x 2" x 2 mm blocks were regularly donated by IBM and were cut with a Buehler saw into 1 cm x 1 cm rectangles. They were placed in acetone in a high frequency ultrasonic bath for 30 sec. Before placing in vacuum chamber they were wiped with acetone and just prior to deposition they were given 20 sec sputter clean. Carbon, with its low mass, did not interfere with the detection of most other elements during the RBS analysis.

Silicon wafers (polished both sides, type N, any orientation, 12-17 mil thick, high Ω-cm, 2" and 1" dia.) from the Polishing Corporation of America were used for IR and ESCA measurements. Cleaning consisted of acetone drag-wipe and 60 sec Ar ion sputter clean just prior to deposition.

Humidity tests were performed on 2" x 2" x 0.030 microscope slides from Kodak which underwent the exact same cleaning procedure as the fused silica.

For ESR measurements, VWR microscope coverslips were drag-wiped with acetone and sputter cleaned for 60 sec just prior to deposition.

Unless otherwise stated, immediately after removal from vacuum each film was scribed along a back edge with the run number and a letter indicating its chamber position. VUV samples were stored in a desiccator; all others were stored in air.

## Characterization Techniques

For all of the characterization techniques used in this work the films were measured after exposure to air. Although some of the techniques require measurements to be made in a vacuum the films were transported in air and measured in a different vacuum system.

## UV, Visible, NIR Spectrophotometry

Transmission, reflection, and vacuum-to-air shift measurements were made with a standard spectrophotometer. The majority were made with a Cary 14 and later work was done on a Cary 2415.

The Cary 14 measurements were done in two parts one with the visible lamp and detector from 800 nm to 300 nm and one from 400 nm to 200 nm with the ultraviolet lamp and detector. Reflectance measurements were done with a single bounce attachment. Vacuum-to-air shift measurements were done at a pressure of $10^{-4}$ torr.

The Cary 2415 was used only for transmission measurements in two ranges, the UV-VIS (800-200 nm) and NIR (3100-800 nm). It has a wavelength accuracy of ±0.20 nm (UV-VIS) ±0.80 nm (NIR); a wavelength repeatability of ±0.50 nm (UV-VIS) ±0.20 (NIR); a resolution of 0.07 nm. Detector changes occur at 800 nm and 340 nm.

Optical Constant Calculation

We used an envelope technique developed by Manifacier, Gasiot, and Fillard (1976) which assumes that the film is homogeneous and weakly absorbing. This method was chosen because it requires no reflectance or independent physical thickness measurement but only a spectral transmittance measurement at normal incidence of a single-layer film on a transparent substrate to obtain n and k. Two auxiliary curves are derived for each spectrophotometer trace, one passing through the quarter-wave points and another passing through the half-wave points. These two envelopes provide two data points at each wavelength of interest for each trace. The Tmax envelope shows what the transmittance of the film at any given wavelength would be if the optical thickness of the film were some even number of quarter-waves at that wavelength rather than its actual thickness. Similarly, Tmin shows what the transmittance would be if the film's optical thickness were an odd number of quarter-waves thick at that wavelength. The variables Tmin, Tmax, and m (the order of the extremum at the measurement wavelength) are adequate to calculate unambiguously n, k, and d at the wavelength of the extremum. The following development is a basic outline of the Manifacier et al. (1976) paper and describes the essential steps taken by Bovard, Garcia, Targove, Hwangbo, and Lehan to write an index calculation program available for group use.

The transmittance of a weakly absorbing, homogeneous, single-layer film of index n, extinction coefficient k, and thickness d on a semi-infinite substrate is given by

$$T = \frac{16n_1n^2\alpha}{\left[C_1^2+C_2^2\alpha^2+2C_1C_2\alpha\cos\left[\frac{4\pi nd}{\lambda}\right]\right]}$$

where $n_0$ and $n_1$ are the refractive indices of the incident medium and substrate, respectively, $C_1=(n+n_0)(n_1+n)$, $C_2=(n-n_0)(n_1-n)$, and $\alpha=\exp\left[-\frac{4\pi kd}{\lambda}\right]$. Letting $\frac{4\pi nd}{\lambda}=m\pi$ at the extrema, it follows that the two envelopes are given by

$$Tmax = \frac{16n_0n_1n^2\alpha}{(C_1 + C_2\,\alpha)^2}$$

and

$$Tmin = \frac{16n_0n_1n^2\alpha}{(C_1 - C_2\,\alpha)^2}$$

These equations can be inverted to give

$$\alpha = \frac{C_1}{C_2}\,\frac{\left[1 - \sqrt{\frac{Tmax}{Tmin}}\right]}{\left[1 + \sqrt{\frac{Tmax}{Tmin}}\right]}$$

and

$$n = \sqrt{\left\{ N + \sqrt{N^2-n_0^2n_1^2} \right\}}$$

where

$$N = \frac{[n_0^2+n_1^2]}{2} + 2n_0n_1\left\{\frac{Tmax-Tmin}{TmaxTmin}\right\}$$

The reliance of this method on extrema in T places a requirement on the film thickness. Typically, at least five extrema are desirable in the spectral range of interest. We obtain transmittance values for the envelopes between the data points by performing a linear interpolation of the form (Garcia 1986)

$$T(\lambda) = T(\lambda_1) + \frac{(\lambda-\lambda_1)[T(\lambda_2)-T(\lambda_1)]}{\lambda_2-\lambda_1}$$

where $\lambda_1$ and $\lambda_2$ are the wavelengths of two adjacent known data points and $\lambda$ is the interpolation wavelength.

When the index has been calculated at each turning point, the optical thickness (nd) at the turning points can be divided by the calculated refractive index n at that wavelength to give the physical thickness of the film d. The calculated values of d at each turning point can then be averaged to give an estimate of the film thickness.

VUV Spectrophotmetry

The Acton reflectometer was used for vacuum ultraviolet transmission and reflection measurements. It has a deuterium source with a $MgF_2$ window, a grating monochromator, and a photomultiplier tube with a $MgF_2$ window for a detector. Reflectance measurements were made at an angle of $10^0$. The measurements were discrete and accurate to $\pm 0.5$ Å. The pressure was $10^{-6}$ torr. The instrument belongs to the Jet Propulsion Laboratory and films were sent via overnight carrier to Pasadena, stored in vacuum, and measured by Optical Instrumentation Group members Dave Thiessen and John Bousman.

Infrared Spectrophotometry

Although the $LnF_3$ have absorption bands in the 0.8-2.0 $\mu$m range due to 4f-4f transitions, they do not have much spectral activity in the 2-12 $\mu$m range. Therefore our infrared measurements were strictly for measuring the long wavelength cutoff and estimating the packing density. Bradford, Hass, and McFarland (1972) have shown that thin films display an absorption band centered around 3 $\mu$m due to absorption by the water trapped in the film. The strength of this water band therefore provides a qualitative measure of the water content of the film and, if we assume that the water is filling the voids in the film, the packing density as well. An absorption band at 2.7 $\mu$m due to $OH^-$ radicals is also present in some films.

Infrared transmission and reflection was measured for coatings 4000 Å thick on average deposited onto silicon wafers. Two sets of measurements were made. Immediately after deposition, the transmission was measured on an Analect model FX-6200 FTIR which had a range of 2.27-23 $\mu$m. The sample compartment of the Analect instrument contains ambient air, introducing atmospheric absorption bands especially those of water and $OH^-$ which could vary significantly from the background spectrum just while inserting the sample. Since their Perkin-Elmer 938 FTIR Spectrophotometer had the $N_2$ purge and reflectance attachment which we did not, the films were also sent to OCLI where T. H. Allen and T. Tuttle Hart measured transmission and reflection in the 2-12 $\mu$m range. Reflection was measured at a slight tilt ($10^0$) to eliminate back reflections from the rear surface of the thin substrate. The spot size for both instruments was 1".

Rutherford Backscattering Spectrometry

Rutherford backscattering spectrometry is an excellent tool for determining the

elemental composition of thin films (Chu 1985). Elastic collisions between an incoming beam of helium nuclei and the nuclei in the target film enable one to distinguish elements according to their mass. When the nuclei scatter, a light target nucleus will take more energy from the $He^{+4}$ than a heavier target nucleus.

The energy of backscattered He nuclei therefore tells us the atomic species involved in the scattering event. For Q incident He nuclei with energy E (MeV) we can calculate the number of atoms of a particular species in the thin film from the number of backscattered counts A, corresponding to this species using

$$Nt = \frac{AE^2}{\Omega \delta Q},$$

where Nt is the number of atoms of this species per $cm^2$ of target area, $\delta$ = differential scattering crossection measured at 1 MeV and $170^0$ backscattering angle, and $\Omega$ = solid angle of detector. Now we are in a position to calculate the stoichiometry

$$S = \frac{(Nt)F}{(Nt)Ln}\,[F],$$

where (Nt)X represents the areal density of the element in question and F represents the electron shell correction. The atomic concentration can also be calculated by dividing the number of counts of the impurity in question by the total number of counts in the whole spectrum

$$[O] = \frac{(Nt)O}{\{(Nt)F + (Nt)Ln + (Nt)O\}}.$$

Many other things can be derived from the RBS spectrum. For example, the thickness of a film can be determined if the density of a material is known. The book by Chu gives a more detailed account of the possibilities afforded by RBS.

X-Ray Diffraction Analysis

X-ray diffraction is a powerful technique for determining the long range order within the vertical columns of a thermally deposited thin film sample (Klug and Alexander 1974). An amorphous sample will have no strong peaks, only the extremely broad peak from the noncrystalline silica substrate and the noncrystalline film combined. A polycrystalline sample will have the broad peak from the substrate and non-ordered portion of the sample but also a series of sharp peaks representing radiation coherently reflected from crystalline planes in the sample.

We used a Siemens D-500 diffractometer set in a Bragg-Brentano geometry to measure our films. It was the property of the Department of Geosciences at the University of Arizona. A copper x-ray tube was in place for all of our measurements, emitting $CuK\alpha_1$ at $\lambda = 1.54051$ Å and $CuK\alpha_2$ at $\lambda = 1.54433$ Å. The weighted average of these lines, $\lambda = 1.54178$ Å, was used for calculations. Bragg's law was used to calculate the interplanar lattice spacing

$$2d \sin\theta = n\lambda$$

where d = lattice spacing, $\theta$ = angle of x-ray incidence, $\lambda$ = x-ray wavelength, and n is an integer (usually one).

Once the lattice spacings were calculated, we were able to identify which phases and orientations of the material were pr sent in a particular sample by

referring to the data cards published by the Joint Committee on Powder Diffraction Standards (JCPDS). These were also the property of the Department of Geosciences. Our thin film samples always consisted of five or six preferred orientations in one or two phases and our powdered samples of boat or starting materials always matched the powder pattern exactly.

When we calculated crystallite size, it was always for the most intense peak in the spectrum. We used the Debye-Scherrer equation

$$\xi(\text{Å}) = \frac{[89.5\ \lambda(\text{Å})]}{[\text{FWHM}(^{0}2\theta)\ \cos\theta]}$$

where $\xi$ is the structural coherence length perpendicular to the sample surface and FWHM ($^{0}2\theta$) is the full width at half maximum of an x-ray peak minus the instrumental resolution. The instrumental broadening for the Siemens at Geosciences was $0.02^{0}$.

One other calculation of interest for the diffraction data was the areal density of the sample plane primitive cell for a particular orientation of a particular phase. The results of a study using this information is discussed in chapter five so we will show an example here. The (110) plane of the tysonite hexagonal phase has

$$a = b = 6.95\ \text{Å} \quad c = 7.12\ \text{Å} \quad d = 3.48\ \text{Å}$$

where a, b, and c are the sides of the unit cell for the hexagonal structure and d is the lattice spacing in the direction perpendicular to the substrate plane (JCPDS). The (110) plane intersects the primitive cell in a rectangle having sides of length c and $2a \sin 60^{0}$ (Hall 1974). The area is therefore given by

$$A = 2ac \sin 60^0 = 85.71 \text{ Å}^2.$$

and the areal density is given by

$$AD = \frac{1 \text{ molecule}}{85.71 \times 10^{-16} \text{cm}^2} = 1.17 \times 10^{14} \frac{\text{molecules}}{\text{cm}^2}.$$

Similar calculations were done for all relevant faces.

Electron Spectroscopy Chemical Analysis

The chemical bonding and surface composition of our films was of interest and we used Electron Spectroscopy Chemical Analysis (ESCA) or X-Ray Photoelectron Spectroscopy (XPS) to get this information. We contracted with Dr. Ken Nebesney to perform measurements on three samples of IAD $SmF_3$ using the apparatus at the University of Arizona Chemistry Department. ESCA employs a monoenergetic x-ray beam to irradiate a sample and cause photoionization of core electrons. The binding energy of the original electron state is given as the difference in energy between the incident x-ray and the photoelectron. The whole experiment is contained in an ultra high vacuum ($<10^{-9}$ torr) and for samples of dielectric material such as ours there can be a shift in the energies due to charging. We prevented the problem by depositing the films on silicon substrates. This technique is surface sensitive since the escape depth of the photoelectron is only about 100 Å. Data is discussed in chapter five.

# CHAPTER 4

## COMPOSITION AND STRUCTURE OF LANTHANIDE TRIFLUORIDE THIN FILMS

This chapter describes an experiment in which we thermally evaporated thin films of a series of lanthanide trifluorides, $LnF_3$ [Ln=Pr,Sm-Lu] onto fused silica and carbon substrates at ambient temperature, 100°C and 200°C. Using the techniques of RBS and Bragg-Brentano x-ray diffractometry we examined the films composition and crystal structure for comparison with the bulk materials.

Recall that the properties of a thin film differ from those of the bulk material. There are many reasons for this, the three main ones being the non-equilibrium nature of the deposition processes, the possibility for great variation in stoichiometry between the source material and the condensate, and the large surface to volume ratio of thin films. First we consider the fact that thermal evaporation is not an equilibrium process.

The earliest prediction that a solid which has not reached the solid state under equilibrium conditions may not be in the stable but instead in a metastable configuration was made by Ostwald in 1897. The phenomenon is now understood as a competition between the crystallization process and the solidification process as depicted in Figure 4.1. If crystallization proceeds at a higher rate than solidification, the result is a crystal in the most stable phase possible for that

material at the existing temperature and pressure conditions. If solidification proceeds at a higher rate, then the material can adopt some metastable phase (Zallen 1983). Metastable in this case includes any higher temperature phases, non-crystalline material, or combination of these. We expected the $LnF_3$ films to be amorphous or to contain their respective high temperature phases as defined in chapter two.

The most straightforward way to affect the thermal evaporation process is by heating the substrate. It works by bringing the substrate temperature closer to the effective temperature of the incoming atoms, thereby making the condensation process closer to equilibrium. It is particularly relevant in this study of physical properties of coating materials since it is a common method of obtaining more densely packed films. We expected our high temperature films to be more ordered than the low temperature films. This could show up only as larger crystallites and higher intensity x-ray peaks or in the sighting of the low temperature phases.

Regarding composition, all molecules do not behave in a similar manner upon evaporating. For instance, ZnS dissociates, cryolite, $Na_3AlF_6$, splits into two parts, $NaF_3$ and $AlF_3$, and $MgF_2$ remains together. All of these, however, form stoichiometric films (Pulker 1984). We expected the $LnF_3$ to remain intact, with a minimum of fluorine loss, and to form stoichiometric films. We based our expectations on several factors. Primarily, that these compounds are ionic and the fluorine should stay bonded unless a more energetically favorable reaction was possible. The most probable reaction would be that of $H_2O + LnF_3 = 2HF + LnF$ but we had so little water in the chamber it was not likely to have a large scale effect. Also the work of Zmbov and Margrave (1966 and 1967) on dissociation of $LnF_3$ upon heating showed that it was difficult to break the Ln-F bonds. Finally,

we had previous results on $LnF_3$ [Ln=La-Nd]. The films were stoichiometric but the compounds differed from $LnF_3$ [Ln=Pr,Sm-Lu] in that they sublime rather than melt (Targove 1987).

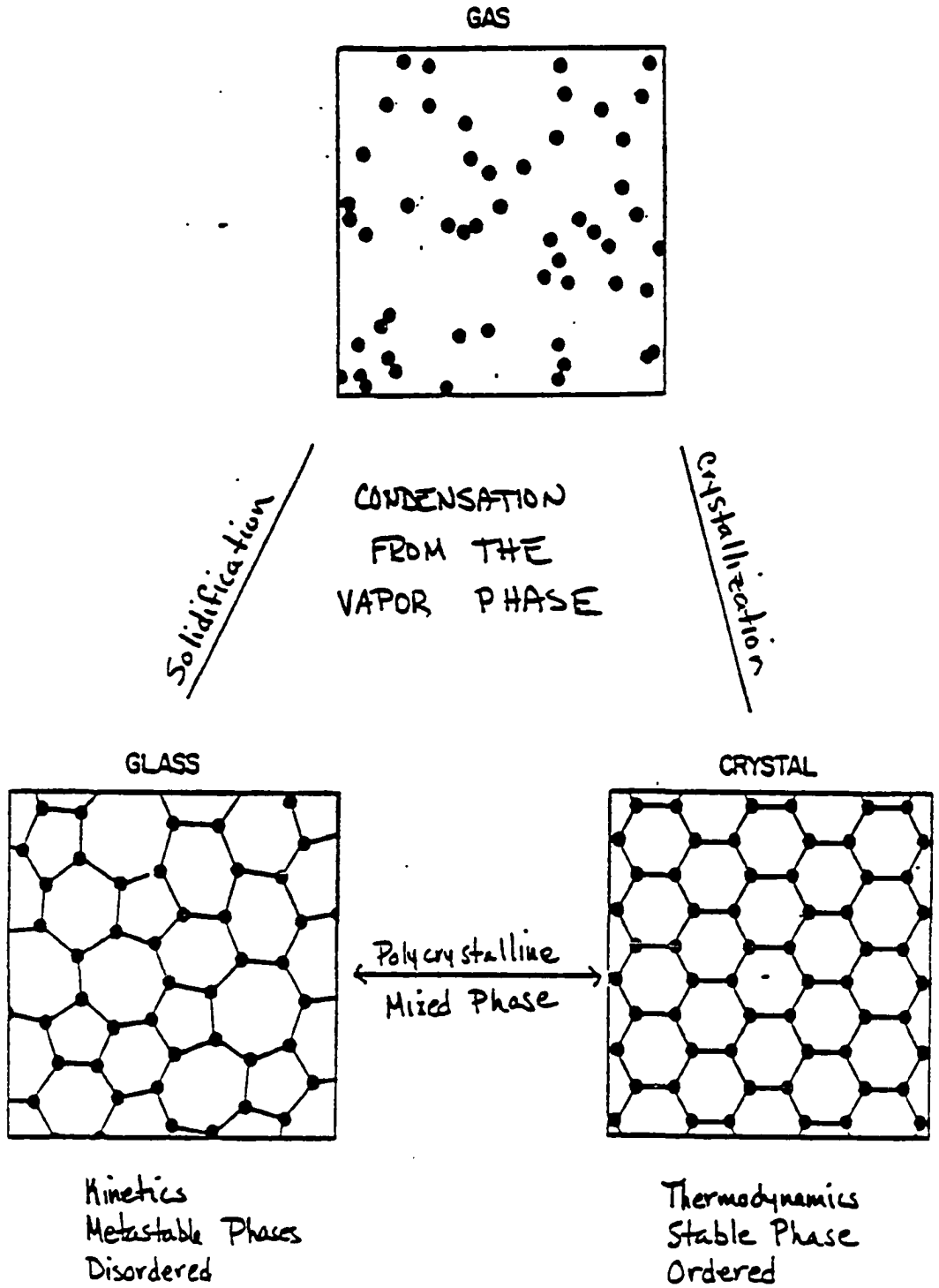


Figure 4.1 Solidification versus crystallization (after Zallen 1983).

Composition

Film composition was tested by depositing a 1000 Å thick $LnF_3$ film onto a carbon substrate, according to the methods described in chapter 3, and passing it to Prof. Leavitt's group at the University of Arizona Physics Department for Rutherford Backscattering Spectrometry analysis.

Table 4.1 contains the results. We see that the films were stoichiometric and most of the values for the different materials were within uncertainty of one another. Notice that there was no relation between temperature of substrates and stoichiometry of films.

The major contaminant in our films is oxygen and it is listed in Table 4.1 as atomic percent. Other elements were sometimes found in the films but in much lower quantities, less than one atomic percent. Molybdenum, tantalum and carbon were the most common ones in these films. Since the rare earths are so hard to separate there is also the possibility that, for example, a film of $PrF_3$ could contain a few ppm Ce or other lanthanide. That is the level of metal contamination listed in the chemical analysis done by Cerac before shipping the starting material to us. This would not be detectable by RBS because heavy elements with such similar masses have overlapping signals (Chu 1978). Nor would it have any effect on the film properties that we are interested in.

The relative amount of oxygen retained by the different groups of $LnF_3$ will become important in our discussion section. Although it did not make a difference for stoichiometry (#F/#Ln), the bakeout associated with the 200°C film deposition caused the high temperature films to have much less oxygen than the ambient temperature films. The $EuF_3$ film deposited at ambient temperature was deposited in the same run as a 200°C optical film but after the chamber had cooled down. It

had therefore been deposited in a cleaner chamber than the rest of the ambient temperature films in this experiment due to the bake-out and it contains less oxygen than those other films. Notice also that the ambient temperature $LnF_3$ [Ln=Tb,Ho] films contain more oxygen than the $LnF_3$ [Ln=Sm,Gd] films and less on average than films of $LnF_3$ [Ln=Er-Lu]. We do not attempt to explain this in terms of the material properties because our base vacuum varied enough from run to run at that time to cause the effect. We do intend to use the fact to make another point in our discussion.

Table 4.1. Composition of lanthanide trifluoride thin films deposited at various temperatures.

| Compound | Thin Film Deposition Temperature | Stoichiometry (# F) (#Ln) | Oxygen Atomic (%) |
|---|---|---|---|
| $PrF_3$ | ambient | 2.96 ± .03 | 1.77 ± .3 |
| $SmF_3$ | ambient | 2.96 ± .03 | 2.24 ± .2 |
| | 100°C | 2.95 ± .03 | 1.35 ± .3 |
| | 200°C | 2.97 ± .03 | 1.34 ± .2 |
| $EuF_3$ | ambient | 3.00 ± .03 | 0.73 ± .2 |
| | 200°C | ——— | ——— |
| $GdF_3$ | ambient | 2.98 ± .03 | 3.85 ± .5 |
| | 200°C | 3.00 ± .03 | 1.19 ± .2 |
| $TbF_3$ | ambient | 2.95 ± .03 | 4.46 ± .3 |
| | 100°C | ——— | ——— |
| | 200°C | 2.99 ± .03 | 0.00 ± .05 |
| $DyF_3$ | ambient | ——— | ——— |
| | 200°C | 3.04 ± .03 | 0.00 ± .05 |
| $HoF_3$ | ambient | 2.94 ± .03 | 4.55 ± .3 |
| | 200°C | 2.98 ± .03 | 0.00 ± .05 |
| $ErF_3$ | ambient | 3.03 ± .03 | 5.11 ± .2 |
| | 100°C | 2.94 ± .03 | 5.34 ± .3 |
| | 200°C | 2.99 ± .03 | 0.00 ± .05 |
| $TmF_3$ | ambient | 2.98 ± .03 | 4.46 ± .4 |
| | 200°C | 3.05 ± .03 | 0.52 ± .2 |
| $YbF_3$ | ambient | 2.97 ± .03 | 5.47 ± .24 |
| | 200°C | 3.00 ± .03 | 0.00 ± .05 |
| $LuF_3$ | ambient | 2.96 ± .03 | 6.78 ± .3 |
| | 200°C | 2.98 ± .03 | 2.49 ± .2 |

Structure

X-ray diffraction was performed on 5000 Å films deposited onto fused silica substrates as described in chapter three. Table 4.2 shows the $LnF_3$, the deposition temperature, the crystal structure and the crystallite size. Again the series can be split into four groups, based on thin film crystal structure, but not the same groups as for the bulk. $PrF_3$ was deposited only at ambient temperature and had polycrystalline hexagonal tysonite structure (Figure 4.2). It gave the same results as we got for $LnF_3$ [Ln=La,Ce,Nd] in earlier experiments (Targove 1987). For $LnF_3$ [Ln=Sm,Eu], films deposited at room temperature had polycrystalline hexagonal tysonite structure and films deposited at 200°C had, in addition, crystallites of the orthorhombic geometry (Figures 4.3, 4.4, 4.5, and 4.6). For $LnF_3$ [Ln=Gd-Er], films deposited at room temperature had no detectable structure and films deposited at 200°C had polycrystalline orthorhombic structure (Figures 4.7, 4.8, 4.9, 4.10 and 4.11). $GdF_3$ also has one faint line at $2\theta=29^0$ from what would be the corresponding hexagonal (111) peak. There is no JCPDS card for this phase since it is too difficult to quench to low temperatures to obtain a powder. For $LnF_3$ [Ln=Tm-Lu], films deposited both at room temperature and at 200°C had no detectable structure. We were able to obtain, at a later date, orthorhombic crystallites in a 1000 Å thick $LuF_3$ film. (Please refer to the thickness section in chapter five.)

All of the films have a preferred orientation, that is the relative intensities of peaks in the films are not the same as those in the powder standard for the material. Within a phase, the same planes which were favored in the low temperature depositions were favored in the high temperature depositions but the relative intensities were not always the same. Crystallite size of the strongest peak

in the spectrum increased with deposition temperature. The largest crystallites were found in the boat material.

To examine the effects of substrate structure on the growth phase, several different substrate materials were investigated. For magnesium fluoride, lithium fluoride, polished (221) oriented silicon, and float glass, the crystal phase and orientation were the same as for films grown on fused silica for the identical deposition conditions. In addition, relaxation of metastable phases was studied over a period of approximately one year. On this time scale no relaxation of the metastable to the equilibrium state phase was observed.

Powder diffraction was done on samples of starting material and samples of boat material. The results of the boat material diffractometry, in Table 4.2, indicate that the material reaches the expected low temperature phase when cooling in the boat.

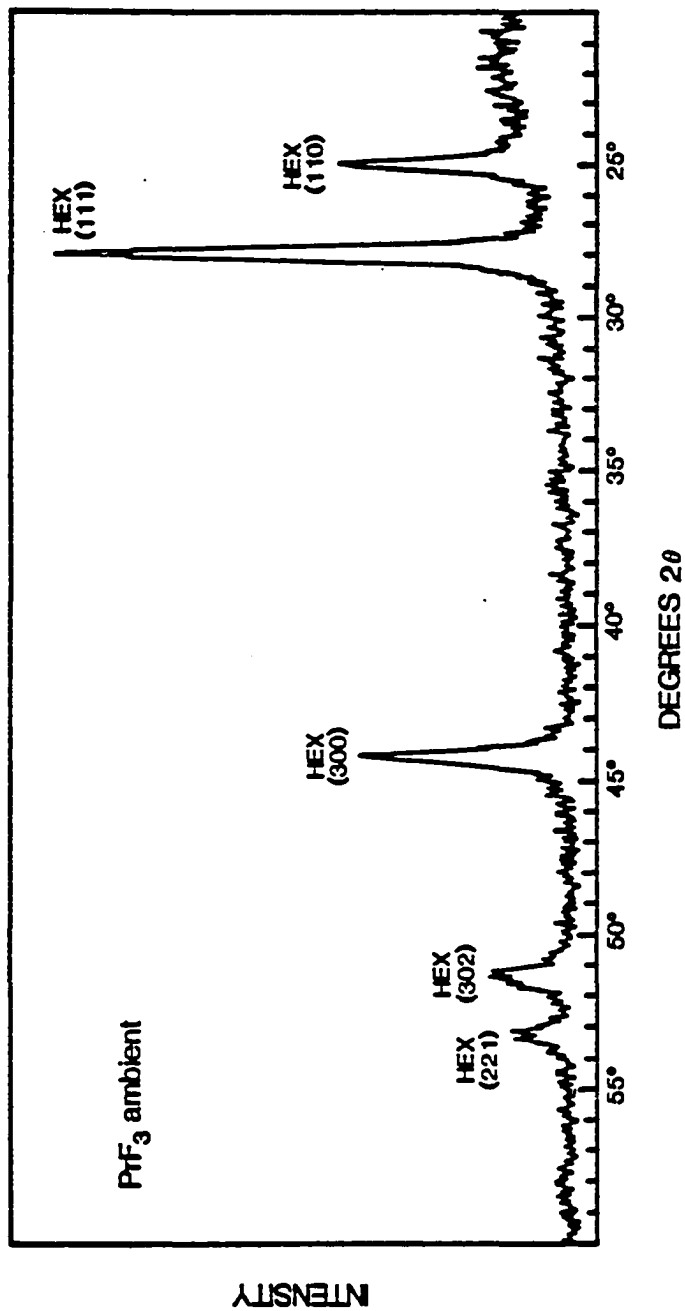


Figure 4.2. X-ray Diffraction Pattern of Praseodymium Trifluoride Film.

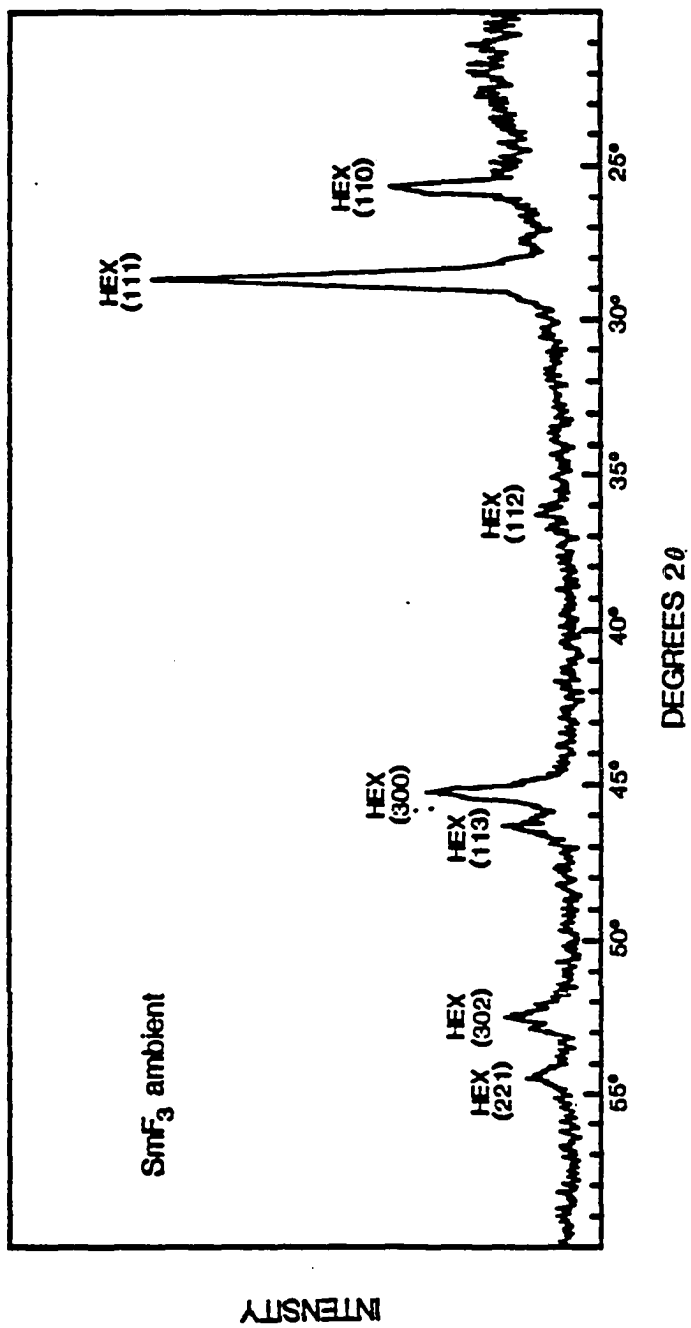


Figure 4.3. X-ray Diffraction Pattern of Samarium Trifluoride Film.

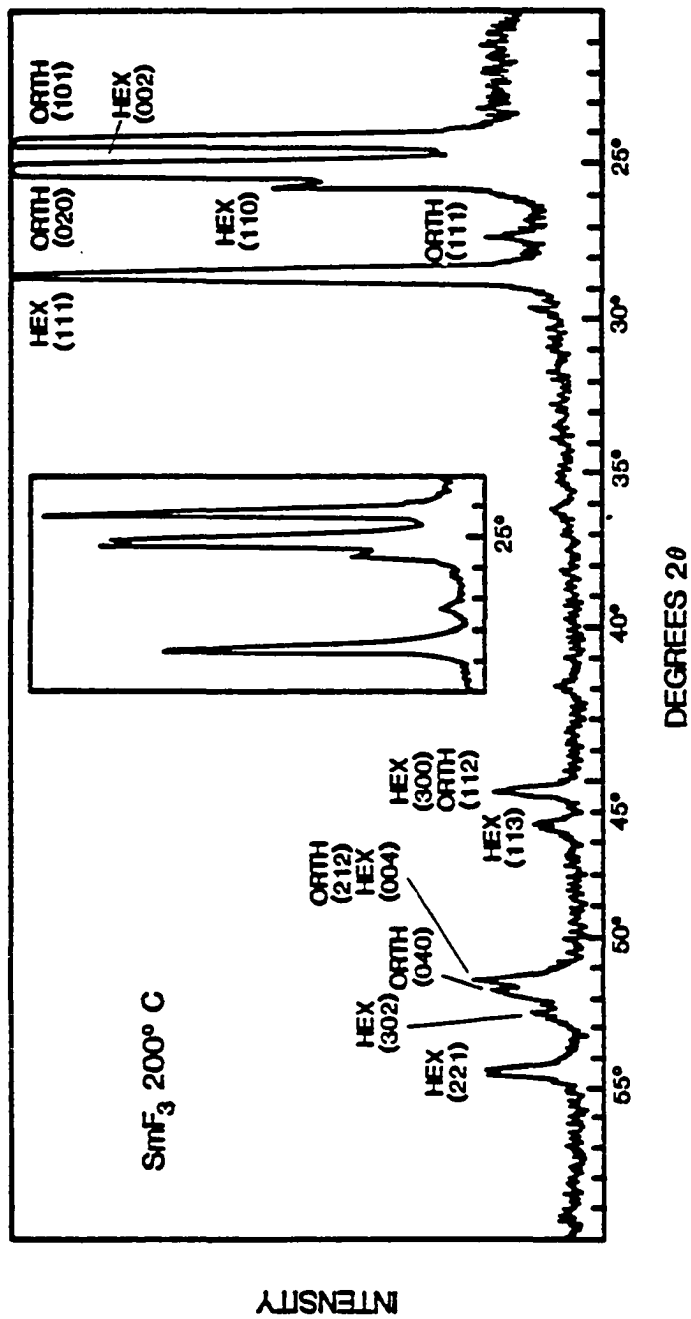


Figure 4.4. X-ray Diffraction Pattern of Samarium Trifluoride Film.

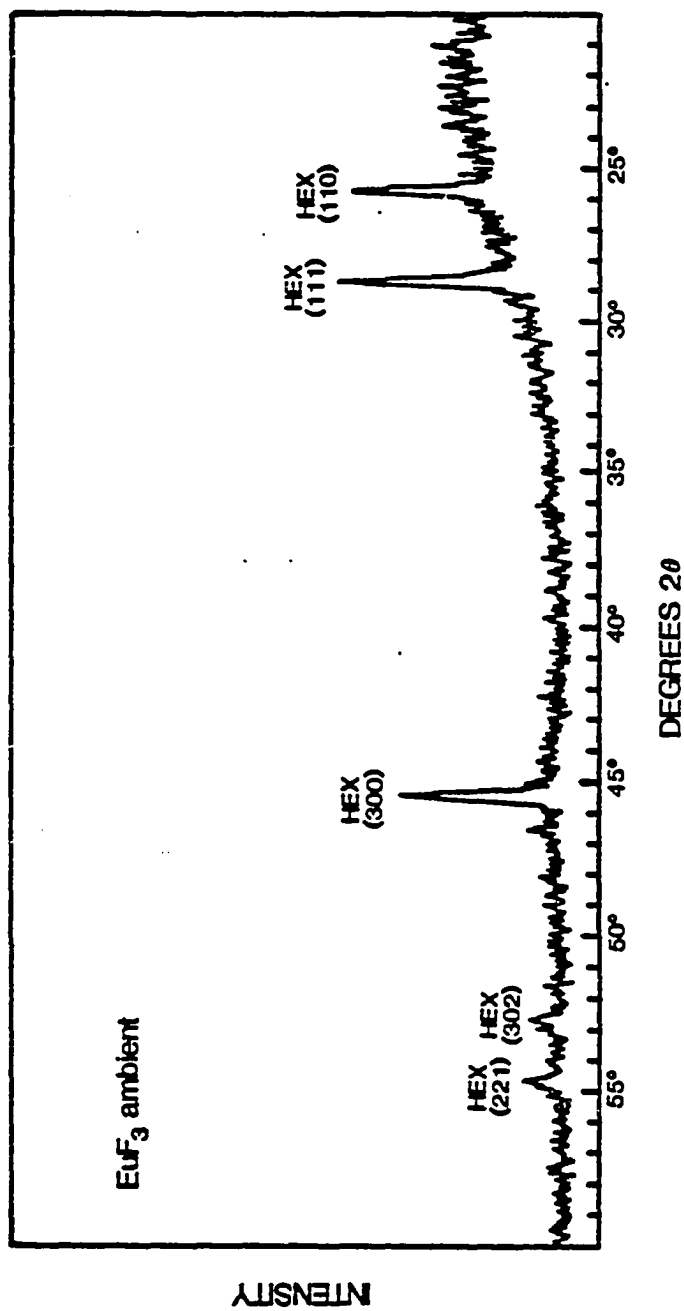


Figure 4.5. X-ray Diffraction Pattern of Europium Trifluoride Film.

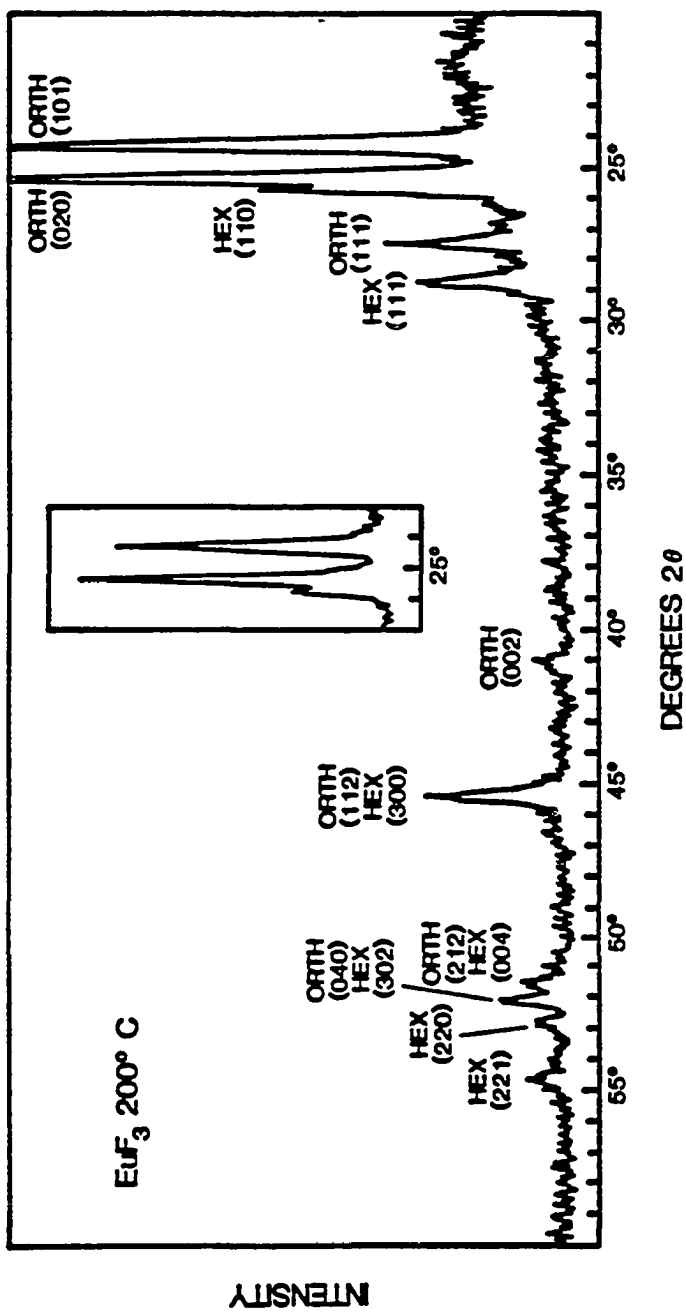


Figure 4.6. X-ray Diffraction Pattern of Europium Trifluoride Film.

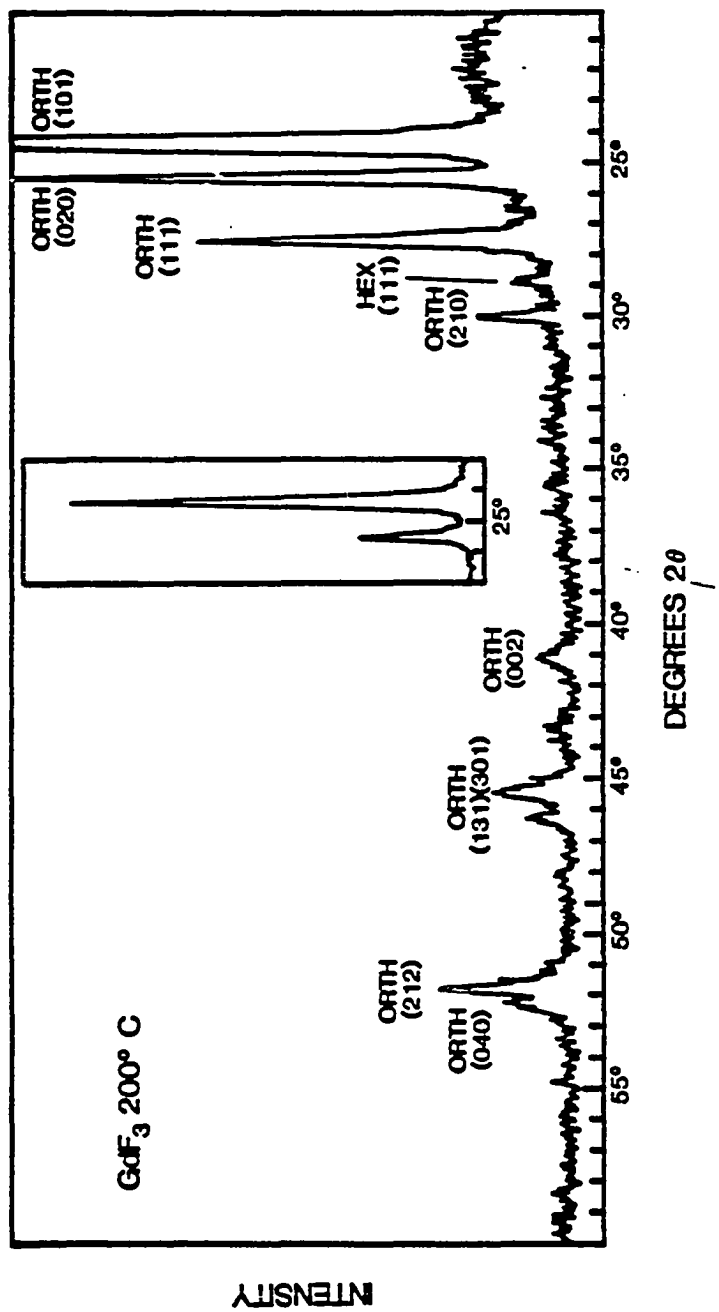


Figure 4.7. X-ray Diffraction Pattern of Gadolinium Trifluoride Film.

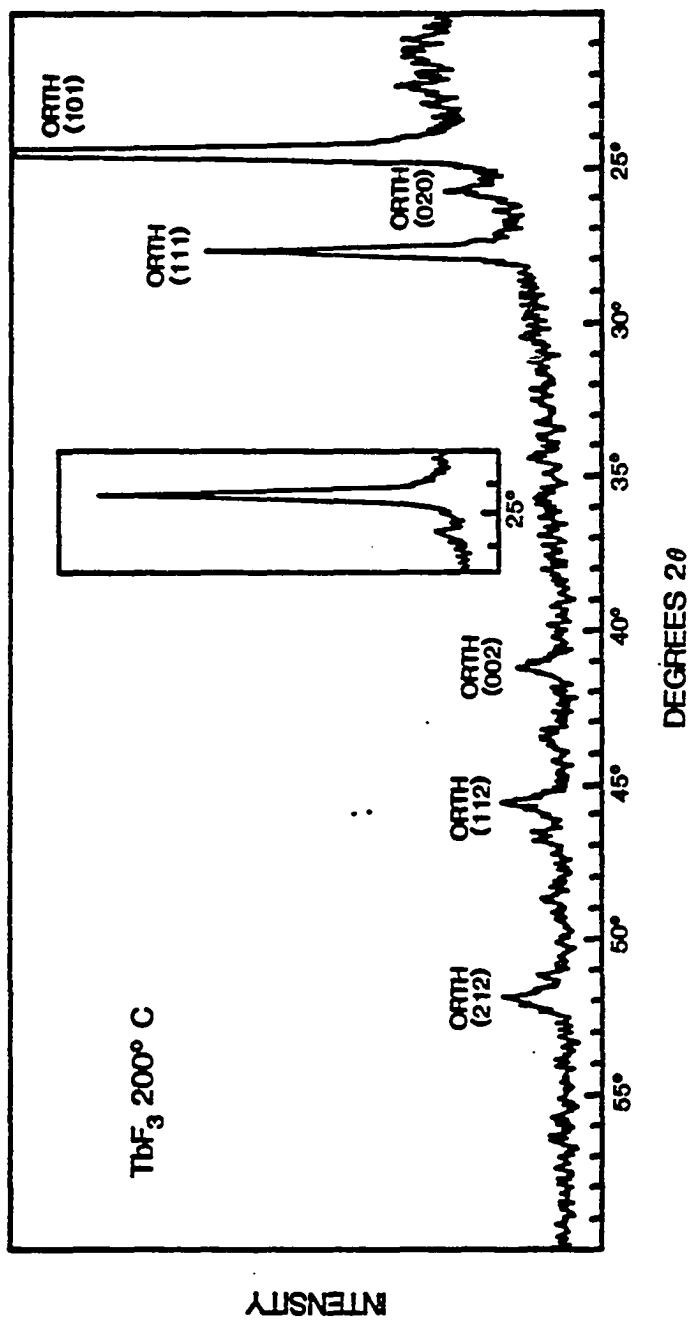


Figure 4.8. X-ray Diffraction Pattern of Terbium Trifluoride Film.

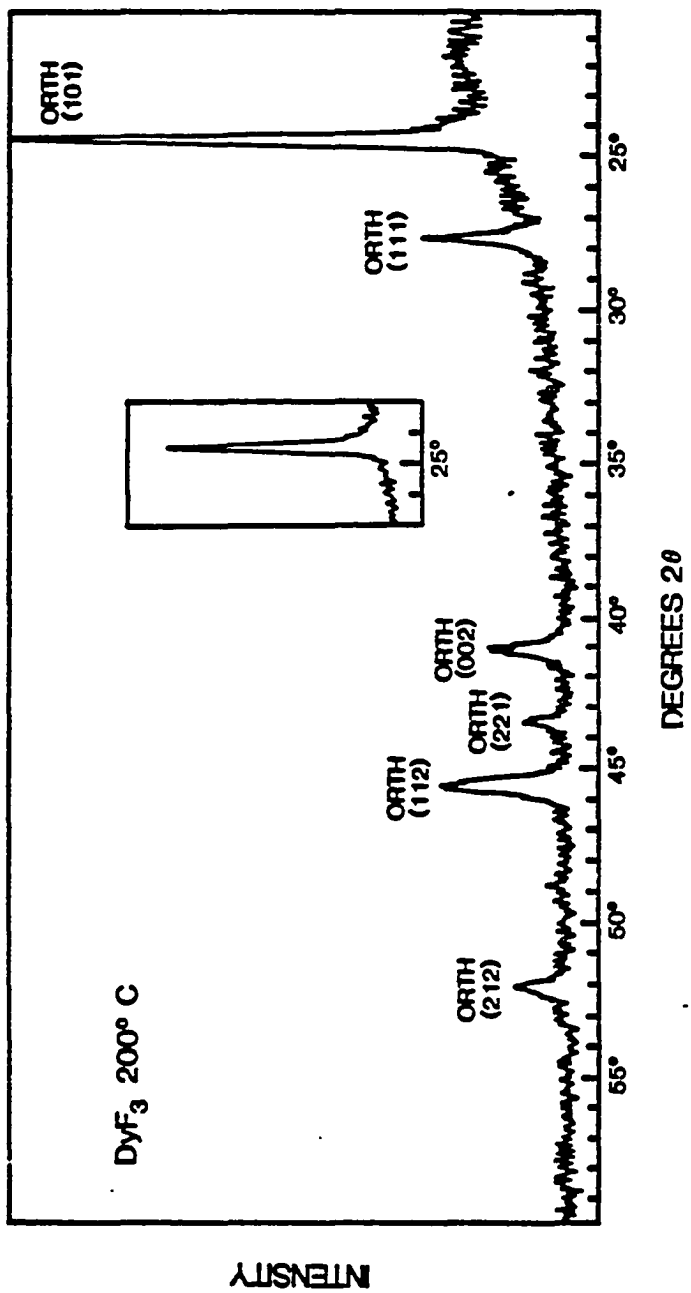


Figure 4.9. X-ray Diffraction Pattern of Dysprosium Trifluoride Film.

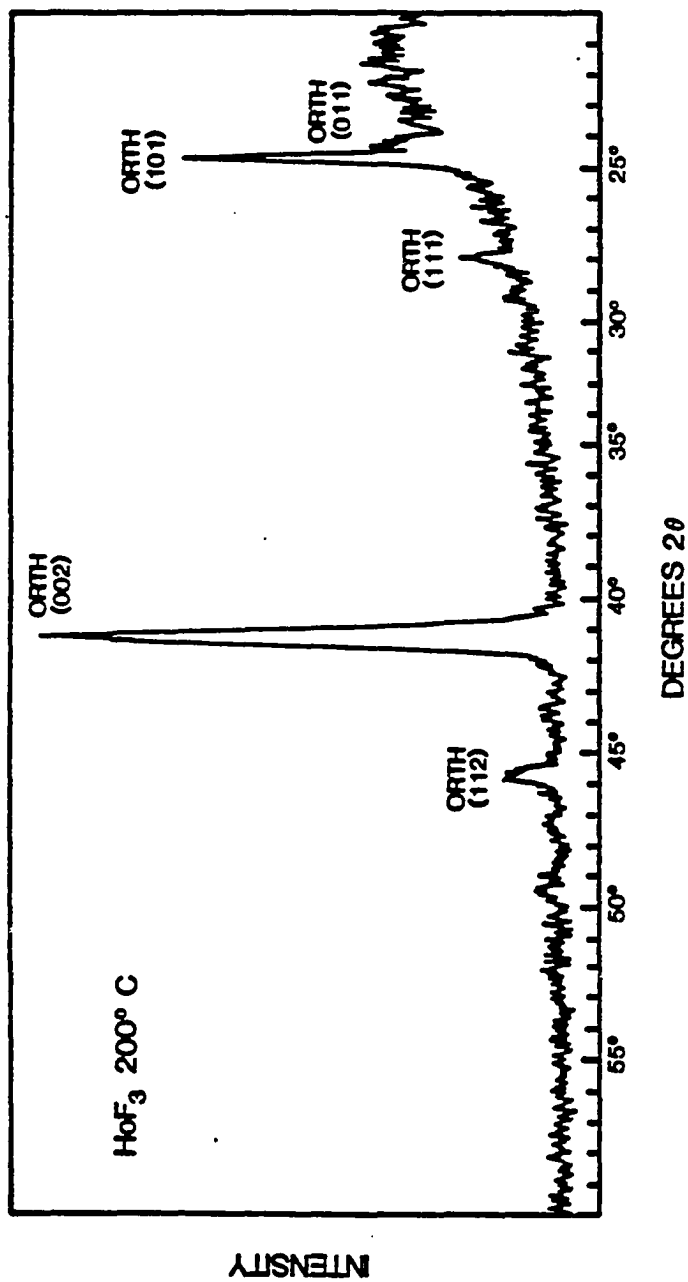


Figure 4.10. X-ray Diffraction Pattern of Holmium Trifluoride Film.

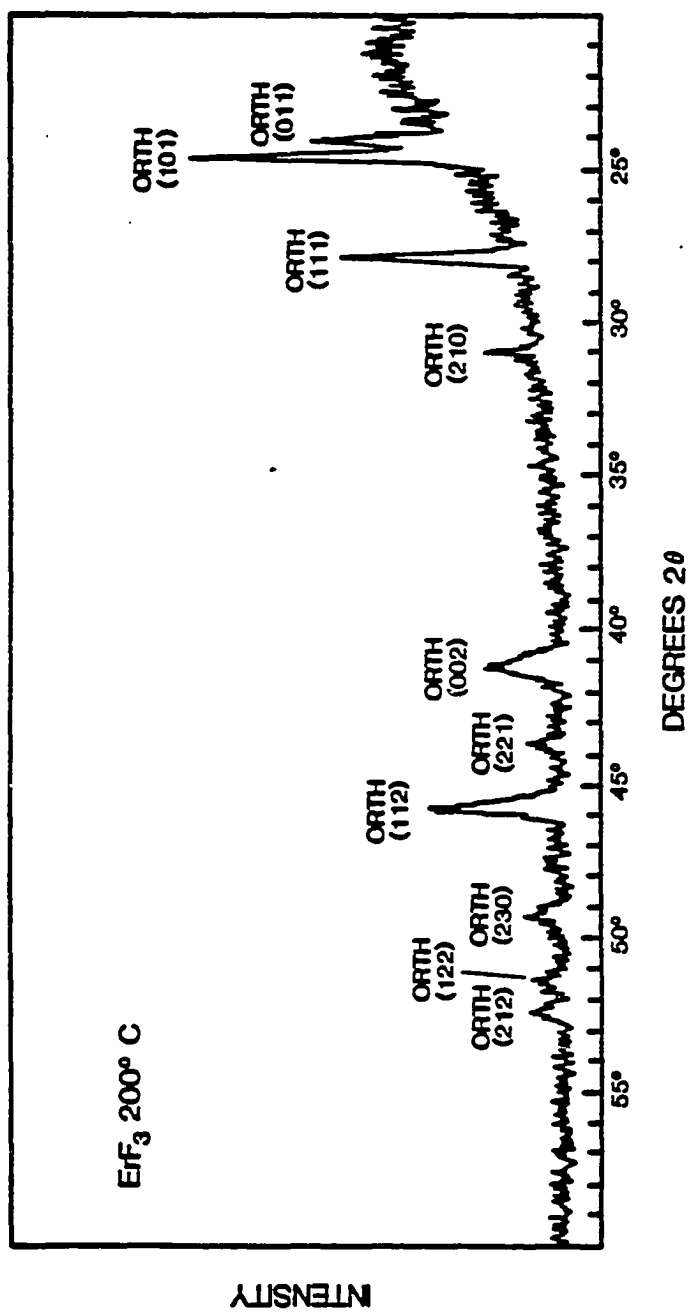


Figure 4.11. X-ray Diffraction Pattern of Erbium Trifluoride Film.

Table 4.2. Crystal structure of lanthanide trifluoride thin films deposited at various temperatures.

| Compound | Thin Film Deposition Temperature | Crystal Structure | Crystallite Size (Å) (Strongest Peak) |
|---|---|---|---|
| $PrF_3$ | ambient | hexagonal | 219 |
| | boat | hexagonal | 1094 |
| $SmF_3$ | ambient | hexagonal | 200 |
| | 100°C | hex & orth | 270 |
| | 200°C | hex & orth | 400 |
| | boat | orthorhombic | 450 |
| $EuF_3$ | ambient | hexagonal | 322 |
| | 200°C | hex & orth | 450 |
| $GdF_3$ | ambient | noncrystalline | — |
| | 200°C | orthorhombic | 320 |
| | boat | orthorhombic | 530 |
| $TbF_3$ | ambient | noncrystalline | — |
| | 100°C | orthorhombic | 300 |
| | 200°C | orthorhombic | 391 |
| $DyF_3$ | ambient | noncrystalline | — |
| | 200°C | orthorhombic | 321 |
| $HoF_3$ | ambient | noncrystalline | — |
| | 200°C | orthorhombic | 300 |
| $ErF_3$ | ambient | noncrystalline | — |
| | 100°C | noncrystalline | — |
| | 200°C | orthorhombic | 400 |
| $TmF_3$ | ambient | noncrystalline | — |
| | 200°C | noncrystalline | — |
| $YbF_3$ | ambient | noncrystalline | — |
| | 200°C | noncrystalline | — |
| | boat | orthorhombic | 790 |
| $LuF_3$ | ambient | noncrystalline | — |
| | 200°C | noncrystalline | — |

Discussion

Judging from the phase and crystallite size results, the $LnF_3$ films appear to strictly and simply follow Ostwald's rule. It states that a system transforms from an initial phase to a final phase by successively assuming those states whose free energies lie between the free energy of the initial and final states along the reaction path. Furthermore, there is the possibility that the system can be trapped in a metastable state if there is not enough activation energy to push it along the reaction path to the next phase (Sachtler 1966). As we anticipated, most of our films were in metastable phases. And most of the films deposited at elevated temperatures displayed a higher degree of order, as demonstrated by the presence of some low temperature phases and larger crystallites, but were still in metastable phases. However, there are several factors in addition to the quenching of the high temperature phase that can produce the results we have seen. Let us compare our results in more detail to the literature.

Supercooling, which happens during the quenching process, for solid-solid first order transitions has been observed in the $LnF_3$ by several groups (Spedding 1971 and Sobolev 1976 and Greis 1985) but the data for that process has remained unpublished because it was not helpful in determining the thermodynamic constants of the materials. Therefore, we must compare our results to the equilibrium results obtained by heating. Phase transitions in these types of experiments are caused by an increase in kinetic energy of the system due to an increase in temperature (Turnbull 1956 and Kingery 1976). The positions of the atoms change with respect to one another, then the number of nearest neighbors is different, the cation is pushed over a coordination threshold and the material must adopt another structure. These occur at characteristic temperatures or temperature ranges. It has been found

that the transition temperature can be changed by the presence of oxygen as well as absence of fluorine in the $LnF_3$. These two composition effects cause anion vacancies and are equivalent to a change in effective coordination number caused by heating. Recall from chapter two that the lanthanide contraction also has this effect (Sobolev 1976).

We are interested in whether our thin films have adopted their structure because of fluorine deficiency, oxygen contamination, or supercooling. In the case of bulk dimorphic trifluorides from $SmF_3$ to $GdF_3$, admixture of oxygen clearly shows a pronounced thermal stabilization of the high-temperature modification of tysonite structural type. The orthorhombic to tysonite transition is particularly sensitive because it is a low activation energy displacive transition. For several $LnF_3$ that do not have tysonite modifications, partial hydrolysis leads to formation of $LnF_{3-2x}O_x$ phases ($0 \leq x \leq 0.2$) that apparently have a tysonite structure. Previously, these phases were often taken to be high-temperature forms of pure $LnF_3$ (Thoma and Brunton 1966).

Let us review our composition and structure results with this knowledge in mind. If oxygen inclusion were a strong influence on the structure of our films as it was for the bulk samples of Thoma and Brunton, Spedding, and Sobolev we should have gotten different results for our ambient temperature films. Our ambient temperature $LnF_3$ [Ln=Tb-Ho] films contained about 4.5% oxygen yet they were not induced into an orthorhombic LnOF structure. Furthermore, the ambient temperature $EuF_3$ film contained only about 0.7% oxygen and it exhibited the same structural patterns as the $SmF_3$ which contained about 2.3% oxygen. The $GdF_3$ ambient temperature film, containing approximately 3.9% oxygen, was amorphous not orthorhombic. We conclude that anion vacancies in our films caused by oxygen

inclusion do not have the same importance in determining structure as they do in the bulk equilibrium experiments.

Now that we have shown that our thin film structures are due to Ostwald's rule and not composition variations, we can explain our structure distribution in those terms. Quenching is the freezing of existing order. The resulting phase of a freshly deposited thin film depends upon the existing order at the time the molecules lose enough kinetic energy to stop transitions between alternative phases. The reason many of the materials do not adopt their high temperature structures in the thin films is because the time the film spends in the temperature range, during cooling, where this phase is stable is too small. This can be because the cooling rate is too fast or because the temperature range where the phase is stable is too small. For example, the $GdF_3$ never adopts the hexagonal structure because it is not energetically favorable over a wide enough temperature range, likewise the $LnF_3$ [Ln=Er-Lu] with their respective hexagonal structure. This reasoning also explains why a high temperature substrate encourages stabilization of the high temperature phase as observed in $LnF_3$ [Ln=Sm,Eu]. It is not clear why the $LnF_3$ [Ln=Er-Lu] do not crystallize in their orthorhombic structure when deposited at 200°C. Possibly they begin to crystallize in the hexagonal structure and are in the throes of a reconstructive transition when they freeze or they may need more energy to adopt the orthorhombic configuration from a disordered state than the other $LnF_3$ do.

# CHAPTER 5

# EFFECT OF ION-ASSISTED DEPOSITION ON SAMARIUM TRIFLUORIDE THIN FILMS

## Introduction

Ion-assisted deposition (IAD) was made possible by Kaufmann's invention of the hot cathode ion source. The size and shape of the ion source made it possible to place it inside a vacuum evaporator and aim it at a growing thin film. The ion bombardment of a thin film during growth has become known as ion-assisted deposition (Hirsch and Varga 1980). The IAD process has generated and continues to generate much interest in the optical coatings community (Martin 1986). Some of the positive effects it can have on a growing film are: an increase in packing density and real refractive index, a change in the crystalline phase and orientation, a change in adhesion, and a change in stress. However, it can also cause an increase in absorption and allow the bombarding species to become included in the film. Its desirable effects must be balanced by the undesirable effects so it has found numerous applications in industry but is not as complete a solution to coatings problems as had been hoped. As we mentioned in chapter one, we can only take full advantage of IAD if we understand it. In this chapter we describe a series of experiments designed to characterize IAD for use with fluorides.

In these experiments we examine the influence of ion-assisted deposition (IAD)

and deposition temperature on thin films of $SmF_3$. Other recent work involving ion-assisted deposition and fluorides has been reported for $MgF_2$ (Wood 1984, Martin 1987) and for $LaF_3$ (Targove 1988). While $MgF_2$ and $LaF_3$ are the more important coating materials, $SmF_3$ is a better choice for a systematic study of the deposition conditions because of its multiple valency and dimorphism. The samarium cation is both divalent and trivalent and therefore the trifluoride and difluoride both exist. The trifluoride is pale yellow in bulk form and the difluoride is blood red (Catalano 1969). Also, recall from chapter 4 that the trifluoride is dimorphic. We found that $SmF_3$ naturally grows in the hexagonal high temperature phase when deposited onto a room temperature substrate and it grows in the orthorhombic low temperature phase when deposited onto a heated substrate. Use of $SmF_3$ provides us with further insight into the affects of ion-assisted deposition than other materials can because the indicators of fluorine deficiency, recrystallization, and even phase transition are so much more pronounced.

Previously ion bombardment was known to effect solids by producing color centers in ionic solids, by producing interstitial-vacancy pairs in metals or by recrystallization. The mechanism for these effects have been explained in several alternative models developed by Seitz and Kohler (1957) and by Brinkman (1956). The most widely accepted theory is based on a collision cascade. When ions hit the solid they undergo a series of collisions loosing momentum as they proceed further and further into the solid. They also trigger a series of collisions between the atoms they have hit and their neighboring atoms. This multiple momentum transfer results in the rearrangement of many atoms. An alternative theory holds that although the ions undergo some collisions, the thing responsible for the bulk of the solid's rearrangement is a thermal spike which occurs at the resting place of the ion. The

remaining energy of the ion which is not transferred in the collision is converted into heat causing local annealing and lattice vibrations. Evidence of local annealing would be the recrystallization seen in bombarded solids (Brinkman 1953). No one has succeeded, to date, in actually proving that either the thermal spike or the collision cascade is dominant for the case of ion bombardment of solids (Kelly 1984) or for the case of ion-assisted deposition (Muller 1987). It is difficult to find some effect of IAD which is reasonable to observe and does not have multiple causes.

Our work using $SmF_3$ films covered a wide range of variable parameters and characterization techniques. Our major variables were substrate temperature, ion current density, ion energy and film thickness. Our major characterization techniques were x-ray diffraction for crystal structure on a subcolumnar level and Rutherford backscattering spectrometry for elemental composition. To try to learn more about the mechanism of IAD, we attempted to separate the effects of ion current density and ion energy and to compare IAD to temperature.

Examining separately the effects of current density and energy was straightforward and the results are presented later in this chapter and in chapter six. But the comparison of IAD and temperature requires some qualification. For IAD, both hypothetical mechanisms are kinetic. A collision cascade is a momentum transfer. A thermal or displacement spike has an extremely short relaxation time. The comparison of this effect with high temperature deposition which drives the process of condensation closer to equilibrium is only valid with certain restrictions. If IAD gives the orthorhombic phase we can conclude that the thermal spike has a relaxation time comparable to that of the quenching time of the film with the substrate at 200°C. If it never gives the orthorhombic phase we are left with three possibilities which we cannot distinguish between : that thermal spike is still the

mechanism but the material affected by the spike quenches too fast to give the equilibrium phase, that the thermal spike is not the responsible mechanism, or that both mechanisms are at work.

In addition to the two experiments described above our goals included explaining some of the previously observed effects of IAD in more detail and more quantitatively by using $SmF_3$. We were able to find a more exact threshold for preferential fluorine sputtering, that is, at what current density and ion energy it begins for a typical fluoride. We found a way to prove that packing density can be controlled with IAD. We have examined in detail the composition of $SmF_3$ films within the parameter set of this experiment. This has led us to question whether or not old explanations for increase in refractive index were valid.

Composition

The data on composition of $SmF_3$ thin films as a function of deposition temperature, ion energy, and current density is presented Tables 5.1 through 5.6. We felt it was better to use tables than graphs because so many graphs would be required to include all the data and to put only a few could be misleading. For tables 5.1, 5.2, and 5.3 the same film was used to obtain the data for corresponding positions on all three tables.

Table 5.1 gives stoichiometry of 1000 Å films of samarium trifluoride evaporated onto carbon substrates from a Mo boat. It contains our data on the effects of temperature, argon ion energy and argon current density on stoichiometry. Deposition temperature has no effect on stoichiometry. Based on previous results (Targove 1988), we expected a decrease in the fluorine to samarium ratio with increasing current density and with increasing ion energy. Actual trends of this

nature were not present in our data, as one can see in Table 5.1, however, we can say that usually a heavily bombarded sample has a lower stoichiometry than a non-IAD sample.

The argon content of the $SmF_3$ films, shown in Table 5.2, behaved more like we predicted. The atomic percent of argon increased as ion energy increased, this makes sense since the greater the ion's energy, the less chance it will be deflected at the surface. The atomic percent of argon in the films increased as current density increased. Since the exposure time to the ion beam is constant, this is reasonable. There was also a decrease in argon content with increase in deposition temperature. The increased temperature of the substrate may have given the argon enough energy to reevaporate after sticking.

In contrast to the behavior of argon, the oxygen content of the films was not regular. The atomic percent of oxygen in the $SmF_3$ films, listed in Table 5.3, followed no trends in temperature. With regard to ion energy and current density we can say that those films which have been bombarded with argon during growth have 2-4% oxygen in them. And those which were not bombarded have much less. Oxygen content can be thought of as a step function. Oxygen in fluoride films is thought to have two possible sources, residual water and residual oxygen in the vacuum chamber. We expected to see less oxygen in the films deposited at higher temperatures because we baked out the chamber for those runs. This would have gotten rid of oxygen coming from the reactions : $H_2O + SmF_3 = 2HF + SmOF$ and $H_2O + 2SmF_3 = 2HF + 2SmF_2 + O$. Since we did not see this, we checked our gas lines for leaks but found none. We also tried ion-assisted deposition with UHP argon. Table 5.4 shows that these films had just as much oxygen as those deposited with the less pure welding grade oxygen. Our only conclusion was that the oxygen

must be residual oxygen in the vacuum chamber getting pushed into the films by the ion beam. (This appears to contradict the composition results of chapter four. However the two experiments were done almost a year apart and in between them our vacuum system was overhauled. Thus the second experiment was done with an average pressure of $5x10^{-7}$ mbar and the first set of low temperature films was made with an average pressure of $5x10^{-6}$ mbar.)

Tables 5.5 and 5.6 contain the results of nitrogen and krypton ion-assist. We see that nitrogen sticks in the films approximately four times as much as the inert krypton and argon (Table 5.2).

Table 5.1. **Stoichiometry of Samarium Trifluoride Films.**

| E (eV) | J ($\mu$A)/(cm$^2$) | # F / #Sm | E (eV) | J ($\mu$A)/(cm$^2$) | # F / #Sm | E (eV) | J ($\mu$A)/(cm$^2$) | # F / #Sm |
|---|---|---|---|---|---|---|---|---|
| 200°C | | | 200°C | | | 200°C | | |
| — | — | 3.02 ±.03 | — | — | ——— | — | — | ——— |
| 250 | 10 | 2.93 ±.03 | 500 | 10 | 2.94 ±.03 | 750 | 10 | 3.01 ±.03 |
| 250 | 20 | 2.90 ±.03 | 500 | 20 | 2.82 ±.03 | 750 | 20 | 2.86 ±.03 |
| 250 | 30 | 2.86 ±.03 | 500 | 30 | 2.78 ±.03 | 750 | 30 | 2.72 ±.03 |
| 250 | 40 | 2.82 ±.03 | 500 | 40 | 2.88 ±.03 | 750 | 40 | 2.78 ±.03 |
| 100°C | | | 100°C | | | 100°C | | |
| — | — | 2.99 ±.03 | — | — | ——— | — | — | ——— |
| 250 | 10 | 2.93 ±.03 | 500 | 10 | 2.91 ±.03 | 750 | 10 | 2.97 ±.03 |
| 250 | 20 | 2.89 ±.03 | 500 | 20 | 2.91 ±.03 | 750 | 20 | 2.92 ±.03 |
| 250 | 30 | 2.90 ±.03 | 500 | 30 | 2.85 ±.03 | 750 | 30 | 2.71 ±.03 |
| 250 | 40 | 2.82 ±.03 | 500 | 40 | 2.76 ±.03 | 750 | 40 | 2.84 ±.03 |
| ~25°C | | | ~25°C | | | ~25°C | | |
| — | — | 3.01 ±.03 | — | — | ——— | — | — | ——— |
| 250 | 10 | 2.88 ±.03 | 500 | 10 | 2.90 ±.03 | 750 | 10 | 2.89 ±.03 |
| 250 | 20 | 2.89 ±.03 | 500 | 20 | 2.70 ±.03 | 750 | 20 | 2.86 ±.03 |
| 250 | 30 | 2.81 ±.03 | 500 | 30 | 2.72 ±.03 | 750 | 30 | 2.78 ±.03 |
| 250 | 40 | 2.87 ±.03 | 500 | 40 | 2.76 ±.03 | 750 | 40 | 2.61 ±.03 |
| 50 | 6 | 2.97 ±.03 | 100 | 10 | 3.00 ±.03 | 1000 | 40 | 2.62 ±.03 |

Table 5.2. **Atomic Percent of Argon in Samarium Trifluoride Films.**

| E (eV) | J ($\mu A$)/($cm^2$) | %Ar | E (eV) | J ($\mu A$)/($cm^2$) | %Ar | E (eV) | J ($\mu A$)/($cm^2$) | %Ar |
|---|---|---|---|---|---|---|---|---|
| 200°C | | | 200°C | | | 200°C | | |
| — | — | 0.1 ± .05 | — | — | ——— | — | — | ——— |
| 250 | 10 | 0.2 ± .1 | 500 | 10 | 0.4 ± .1 | 750 | 10 | 0.6 ± .1 |
| 250 | 20 | 0.5 ± .1 | 500 | 20 | 0.8 ± .05 | 750 | 20 | 1.2 ± .1 |
| 250 | 30 | 0.9 ± .1 | 500 | 30 | 1.3 ± .05 | 750 | 30 | 1.4 ± .1 |
| 250 | 40 | 0.9 ± .1 | 500 | 40 | 1.3 ± .1 | 750 | 40 | 1.7 ± .1 |
| 100°C | | | 100°C | | | 100°C | | |
| — | — | 0.1 ± .1 | — | — | ——— | — | — | ——— |
| 250 | 10 | 0.0 ± .05 | 500 | 10 | 0.4 ± .1 | 750 | 10 | 0.6 ± .1 |
| 250 | 20 | 0.7 ± .05 | 500 | 20 | 1.0 ± .1 | 750 | 20 | 1.2 ± .1 |
| 250 | 30 | 1.0 ± .1 | 500 | 30 | 1.5 ± .1 | 750 | 30 | 1.9 ± .1 |
| 250 | 40 | 1.1 ± .1 | 500 | 40 | 1.8 ± .05 | 750 | 40 | 2.5 ± .1 |
| ~25°C | | | ~25°C | | | ~25°C | | |
| — | — | 0.1 ± .05 | — | — | ——— | — | — | ——— |
| 250 | 10 | 0.5 ± .1 | 500 | 10 | 0.9 ± .1 | 750 | 10 | 1.0 ± .1 |
| 250 | 20 | 1.5 ± .1 | 500 | 20 | 2.0 ± .1 | 750 | 20 | 2.2 ± .4 |
| 250 | 30 | 2.1 ± .1 | 500 | 30 | 2.3 ± .1 | 750 | 30 | 3.1 ± .1 |
| 250 | 40 | 2.2 ± .1 | 500 | 40 | 3.2 ± .05 | 750 | 40 | 2.4 ± .1 |
| 50 | 6 | 0.0 ± .05 | 100 | 10 | 0.0 ± .05 | 1000 | 40 | 3.0 ± .1 |

Table 5.3. **Atomic Percent of Oxygen in Samarium Trifluoride Films.**

| E (eV) | J ($\mu A$)/($cm^2$) | %O | E (eV) | J ($\mu A$)/($cm^2$) | %O | E (eV) | J ($\mu A$)/($cm^2$) | %O |
|---|---|---|---|---|---|---|---|---|
| 200°C | | | 200°C | | | 200°C | | |
| — | — | 1.5 ± .2 | — | — | ——— | — | — | ——— |
| 250 | 10 | 1.6 ± .4 | 500 | 10 | 1.8 ± .4 | 750 | 10 | 0.9 ± .2 |
| 250 | 20 | 3.4 ± .3 | 500 | 20 | 3.5 ± .2 | 750 | 20 | 2.8 ± .2 |
| 250 | 30 | 3.1 ± .2 | 500 | 30 | 4.4 ± .1 | 750 | 30 | 3.6 ± .2 |
| 250 | 40 | 3.6 ± .2 | 500 | 40 | 4.7 ± .4 | 750 | 40 | 4.2 ± .3 |
| 100°C | | | 100°C | | | 100°C | | |
| — | — | 1.3 ± .2 | — | — | ——— | — | — | ——— |
| 250 | 10 | 2.4 ± .1 | 500 | 10 | 2.5 ± .4 | 750 | 10 | 1.6 ± .4 |
| 250 | 20 | 2.8 ± .1 | 500 | 20 | 2.7 ± .5 | 750 | 20 | 2.7 ± .6 |
| 250 | 30 | 3.1 ± .4 | 500 | 30 | 3.3 ± .5 | 750 | 30 | 2.9 ± .2 |
| 250 | 40 | 3.8 ± .4 | 500 | 40 | 5.6 ± .2 | 750 | 40 | 1.6 ± .4 |
| ~25°C | | | ~25°C | | | ~25°C | | |
| — | — | 2.0 ± .3 | — | — | ——— | — | — | ——— |
| 250 | 10 | 2.9 ± .6 | 500 | 10 | 0.9 ± .1 | 750 | 10 | 2.7 ± .6 |
| 250 | 20 | 3.5 ± .6 | 500 | 20 | 4.2 ± .6 | 750 | 20 | 2.2 ± .2 |
| 250 | 30 | 3.4 ± .4 | 500 | 30 | 5.5 ± .6 | 750 | 30 | 3.3 ± .1 |
| 250 | 40 | 2.5 ± .1 | 500 | 40 | 2.0 ± .1 | 750 | 40 | 5.0 ± .5 |
| 50 | 6 | 2.2 ± .2 | 100 | 10 | 3.6 ± .2 | 1000 | 40 | 6.2 ± .2 |

Table 5.4. **Composition of Films With UHP Argon Ion-Assist.**

| E (eV) | J ($\mu A$)/($cm^2$) | # F / #Sm | E (eV) | J ($\mu A$)/($cm^2$) | %UHP Ar | E (eV) | J ($\mu A$)/($cm^2$) | %O |
|---|---|---|---|---|---|---|---|---|
| ~25°C | | | ~25°C | | | ~25°C | | |
| — | — | 2.95 ±.03 | — | — | 0.0 ± .05 | — | — | 2.1 ± .2 |
| 500 | 20 | 2.78 ±.03 | 500 | 20 | 2.4 ± .1 | 500 | 20 | 3.7 ± .3 |
| 750 | 20 | 2.72 ±.03 | 750 | 30 | 2.8 ± .2 | 750 | 20 | 3.9 ± .2 |

Table 5.5. **Composition of Films With Nitrogen Ion-Assist.**

| E (eV) | J ($\mu A$)/($cm^2$) | # F / #Sm | E (eV) | J ($\mu A$)/($cm^2$) | %N | E (eV) | J ($\mu A$)/($cm^2$) | %O |
|---|---|---|---|---|---|---|---|---|
| ~25°C | | | ~25°C | | | ~25°C | | |
| 250 | 10 | 2.81 ±.03 | 250 | 10 | 3.5 ± .2 | 250 | 10 | 3.2 ± .4 |
| 500 | 20 | 2.55 ±.03 | 500 | 20 | 8.3 ± .4 | 500 | 20 | 4.0 ± .3 |
| 750 | 20 | 2.56 ±.03 | 750 | 20 | 8.0 ± .3 | 750 | 20 | 3.2 ± .1 |

Table 5.6. **Composition of Films With Krypton Ion-Assist.**

| E (eV) | J ($\mu A$)/($cm^2$) | # F / #Sm | E (eV) | J ($\mu A$)/($cm^2$) | %Kr / %Ar | E (eV) | J ($\mu A$)/($cm^2$) | %O |
|---|---|---|---|---|---|---|---|---|
| ~25°C | | | ~25°C | | | ~25°C | | |
| 500 | 15 | 2.87 ±.03 | 500 | 15 | 1.7 ± .1<br>0.5 ± .1 | 500 | 15 | 3.8 ± .2 |

Structure

X-ray diffraction is a powerful technique for analyzing the distribution of crystalline phases in our thin films. In this paper we have made use of two XRD spectrum parameters: peak position and relative peak height. Peak position identifies compounds, particular crystalline structures of a given compound, and preferred orientation of crystallites possessing a particular crystalline structure. Relative peak height within a scan is an indication of what percentage of the crystallites are of a particular orientation relative to the substrate plane (Cullity 1978). The uncertainty of a normalized peak intensity is ±10%.

Recall that in chapter four we showed the effects of elevated temperature deposition on the crystal structure of $LnF_3$ thin films. The result for $SmF_3$ was that the films were more crystalline and that the low temperature phase (orthorhombic) appeared and dominated the high temperature phase (hexagonal tysonite). We consider this the effect of temperature on deposition and will be referring to it throughout this chapter. The ambient temperature, non-IAD films were slightly crystalline $SmF_3$ and of hexagonal structure with the two main preferred orientations (111) (d = 3.12 Å) and (110) (d = 3.48 Å), with dominant texture being (111). Films deposited onto substrates at 100°C exhibited improved crystallinity by increased peak height. At 200°C the crystallinity increased even more. However, only at 200° C did the orthorhombic phase become evident. In fact the orthorhombic (111) (d = 3.67 Å) peak was more intense than the hexagonal (110).

Figure 5.1 is a comparison of the x-ray diffraction patterns of two $SmF_3$ films, one non-IAD and one IAD. In this figure and in general the IAD films were more crystalline than the non-IAD films with the crystallinity increasing as the ion current density increased. We saw little correlation with ion energy. The dominant peak

at low current densities was hexagonal (110) followed by hexagonal (111). It is the opposite of the non-IAD case as we have shown clearly in Figure 5.1. At higher current densities a new peak appeared which is characteristic of several samarium fluoride compounds which have a F to Sm ratio less than three. They are: $SmF_2$ cubic (111), $Sm_{27}F_{64}$ cubic (511), $Sm_{13}F_{32-x}$ rhombohedral (131), $Sm_{14}F_{33}$ hexagonal (006), and $Sm_3F_7$ tetragonal (213).

Figures 5.2 through 5.9 are the result of further analysis, showing the normalized intensity of an XRD peak versus the argon ion current density for three different ion energies. Data for the last four figures was taken from films grown at ambient temperature and for the first four figures at 200°C. Each datum represents the relative abundance of the indicated preferred orientation in a separate film. These were measured perpendicular to the substrate plane and converted to the parallel face via the Miller indices. We found that the ion current density had a much more pronounced effect on the structure of the film than the ion energy.

We see that the hexagonal (111) decreases with ion current density at both ambient temperature and 200°C (Figures 5.5 and 5.9). Figures 5.4 and 5.8 show the increase in the hexagonal (110) face with increasing current density. In Figures 5.3 and 5.7, we see the increase in cubic (111) which is associated with $SmF_2$ and other non-stoichiometric samarium fluoride compounds. Finally, Figures 5.2 shows the absence of the orthorhombic phase at ambient temperature and Figure 5.6 shows its presence in the preferred orientation (101) at 200°C. We were careful not to regard the decrease in peak height as a decrease in the actual amount of crystallized material but a decrease in the growth rate as compared to another peak, since our peak intensities are not absolute.

Using the simple geometrical calculations we introduced in chapter three, we

calculated the areal density of each of the relevant faces in the plane parallel to the substrate. Table 5.7 summarizes the results, namely that IAD favors a certain areal density, $1.17 \times 10^{14}$ molecules per $cm^2$ by spreading out more densely packed material and packing in the looser material. Further evidence for this conclusion is given by a thickness study, the results of which are presented in Table 5.8.

Thickness

For the thickness study we grew films of thickness from 300 to 7500 Å. We followed the same data analysis with these films that we used in the previous experiment. Table 5.8 shows the areal density in the left column and values of normalized peak intensity inside the table. We see that for thinner films the areal density is greater and for thicker films the areal density of the most common orientation is less. This is an indication that the in-plane packing density within a column of a thin film is greater for thinner films. We postulate that as the $SmF_3$ films become thicker the in-plane packing density is reduced by stress. Fluorides are in fact known to have tensile stress (Pulker 1984).

We have seen and discussed the effect of ion-bombardment on films 5000 Å thick. We have also seen and discussed the effect of thickness on $SmF_3$ films. Combining the two ideas, we grew IAD films to a thickness of 2500 Å under the following conditions : a) 250 eV and 10 $\frac{\mu A}{cm^2}$, b) 500 eV and 20 $\frac{\mu A}{cm^2}$, and c) 750 eV and 20 $\frac{\mu A}{cm^2}$. All of the films were amorphous. This is further evidence that IAD can reduce the packing density of a film as well as increase it.

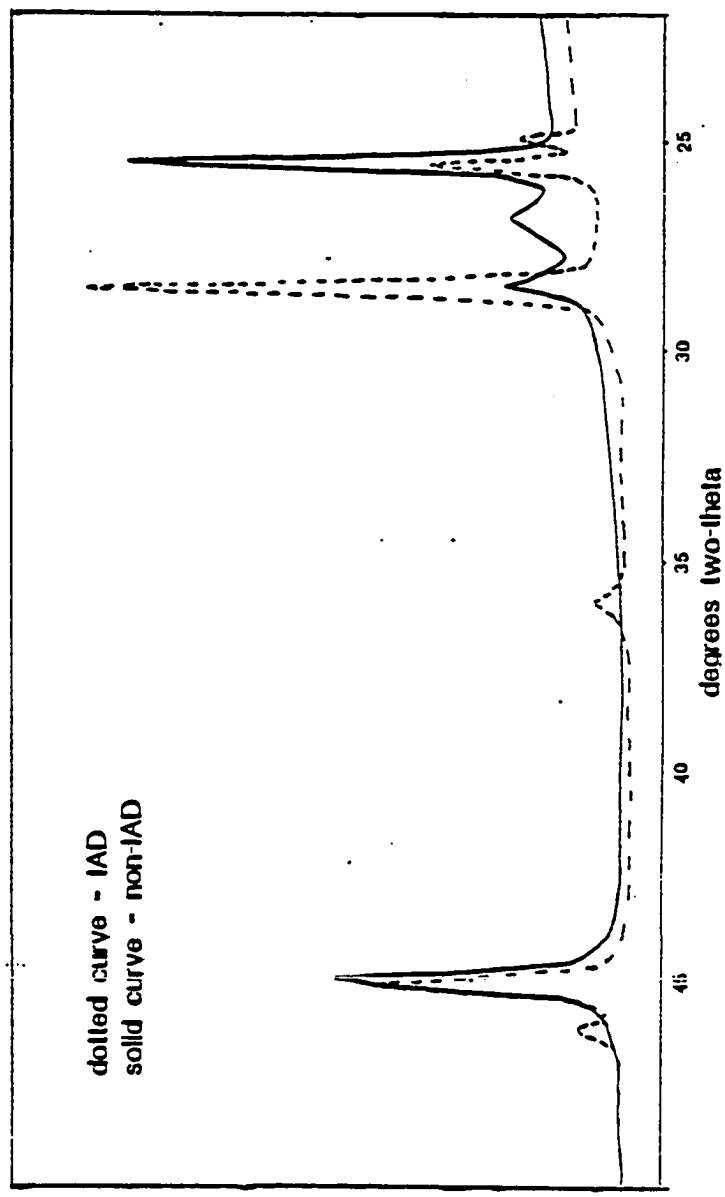


Figure 5.1. X-ray Diffraction Pattern of non-IAD and IAD $SmF_3$.

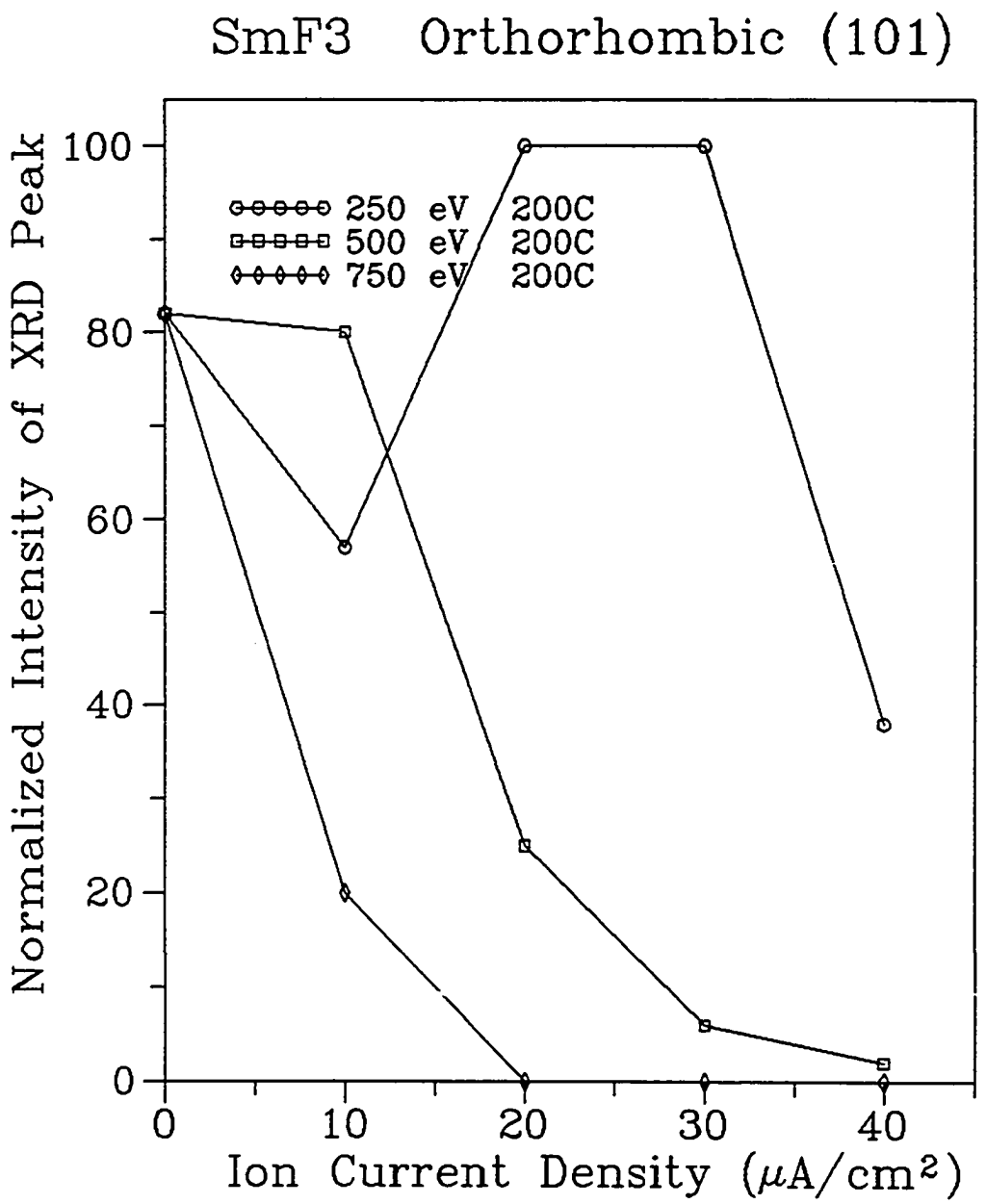


Figure 5.2. Structure of Samarium Trifluoride Thin Films.

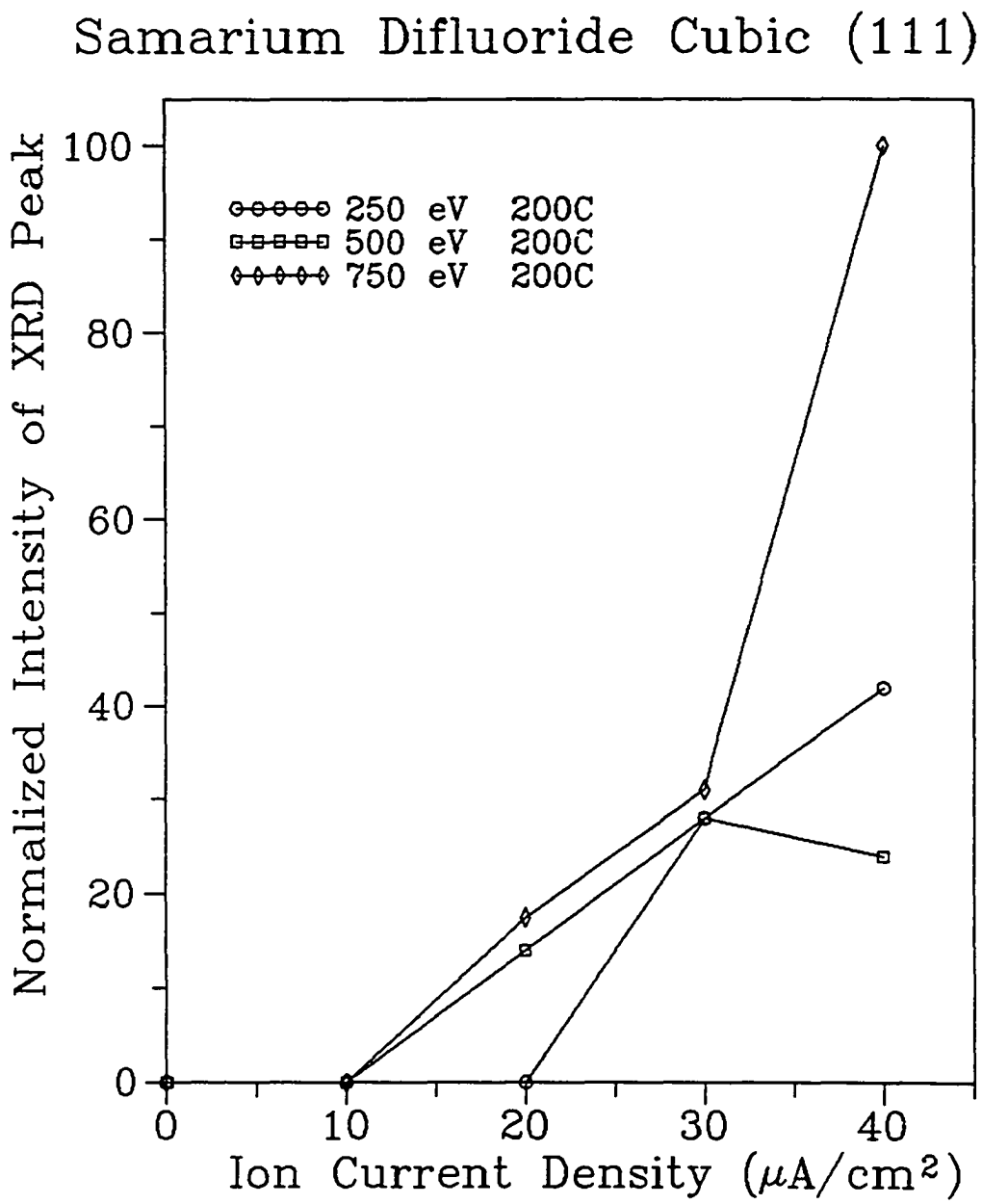


Figure 5.3. Structure of Samarium Trifluoride Thin Films.

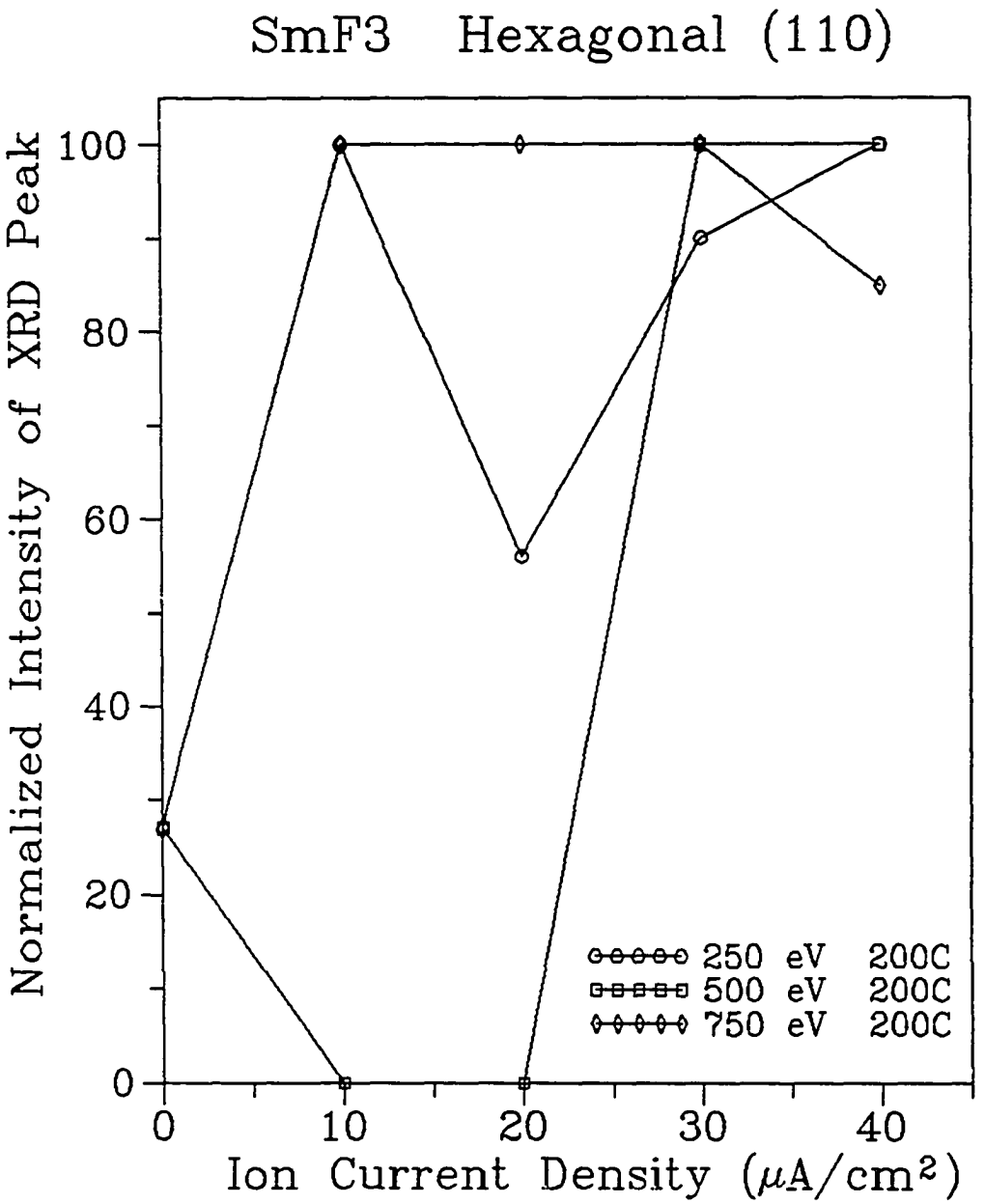


Figure 5.4. Structure of Samarium Trifluoride Thin Films.

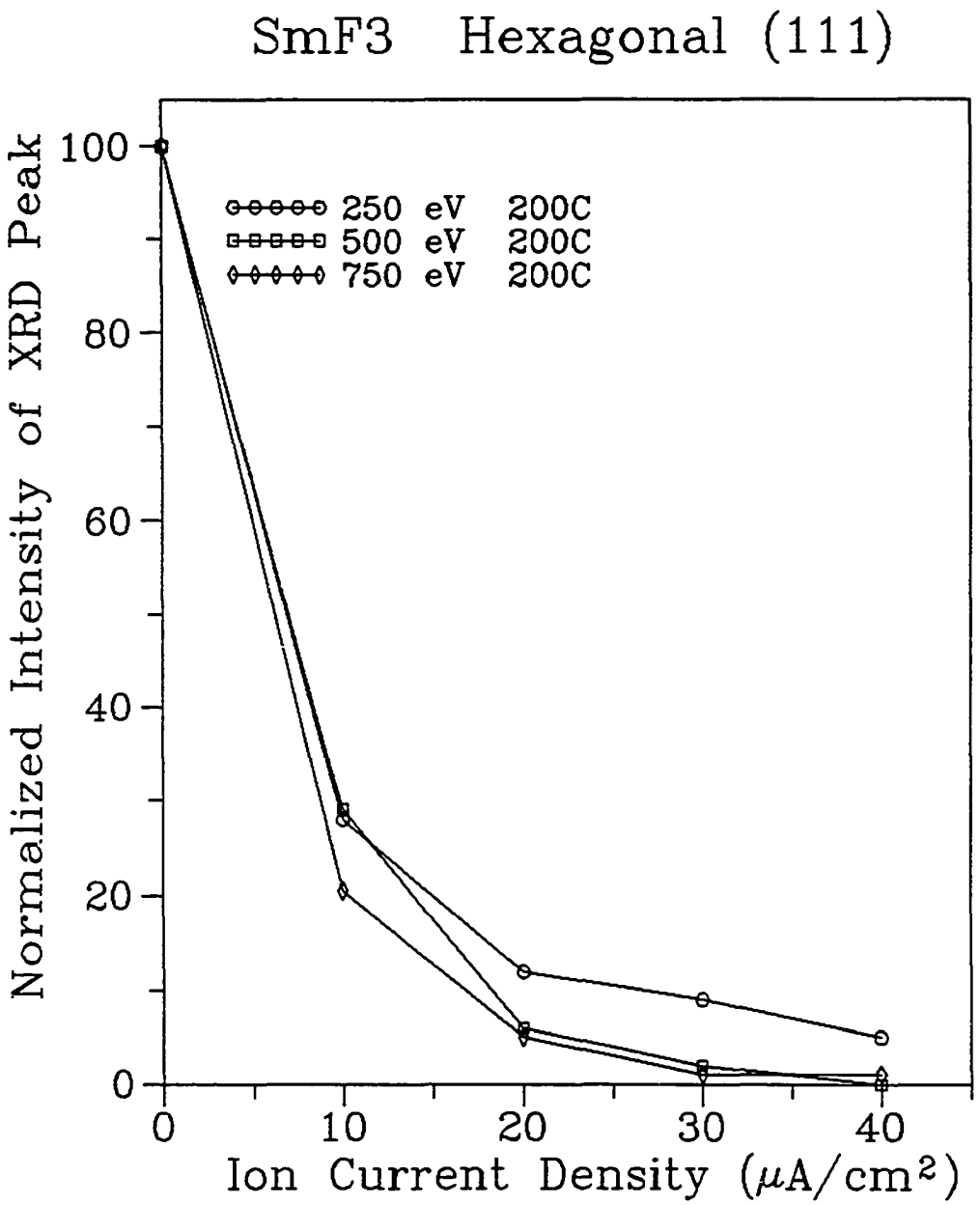


Figure 5.5. Structure of Samarium Trifluoride Thin Films.

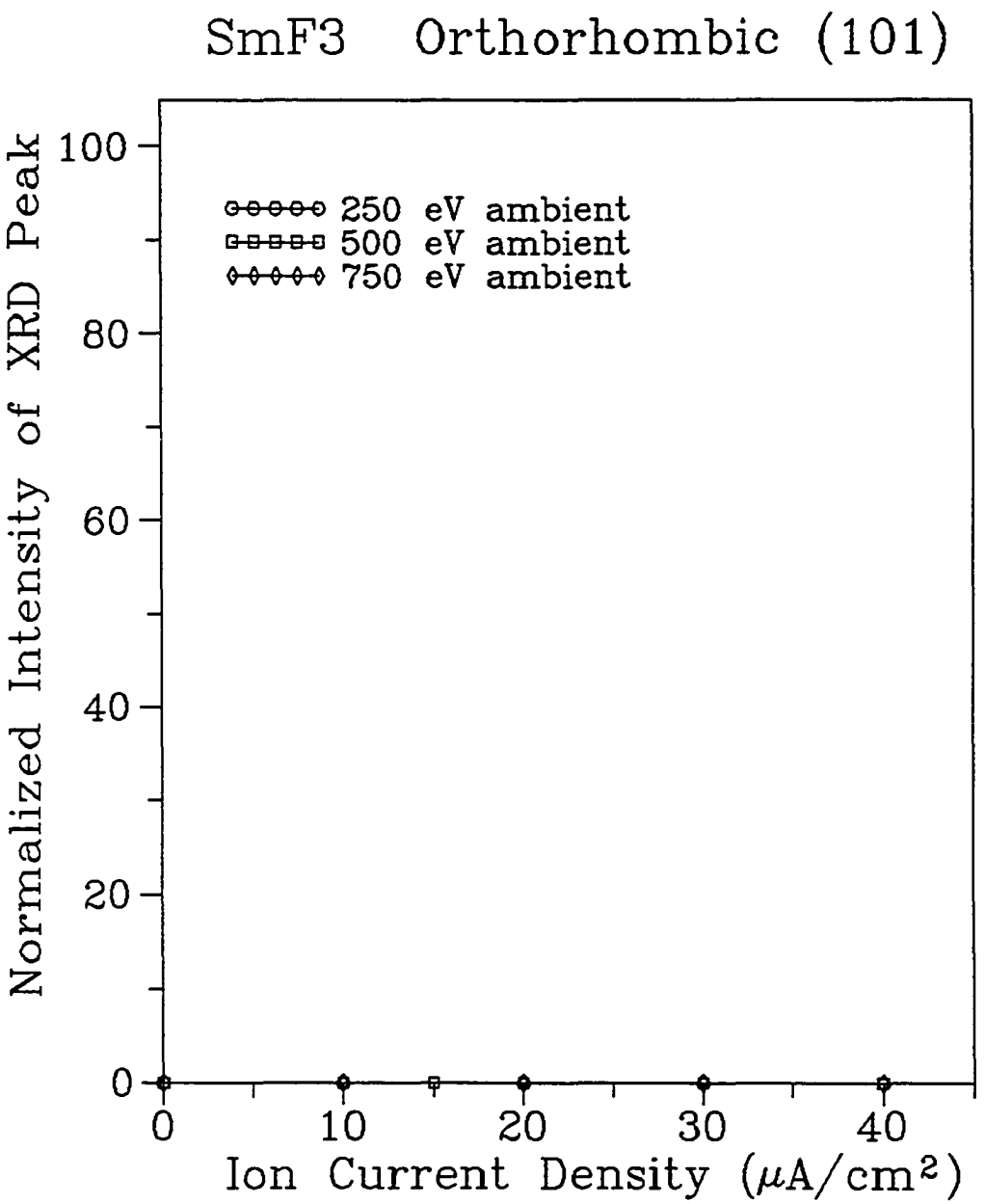


Figure 5.6. Structure of Samarium Trifluoride Thin Films.

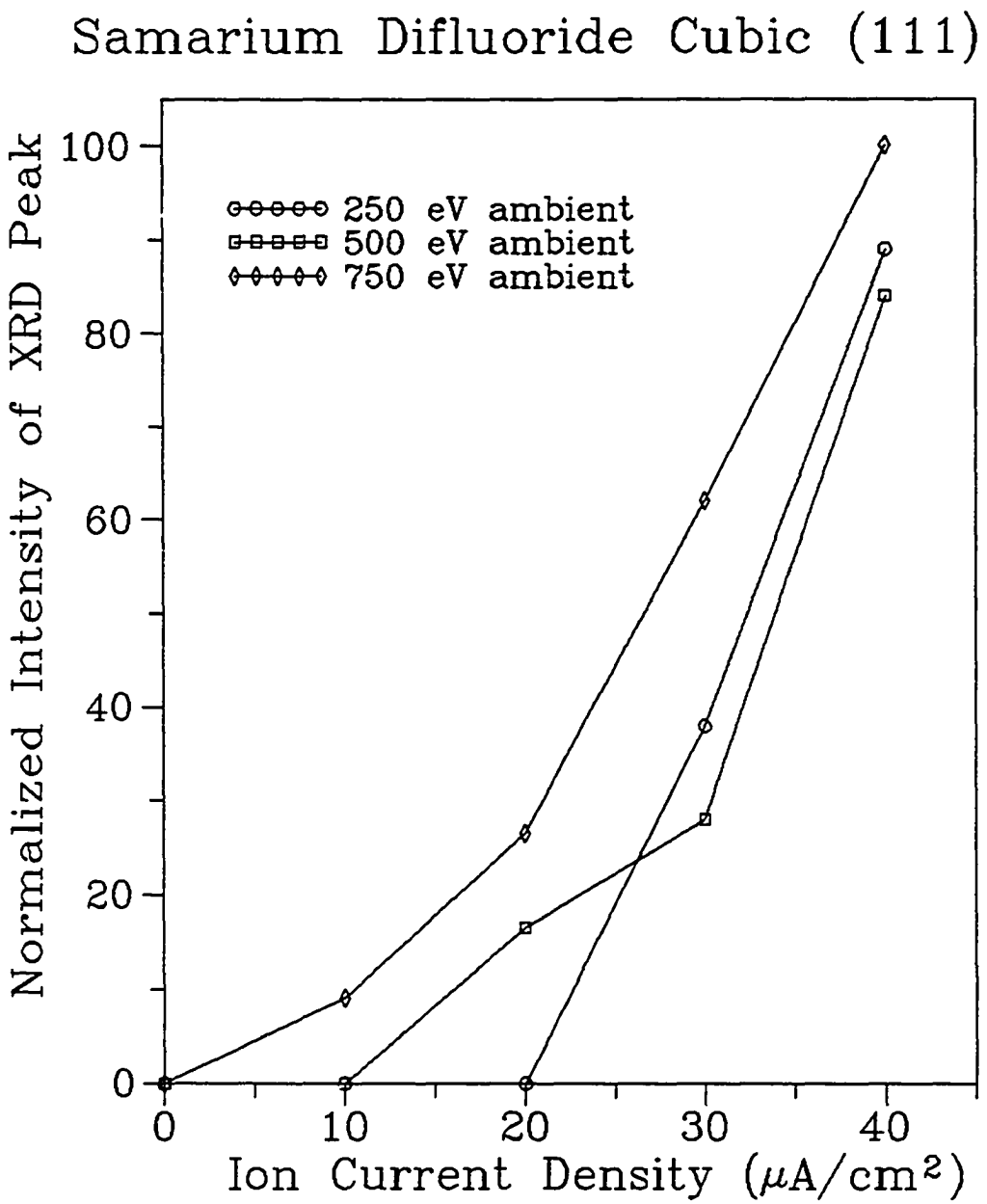


Figure 5.7. Structure of Samarium Trifluoride Thin Films.

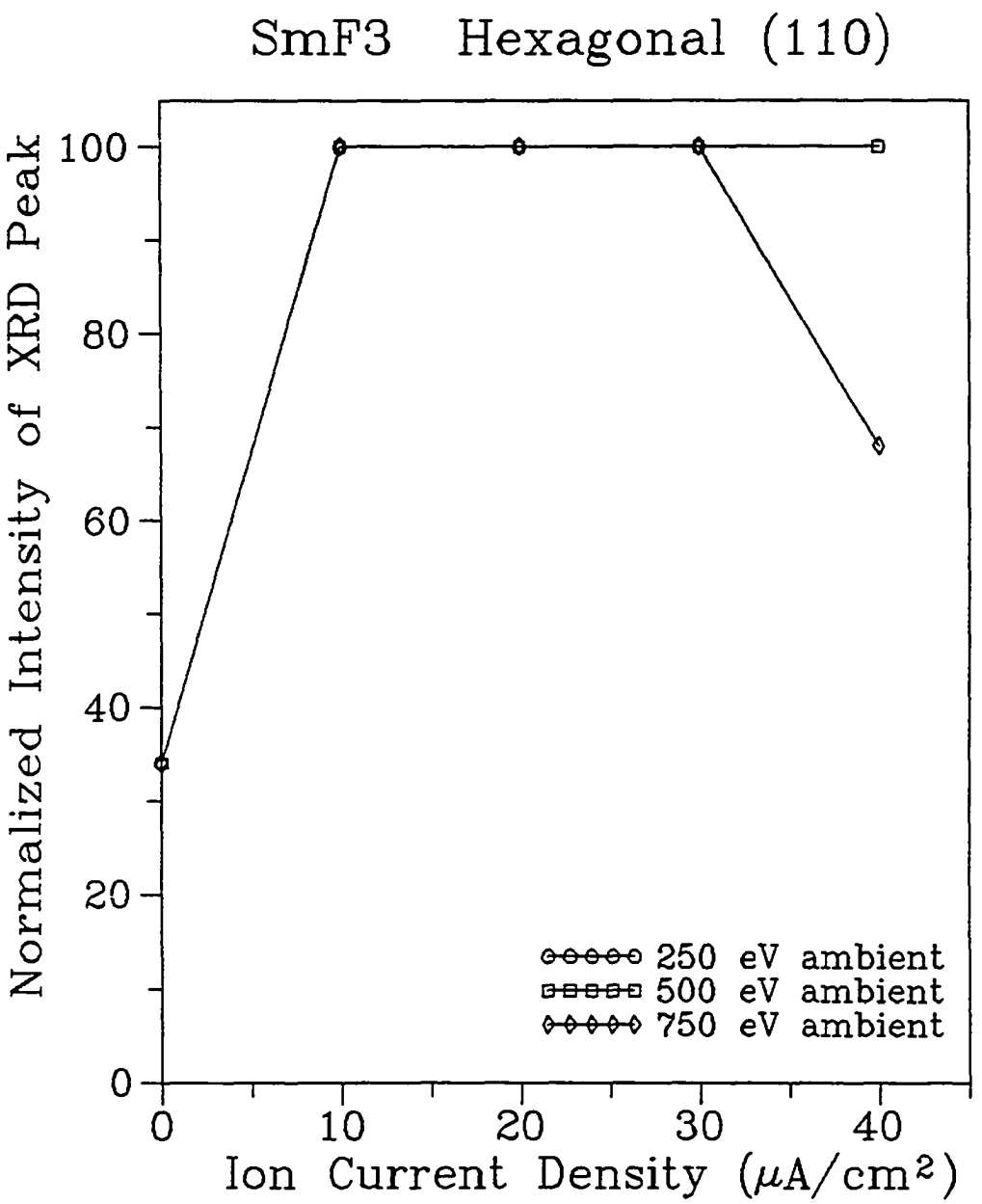


Figure 5.8. Structure of Samarium Trifluoride Thin Films.

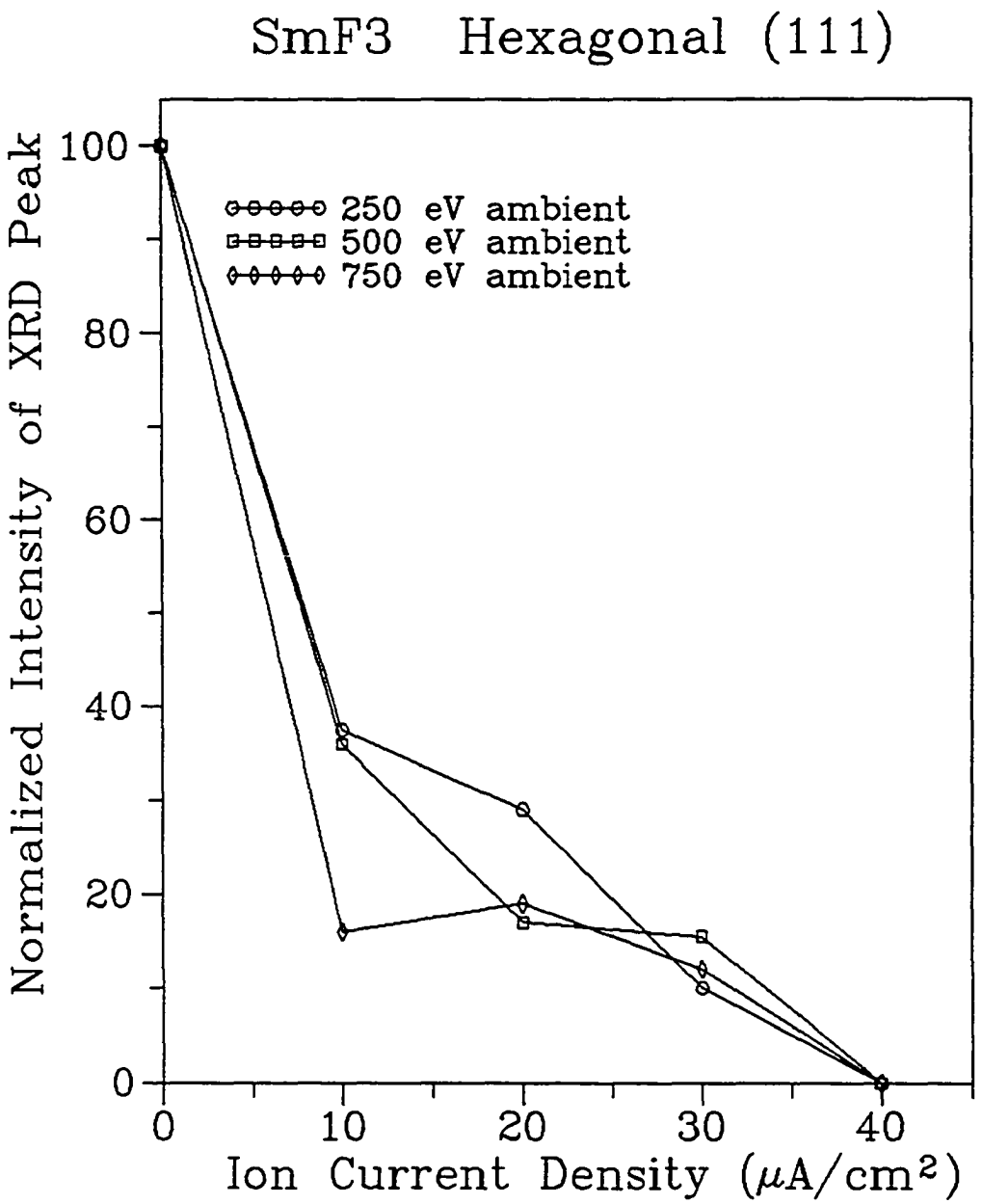


Figure 5.9. Structure of Samarium Trifluoride Thin Films.

Table 5.7. Summary of In-Plane Packing Density Results from a study on the effect of ion-assisted deposition on the structure and two dimensional packing density of samarium trifluoride thin films.

| Plane Dominating Film Structure | In-Plane Density ($x10^{14}$ molecules/$cm^2$) | Deposition Conditions temperature&ion-assist |
|---|---|---|
| hexagonal (111) | 1.05 | ambient & no ion-assist |
| hexagonal (110) | 1.17 | ambient & ion-assist |
| orthorhombic (101) | 1.78 | 200°C & no ion-assist |
| hexagonal (110) | 1.17 | 200°C & ion-assist |

Table 5.8. Summary of Thickness Versus Areal Density Results for non-IAD samarium fluoride films. Table gives normalized intensity of XRD peak detected at lattice spacing corresponding to areal density in first column.

| Areal Density | Thickness (Å) | | | | | | |
|---|---|---|---|---|---|---|---|
| ($x10^{14}$molecules/$cm^2$) | 7500 | 5000 | 2500 | 1500 | 1000 | 500 | 300 |
| 2.39 | 7 | 12 | 25 | 65 | 100 | 100 | 100 |
| 2.08 | 36 | 44 | 40 | 33 | 45 | 43 | 0 |
| 1.17 | 25 | 32 | 48 | 47 | 45 | 57 | 0 |
| 1.05 | 100 | 100 | 100 | 100 | 75 | 86 | 88 |

Spectrophotometry

Thin films of trifluoride which is normally clear in the visible take on a very pale orange or pink tint when very small amounts of the difluoride are present. This can be seen only with the spectrophotometer at the lowest concentrations, at higher concentrations it can be seen by eye and x-ray diffraction analysis. The

phenomenon makes it possible to determine a practical threshold for preferential fluorine sputtering and separate it from the usual evidence of oxygen inclusion which is accepted to be identical with fluorine sputtering in materials which are not multivalent. Refer to the chapter on optical properties to show correlation between optical and x-ray results and the effect of parameters on optical properties.

Surface Composition and Chemical Bonding

ESCA gives information on the bonding state of the compound under analysis. By necessity it gives some idea of which atoms are in the compound and in what ratios but being a surface technique it cannot be used to corroborate the more reliable thin film stoichiometry data obtained by RBS. Figures 5.10 and 5.11 show a comparison of two ambient temperature samarium trifluoride films. The films were deposited onto silicon to avoid charging during the measurement. One film was not bombarded, the other was heavily bombarded with argon during growth. The films were stored in a desiccator for about one month between deposition and ESCA analysis and were measured at a pressure of about $10^{-9}$ torr. Figures 5.10 and 5.11 show number of counts versus binding energy of the electron and the peak around 540 eV represents the 1s electron for oxygen. The conventional film has very little oxygen (552 eV) and the IAD film has quite a lot in comparison (534 eV). This indicates that IAD increases oxygen content and it is a very interesting complementary result to that of the presence of $OH^-$ in IAD films. In the next chapter we will see that the amount of water in the films goes down with IAD as measured in air by infrared transmission analysis. If the IAD films are more densely packed than the conventional films, as indicated by the IR results, but they contain more oxygen, then the oxygen in the films must not be from water but

bound or interstitial molecular oxygen. This corroborates the findings of Targove, Lingg, Lehan and Macleod (1988) in lanthanum fluoride f lms. The resolution of this ESCA data was not good enough to tell whether or not the oxygen was bound to the fluorine and samarium.

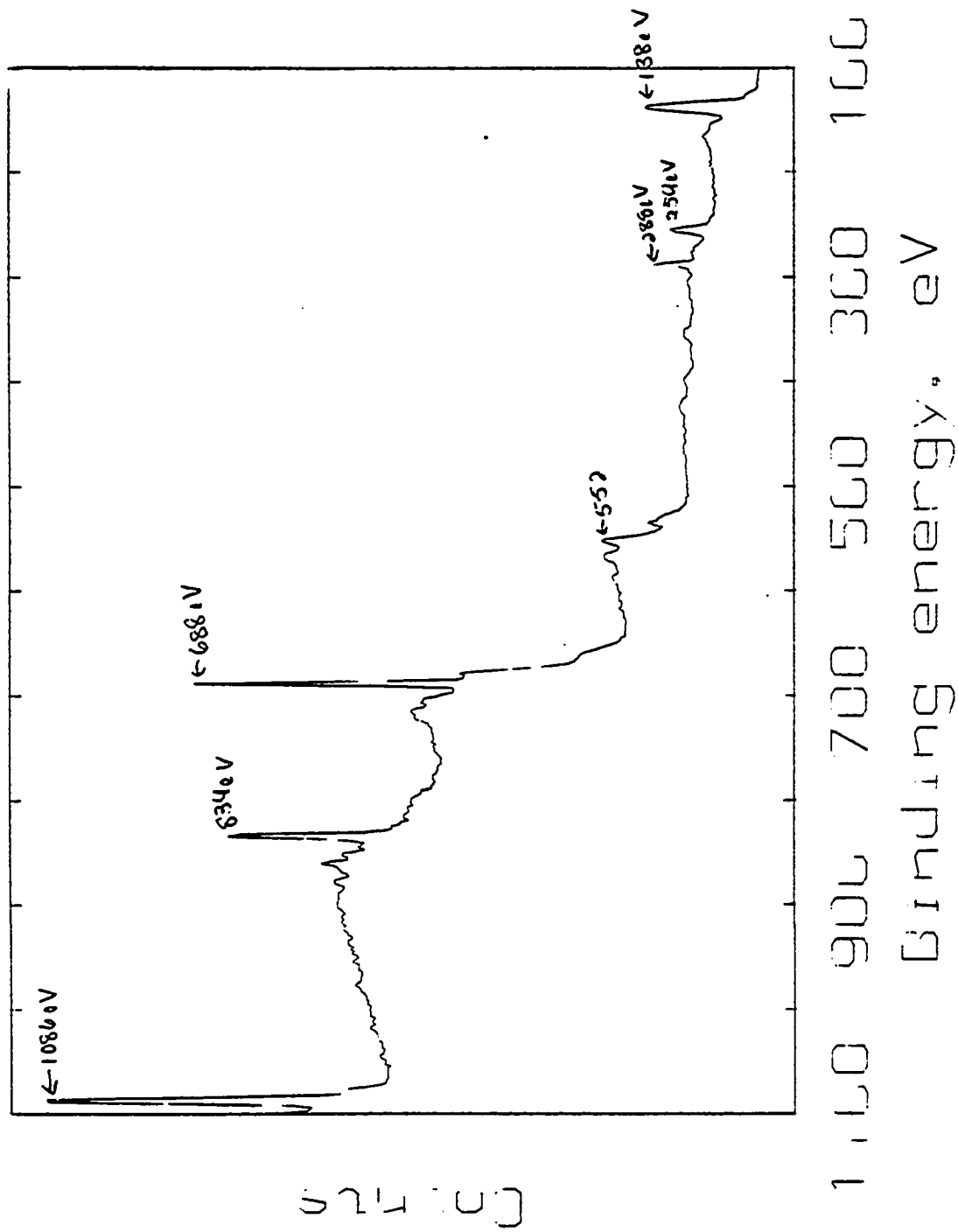


Figure 5.10 Binding Energy Survey of non-IAD $SmF_3$ Thin Film.

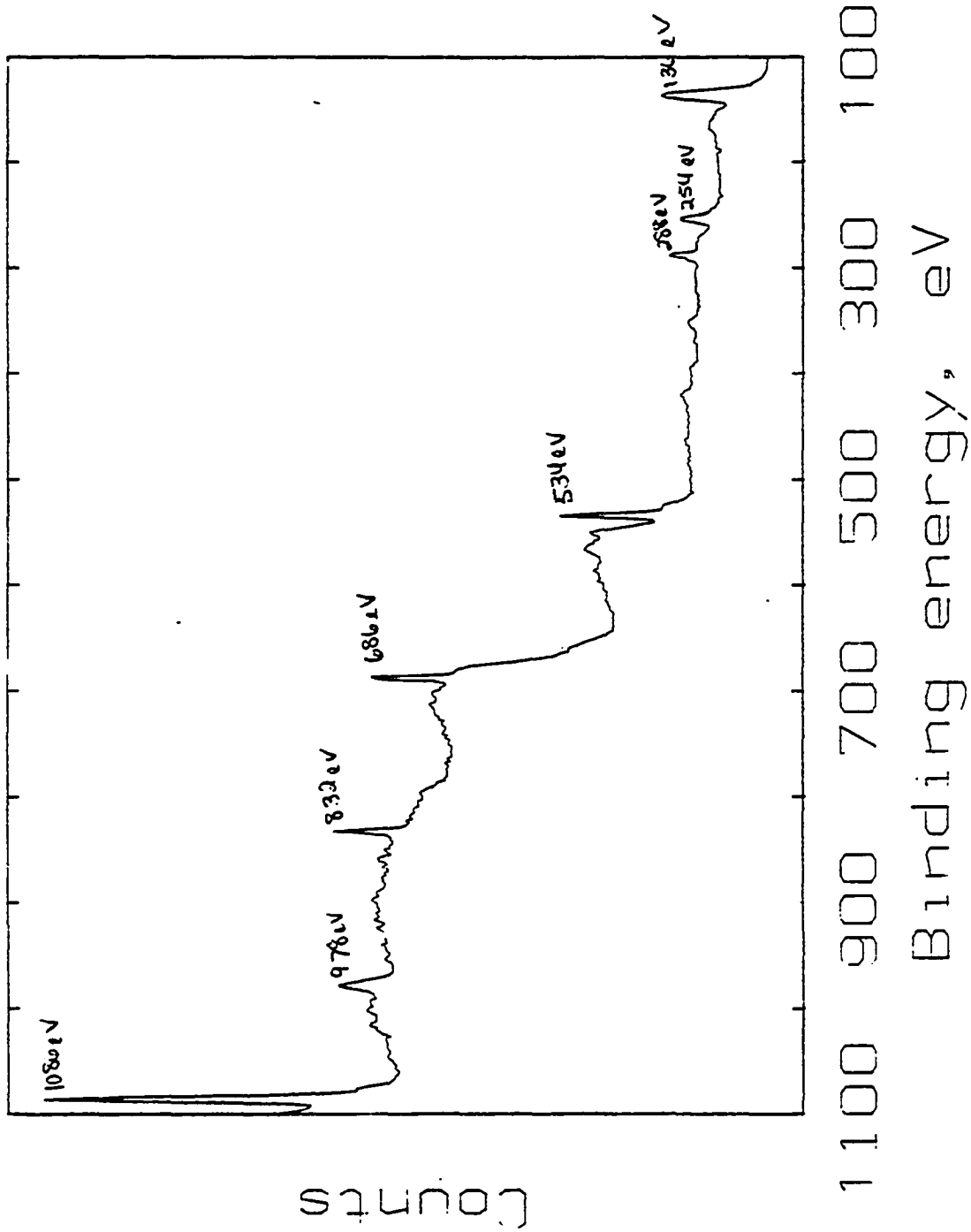


Figure 5.11 Binding Energy Survey of IAD $SmF_3$ Thin Film.

Annealing and Aging

We annealed several $SmF_3$ films in an 50%argon/50%air environment at 500°C for 24 hours. The RBS analysis of the films deposited on carbon showed that oxygen entered the films and fluorine left the films during this process (Table 5.9). XRD analysis of films deposited on fused silica showed that the diffraction pattern matched that of the SmOF. The optical results are shown in Figures 6.28 and 6.29. We attribute this to moisture in the air forming HF. The forming of a new compound was probably not due strictly to the reaction but also to the diffusion afforded by the high annealing temperature.

To examine the effects of aging in the atmosphere, we monitored the composition of the film in Table 5.10 just after deposition and after approximately one year. The RBS showed that, on a smaller scale, fluorine was lost and oxygen gained. We also attribute this to moisture in the air forming HF.

Table 5.9. Effect of Annealing on Composition of samarium trifluoride thin films.

| DEPOSITION AND ANNEALING CONDITIONS | ELEMENTAL COMPOSITION #F/#Sm | %O | %Ar |
|---|---|---|---|
| RBS measured on 5/10/88 | | | |
| 687A 200°C 750 eV 30 $\mu A/cm^2$ | 2.83±.03 | 4.3±0.2 | 1.33±.04 |
| 688A 200°C 750 eV 10 $\mu A/cm^2$ | 2.95±.03 | 2.0±0.2 | 0.62±.03 |
| RBS measured on 5/25/88 anneal in Ar/air 500°C 24hrs. | | | |
| 687A after anneal | 2.31±.03 | 12.4±0.3 | 1.34±.04 |
| 688A after anneal | 2.72±.03 | 6.0±0.2 | 0.62±.03 |

Table 5.10. Effect of Aging on Erbium Trifluoride Film Composition.

| DEPOSITION & AGING CONDITIONS | ELEMENTAL COMPOSITION #F/#Er | %O | %C |
|---|---|---|---|
| RBS 8/20/86 | | | |
| ambient no IAD | 3.08±.03 | 4.7±0.3 | 7.6±1.8 |
| RBS 9/22/87 | | | |
| storage in air | 2.86±.03 | 6.8±0.3 | 7.8±1.0 |

Discussion

Recall both from our work in chapter four and our structural results in this chapter, that high temperature deposition results in films with a higher degree of order than ambient temperature deposition. As we have seen in chapter five, IAD also results in more highly ordered films than non-IAD ambient temperature films. In comparing the two processes, the most important fact is that with increased temperature we were able to switch phases in $SmF_3$ and we were not able to achieve that result with IAD. Therefore, although they both increase the order of the films, high temperature is much more effective.

As we stated in the introduction, the fact that we see different crystal structure results for temperature and IAD is not by itself a proof that IAD involves no thermal spike. We conclude that the quenching time of the material affected by the spike is less than the quenching time for the material landing on the 200°C substrate.

Focusing just on IAD, we were able to compare the importance of ion current density and ion energy to the structure of the films. We found that the preferred

orientations were affected by current density and that energy had little influence. Our energy range for the experiment, not just the results shown in the figures, was 50-1250 eV. It is possible that we are on an energy plateau with respect to bombardment of solids and that the only way to get an increased response within that energy range is to use more ions (increase current density), but in a different regime energy would be the dominant variable. It is also possible that energy always remains secondary.

We proved that IAD can both reduce and increase in-plane packing density. We showed that a material which under normal deposition conditions (ambient temperature, 5000 Å thick) has preferred orientation which is loose, IAD will pack it tighter. And the same material in conditions which would usually have a preferred orientation which is more tightly packed (high temperature or very thin films) IAD will change the orientation to something looser. Up until now the packing density of IAD films has always been said to increase. One must keep in mind that our results are for the material inside the columns, a subcolumnar or submicrostructure level. Packing density results are usually gotten for the microstructure level (Macleod 1985). We hesitate to extrapolate to the microstructure level because there are many complications in doing so. We refer the reader to chapter six for results on microstructure level packing density. One wonders if packing density on the microstructure level reaches a favored value as it does on the subcolumnar level. If this is so then the increase in index, said to be a result of packing density, must have an upper limit of its own and different from that of the bulk low temperature phase. This would be difficult to test since the other reasonable measure of packing density is the $OH^-$ band in the infrared and its disappearance does not necessarily correspond to a unit bulk packing density.

We have also explored the role of oxygen in IAD films. From our composition results we saw that oxygen is included in IAD films but as no discernable function of either current density or energy. It is a powerful enough effect though that it does not decrease with increasing temperature like the argon inclusion does. We have seen no large scale evidence of bonding to form either the fluoride or the oxyfluoride using the x-ray diffraction and the XPS techniques but from the results of Sobolev and others we know that a very small amount of oxyfluoride is very difficult to detect. Considering these facts we are unable to demonstrate that the increase in refractive index is due to packing density when it could be just as readily due to oxygen inclusion.

We have also succeeded in showing very clearly the course of preferential fluorine sputtering in a multivalent fluoride. The decrease in fluorine brought on by the IAD caused the formation of alternative ordered structures which employed no oxygen. We were not able to distinguish between $SmF_2$ crystallites and superstructures of stoichiometry between the tri and difluorides because the x-ray peaks coincided. They were, however, clearly distinct from any oxyfluoride structures.

Whereas the optical properties are often the most sensitive indicator of a change in a thin film's structure, composition, or chemistry, the interpretation or explanation of the phenomenon is very difficult without some additional type of characterization. All of the experiments in this chapter were naturally done in conjunction with optical characterization and full conclusions cannot be drawn without first looking at it. Therefore, we will pick up the ideas from this discussion again in the discussion of chapter six where they support and are supported by our optical data.

# CHAPTER 6

## OPTICAL PROPERTIES AND GENERAL CHARACTERIZATION OF LANTHANIDE TRIFLUORIDE THIN FILMS

We have predicted the optical properties of lanthanide trifluoride thin films based on their bulk physical properties and we have said that they would vary systematically with atomic number. We have seen that the crystal structure and composition of these thin films vary with depositition temperature, and with ion-beam energy and current density. In this chapter we present the results of a systematic study of lanthanide trifluoride thin film optical properties following the dependence on atomic number and on deposition conditions. The optical properties considered here are the transmittance and reflectance from 1216 $\mathring{A}$ to 500 $cm^{-1}$ and real refractive index in the UV and visible. We find that some of the optical properties are directly related to the change in atomic number, some are directly related to coincident changes in structure and composition induced by different deposition conditions, and some are dependent on deposition conditions which have negligable effect on the physical properties we measured. Results on optical properties of the $LnF_3$ are organized by wavelength region and the data within a wavelength region is arranged in order of increasing atomic number. This is a convenient way to compare the series of materials because different absorption mechanisms are active in different spectral regions and also because the optical

applications are frequently limited to one spectral region at a time.

VUV Transmittance

The vacuum ultraviolet includes the electromagnetic spectrum from 500-2000 Å. We obtained measurements of transmittance from 1216-2000 Å using the instrument described in chapter three. As predicted in chapter two, we found that thin films of $LnF_3$ do exhibit transparency in the VUV and also that the absorption edge is higher in energy for the compounds having the smaller ionic radius cation. Figures 6.1 through 6.11 show transmittances of 1000 Å to 1200 Å thick films of the $LnF_3$ on $MgF_2$ substrates. From the figures we can see several important things, namely, the details of the transparency for each of the materials, how the materials may be grouped according to valency, and the effects of temperature and IAD on the films.

One can see by looking at the figures that the absorption edge is not as abrupt as for single crystals and instead has a more rounded sloping curve characteristic of polycrystalline and noncrystalline thin films.

Our first concern was vacuum ultraviolet transparency. $LuF_3$ is the best VUV transmitter and $GdF_3$ the second best. $LuF_3$ was expected to be the best because it has the smallest ionic radius, but based solely on a band gap argument, $GdF_3$ should have VUV transmittance average for this series. The reason it did not is that the $LnF_3$ with partially filled f-shells have atomic electron transitions which overlap the band gap. $LnF_3$ [Ln=Gd,Lu] have half-filled and completely filled f-shells respectively and so have the cleanest spectra of the series along with $LaF_3$ which has a completely empty f-shell. Keeping this in mind, a valid comparison of VUV transmittances can only be drawn between $LnF_3$ [Ln=La,Gd,Lu] since they are

electronically similar. These three materials follow exactly the band gap argument of VUV transparency made in chapter two. $LuF_3$ (Figure 6.11) transmits the farthest followed by $GdF_3$ (Figure 6.4). Although $LaF_3$ was not officially part of our study, we have made and measured $LaF_3$ films. The results are not shown here but $LaF_3$ cuts-off completely by 1500 Å.

$LnF_3$ [Ln=Dy,Ho,Er] (Figures 6.6,7,8) have nearly full f-shells and are strictly trivalent. They do not have obvious absorption bands near the UV edge, however, they are not as transparent as the previous group.

In the remaining cases the absorption edge is seriously obscured by superimposed atomic electron transitions. The tetra- and trivalent $LnF_3$ [Ln=Pr,Tb] (Figures 6.1,5) have large absorption bands in the VUV centered right on top of the absorption edge. The tri- and divalent $LnF_3$ [Ln=Sm,Eu,Tm,Yb] (Figures 6.2,3,9,10) have small absorption bands right near Lyman alpha. The usefulness of these materials is diminished by these bands unless one can take advantage of the absorption bands for an edge filter.

Recall the results of chapter four on the effects of temperature on $LnF_3$ thin films. Those results can be correlated with the high temperature transmittance traces in this section. All of the higher temperature films show an increase in transmittance at shorter wavelengths and a decrease in transmittance at longer wavelengths (Figures 6.2-6.11). The reason for this behavior is twofold. At shorter wavelengths, the interference fringes are not as dominant in determining the transmittance as the absorption properties of the material and its impurities and contaminants. We saw in chapter four that the higher temperature films contained less oxygen than the lower temperature films. As we shall see in the UV and visible section of this chapter and as numerous studies o $MgF_2$ (Messerly 1986) and

$LaF_3$ (Targove 1986) have shown, oxygen causes the short wavelength edge to red shift. Therefore, films with less oxygen are more transparent in the VUV. Recall also the structural change brought about by temperature which we discussed in chapter four. This change is also evident in the UV and visible films as inhomogeneity in the growth direction of a single layer (Figure 6.23). What we see in the lower energy region of the VUV is a continuation of this effect.

The effects of IAD are shown in Figure 6.11. It preserves transparency if low energy and current density are used and it causes absorption if high current density and energy are used. Considering our results from chapter five, that oxygen is included when IAD is used, and our discussion in chapter two, saying that oxygen is not as electronegative as fluorine and would make the potential wells of $LnF_3$ more shallow and therefore narrow the band gap, our optical results make sense. Therefore, IAD can be used to increase the index of films as in Figure 6.44 but it must be done lightly.

We have been very cautious about using numerical values of transmittance to assess the potential value of a $LnF_3$ for coating applications. This is because scattering and interference can be mistaken for physical properties of the material. These figures represent thin films of high refractive index on substrates of low refractive index and the superposition of interference fringes on the spectrum is especially evident in Figures 6.4 and 6.11. A slight change in film thickness can shift the location of the minima and maxima, as we have shown in the two lower curves of Figure 6.4, and a slightly different contrast between film and substrate indices will change the amplitude of the fringes. This can make films of different thickness look like films with different innate optical properties. Furthermore, the fact that the data is taken in discrete increments makes it difficult to draw an

envelope to describe the absorption edge. Scatter is also important in this short wavelength region, since the shorter the wavelength of light the smaller the object from which it can scatter. (Bennett 1967). We tested the effect of scatter on our results by sending two samples to Claude Amra (1987) at the Laboratoire d'Optique des Surfaces et des Couches Minces, Ecole Nationale Superieure de Physique de Marseille for total integrated scatter measurements. He measured a scattering loss at 632.8 nm on transmission for $LuF_3$ at 3.8 x $10^{-3}$ and for $GdF_3$ at 2.0 x $10^{-3}$. The scattering loss on reflection for $LuF_3$ at 0.73 x $10^{-3}$ and for $GdF_3$ at 0.35 x $10^{-3}$. Since the scattering losses were greater for $LuF_3$ than for $GdF_3$ and $LuF_3$ still transmitted more, we concluded that the optical spectra were true to the material and not dominated by surface roughness scatter. Finally, we deposited a whole series of films on LiF substrates and we include in Figure 6.7 typical data from such a sample. The transmittance is far lower than that of an identically deposited sample with a $MgF_2$ substrate. We attribute this partially to scatter since LiF is known to be soft and difficult to polish (we observed sleeks on our substrates) and partially to the hygroscopic nature of LiF.

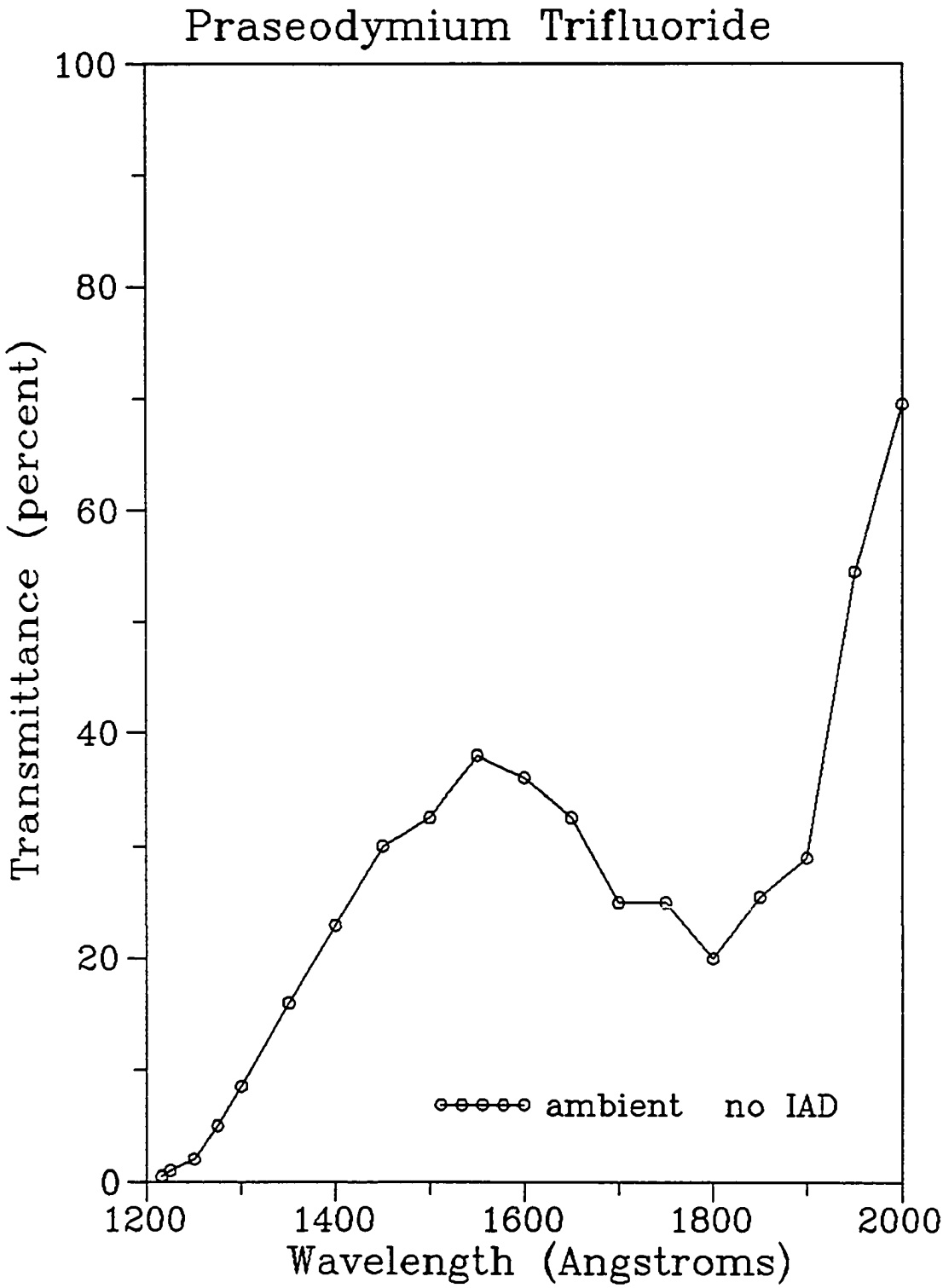


Figure 6.1. Vacuum ultraviolet transmittance of Praseodymium Trifluoride.

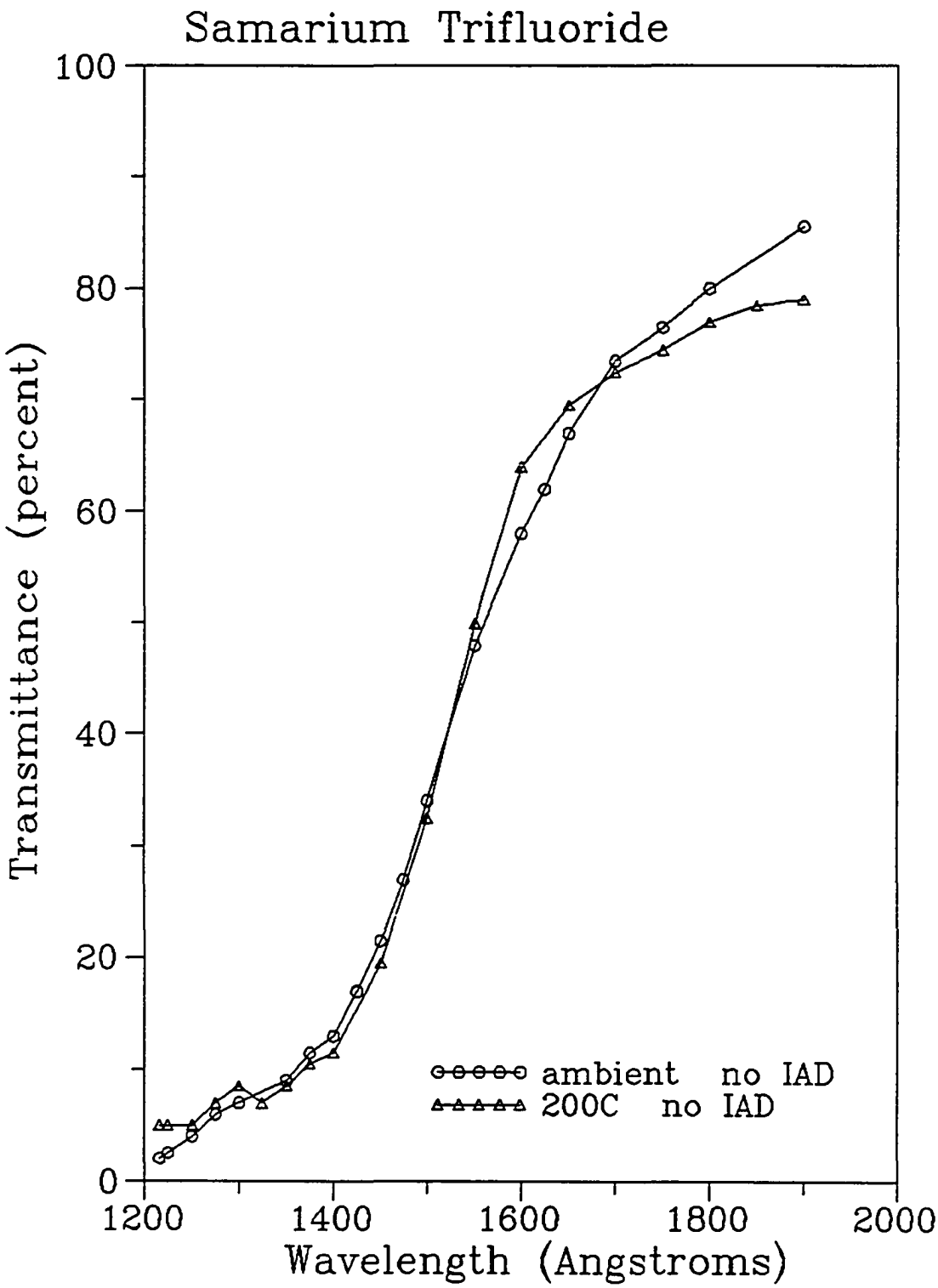


Figure 6.2. Vacuum ultraviolet transmittance of Samarium Trifluoride.

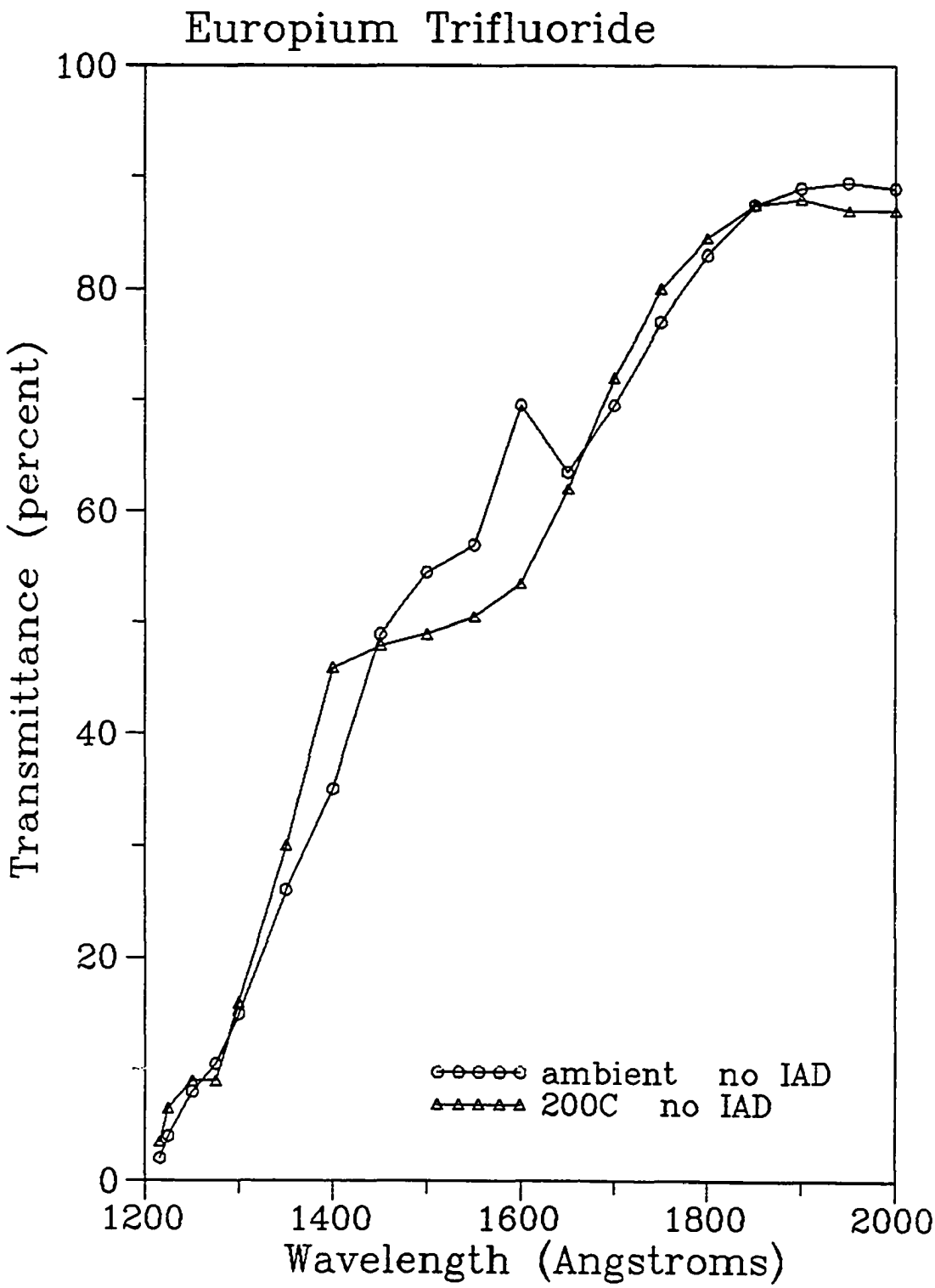


Figure 6.3. Vacuum ultraviolet transmittance of Europium Trifluoride.

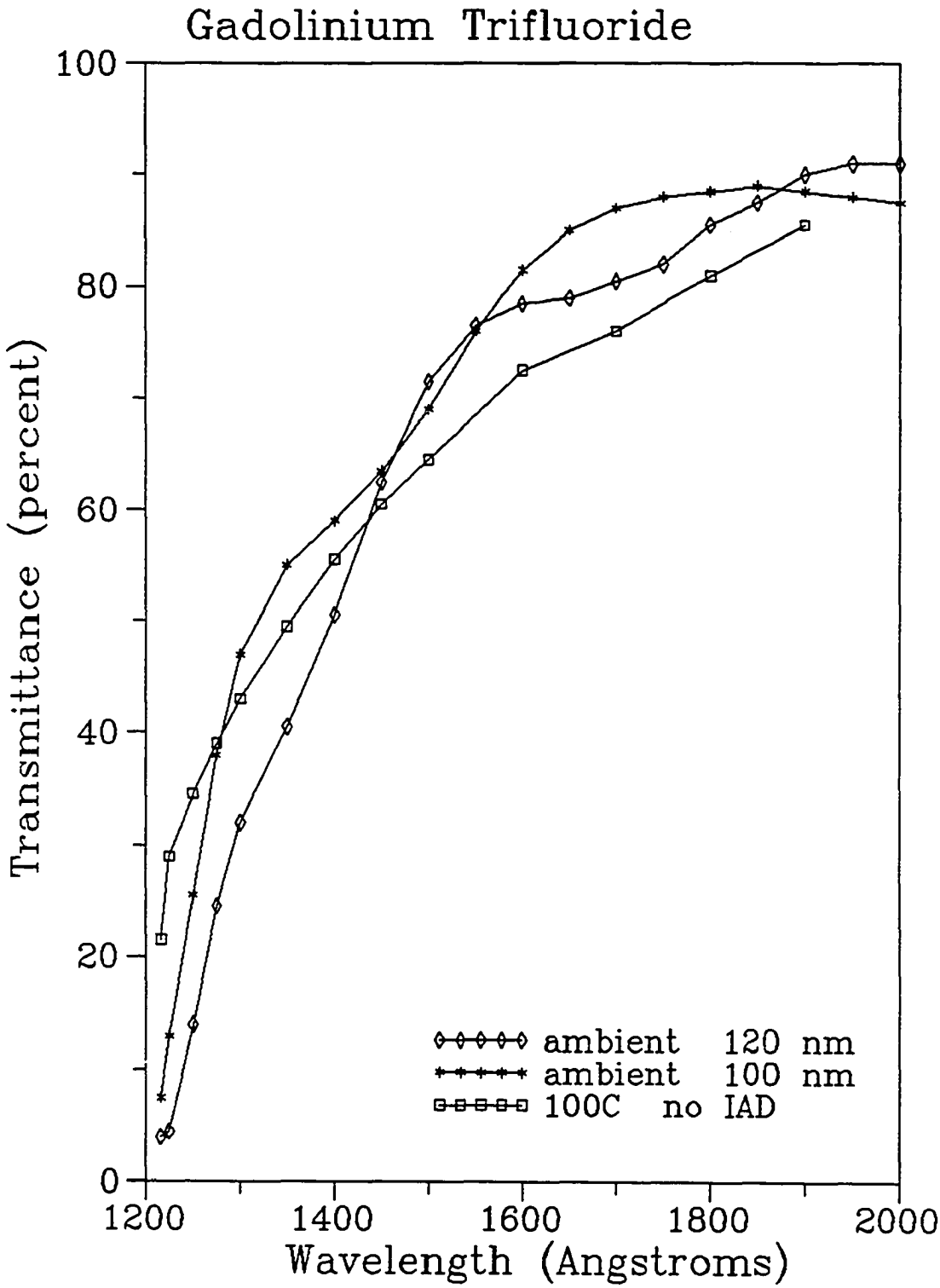


Figure 6.4. Vacuum ultraviolet transmittance of Gadolinium Trifluoride.

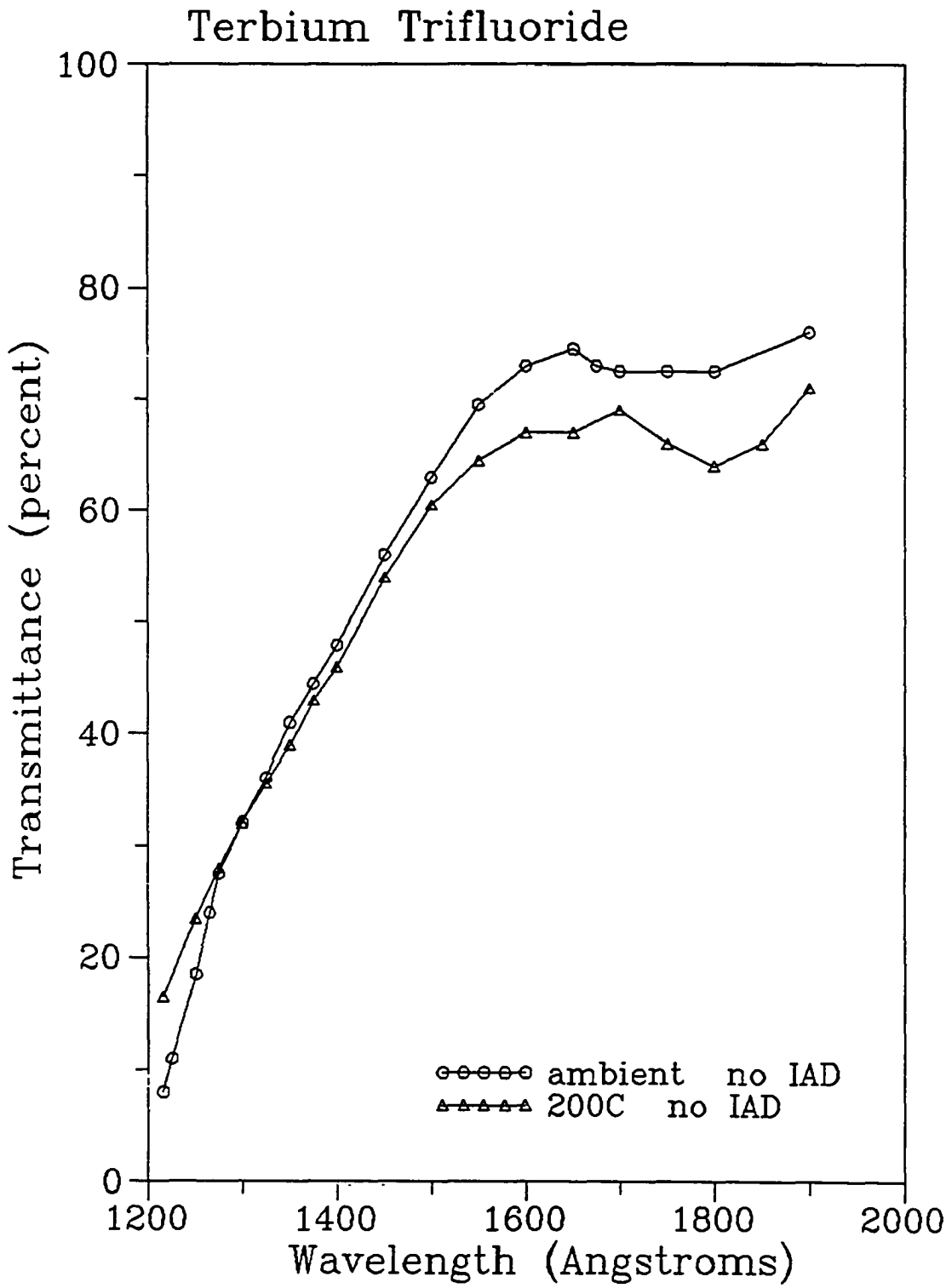


Figure 6.5. Vacuum ultraviolet transmittance of Terbium Trifluoride.

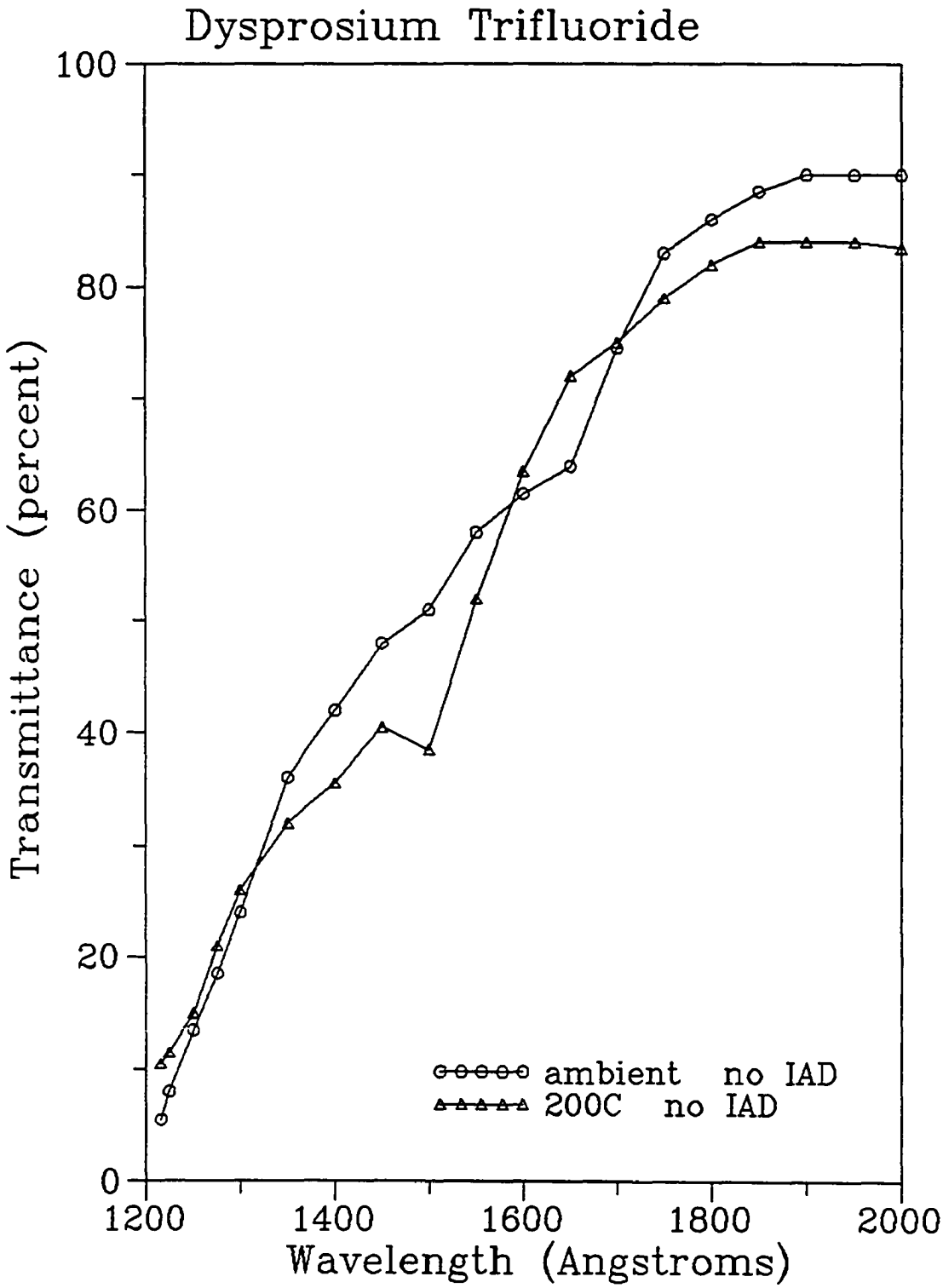


Figure 6.6. Vacuum ultraviolet transmittance of Dysprosium Trifluoride.

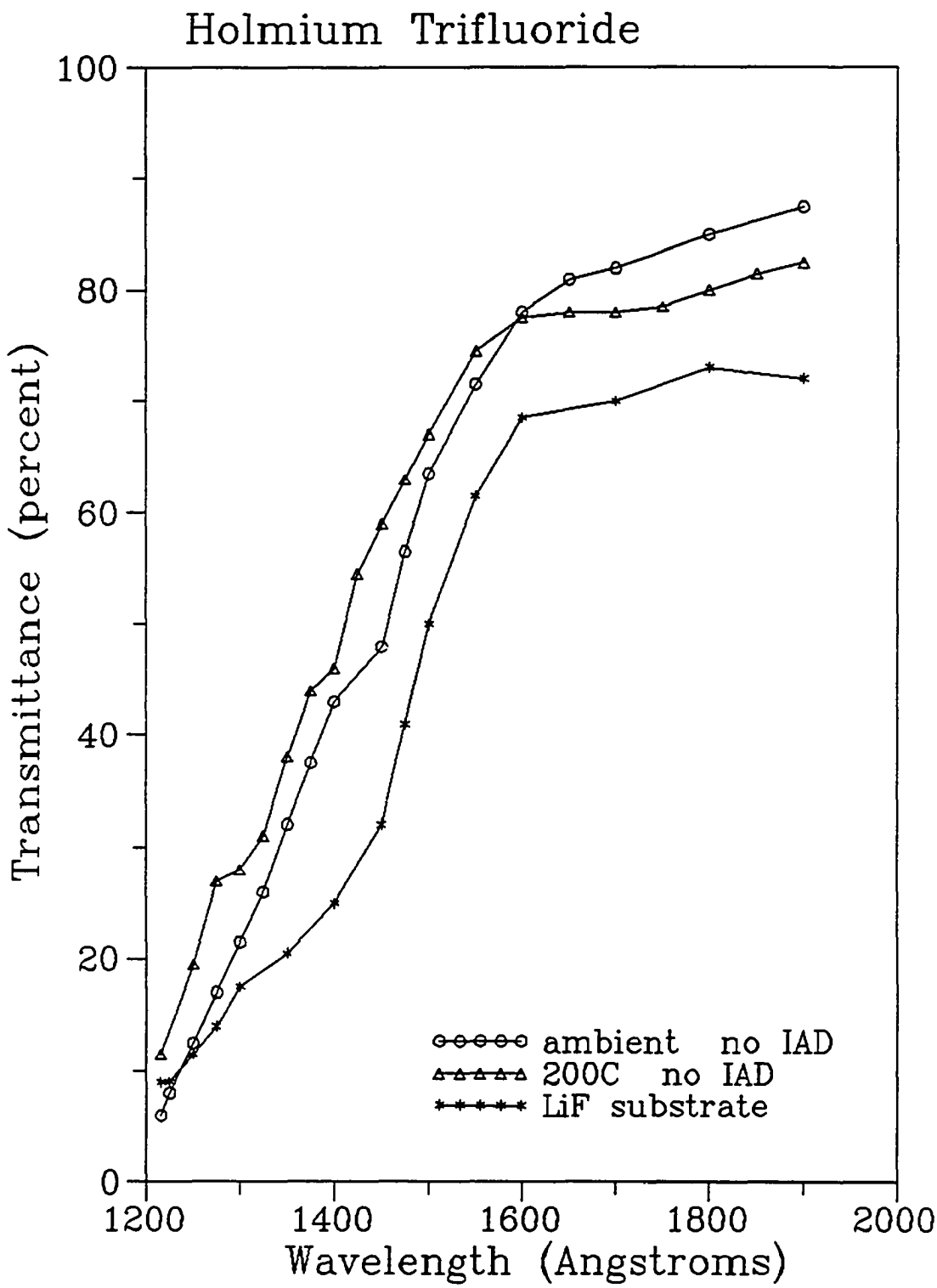


Figure 6.7. Vacuum ultraviolet transmittance of Holmium Trifluoride.

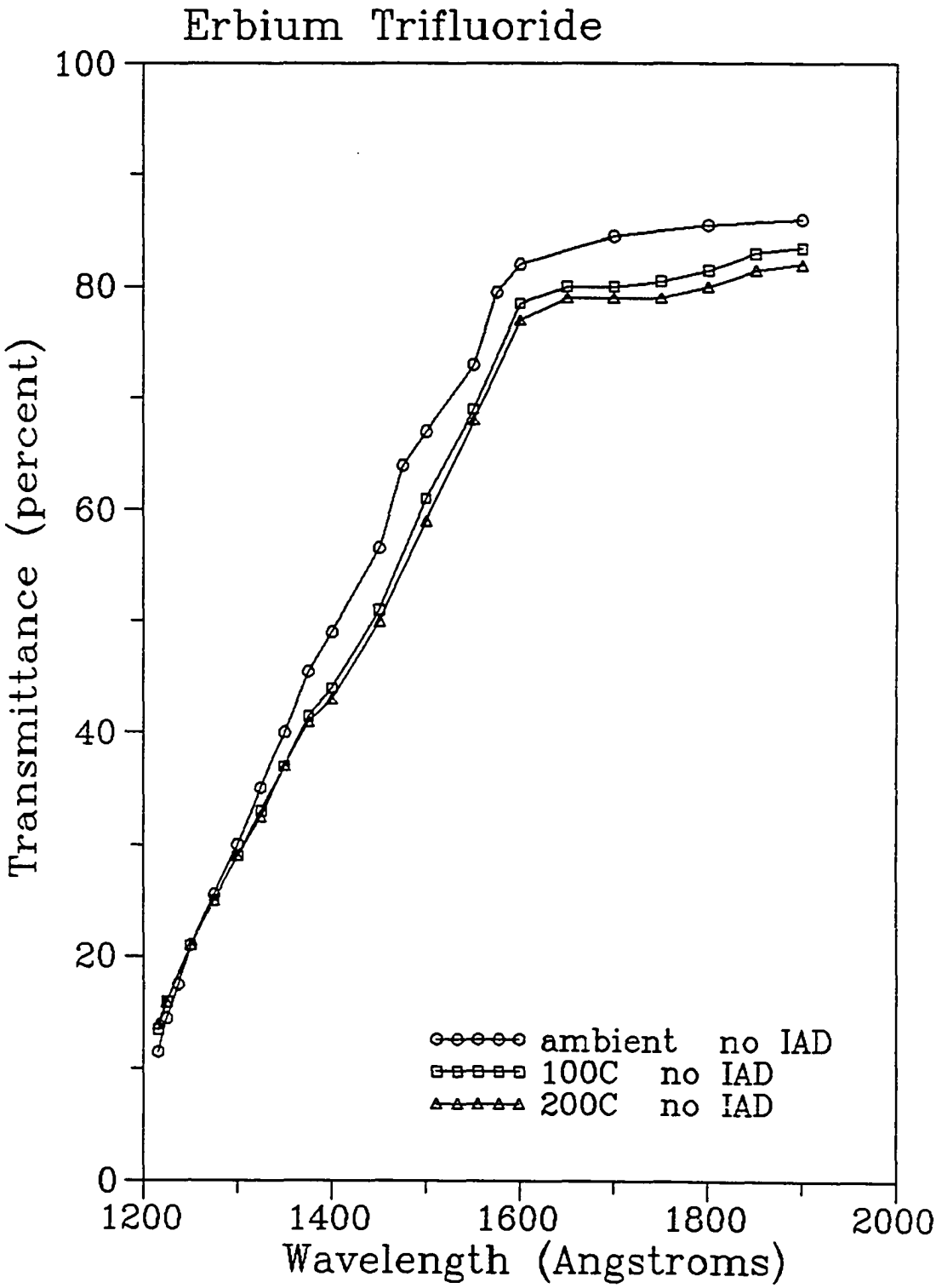


Figure 6.8. Vacuum ultraviolet transmittance of Erbium Trifluoride.

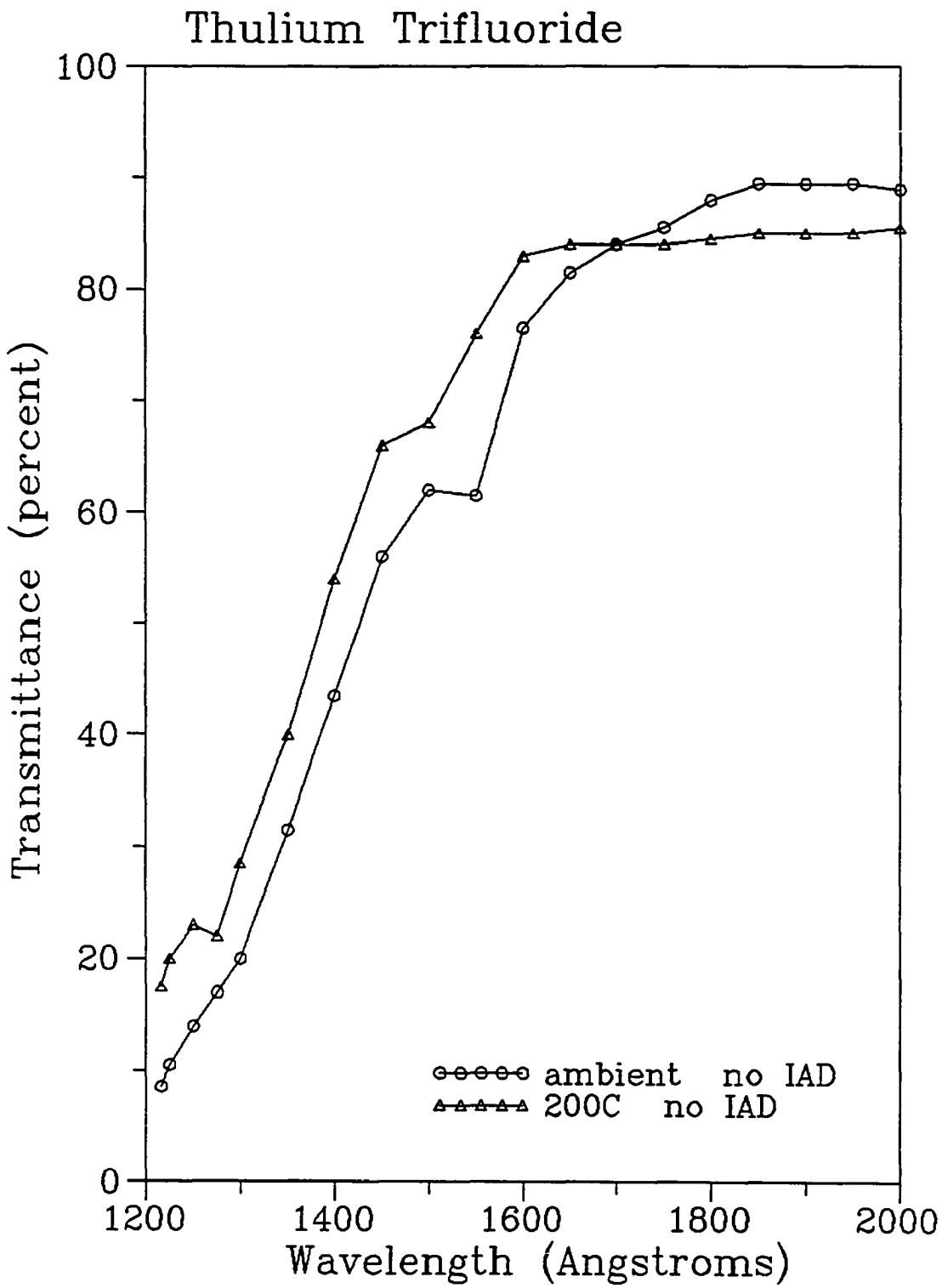


Figure 6.9. Vacuum ultraviolet transmittance of Thulium Trifluoride.

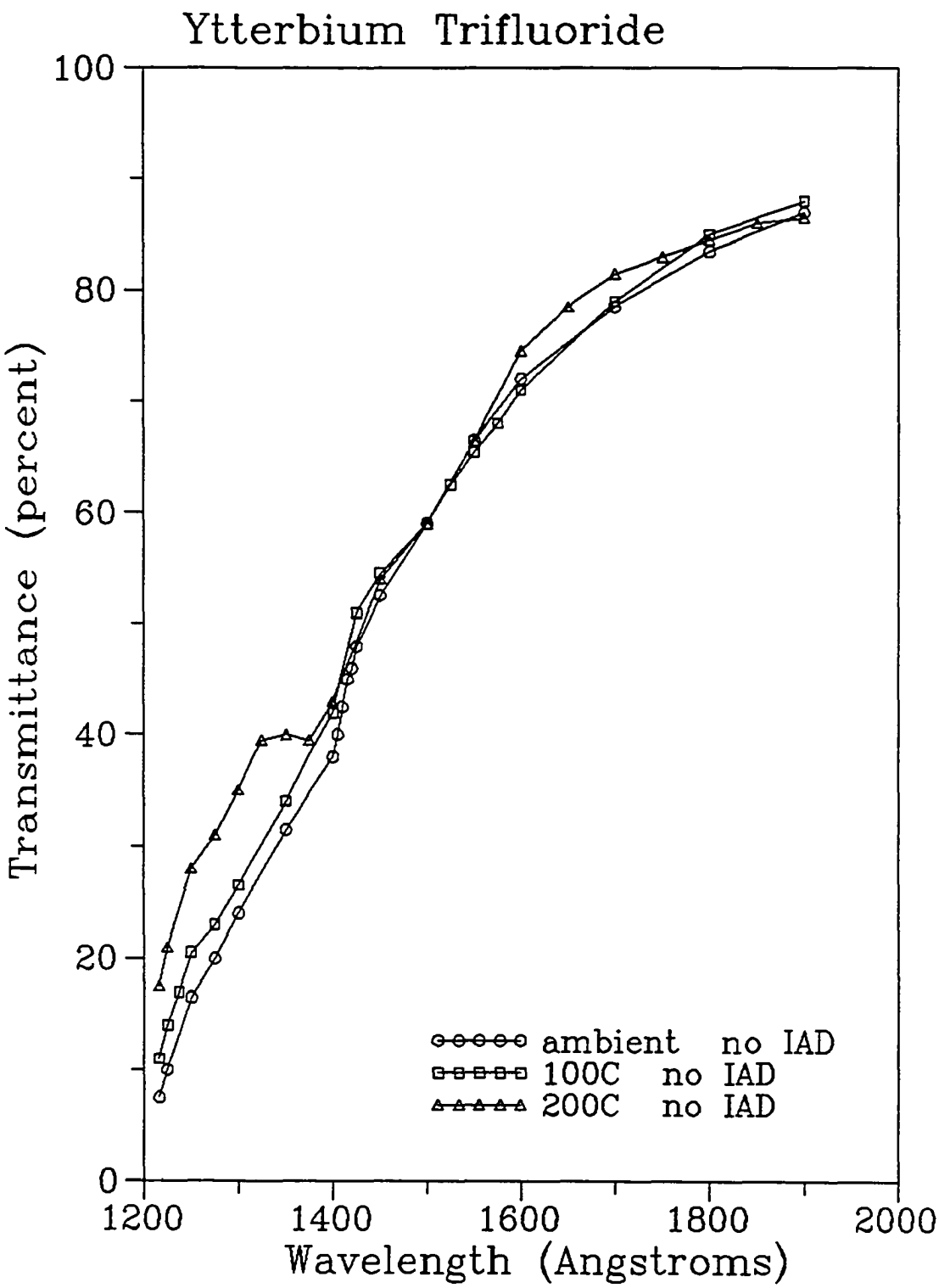


Figure 6.10. Vacuum ultraviolet transmittance of Ytterbium Trifluoride.

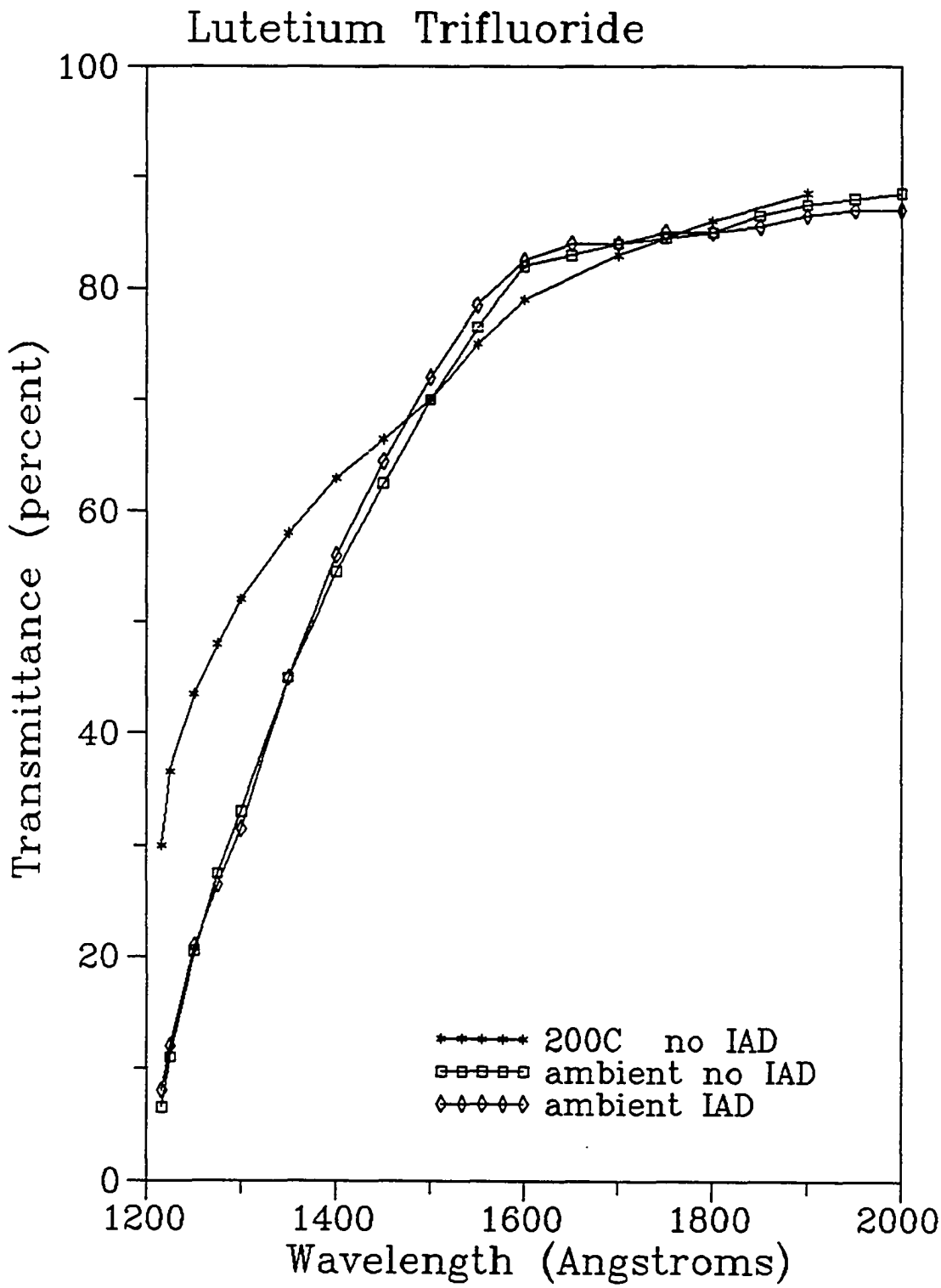


Figure 6.11. Vacuum ultraviolet transmittance of Lutetium Trifluoride.

UV and Visible Transmittance

All of the trifluorides have very high transmittances at near-UV and visible wavelengths exclusive of specific absorption bands and this agrees with the standard spectrum of a wide band gap optical material (Black and Wales) and with our expectations as discussed in chapter two. Figures 6.12 through 6.22 show the near-UV and visible transmittance of the $LnF_3$ [Ln=Pr,Sm-Lu] for films 5000 Å thick. They are scaled down drawings of the original Cary traces and, as described in chapter three, are the source of the refractive index values reported in Figures 6.41 through 6.51. Each figure has three lines for transmittance versus wavelength. The uppermost is a 100% line showing the calibration of the spectrophotometer, the middle line which is also stright represents the transmittance of an uncoated fused silica substrate, and the wavy line is the transmittance of the film plus the substrate. The dotted vertical line represents the point at which we put together two traces, the UV and visible, since they were each taken with different sources when using a Cary 14.

Again the point of including a separate trace for each material is to enable one to group the materials according to electronic structure. Then in choosing one for an application it is not necessary to remember where the absorption bands are for each material separately and wonder whether they are weak or strong or sharp or broad. Figures 6.15 and 6.22 represent nsmittance for $LnF_3$ [Ln=Gd,Lu] respectively. They show no absorption bands, as expected. Notice that the fringes are shallower for $LuF_3$, this is because it has an index extremely close to that of the substrate. Keeping the same divisions as for the VUV section works again but since the size of our figures is very much smaller than the original size, a series of absorption peaks which are about 1% of the transmittance do not always show up

well. Figures 6.17, 6.18, and 6.19 are the spectra of $LnF_3$ [Ln=Dy,Ho,Er]. These small absorption bands were exaggerated by the artist to make them visible in $HoF_3$ (2500, 2800, 3500, 4500 and 5300 Å) and $ErF_3$ (3800 and 5200 Å) but they did not occur at all in $DyF_3$. Transmittance spectra for $LnF_3$ [Ln=Sm,Eu,Tm,Yb] are in Figures 6.13, 6.14, 6.20, 6.21. The $EuF_3$ trace is the best example shown here of a fluorine deficient divalent $LnF_3$. It has a wide absorption band around 2500 Å. All four of these films were deposited under the same conditions, ambient temperature and no-IAD. The $EuF_3$ is fluorine deficient either because the starting material was or because it has more of a tendency to dissociate in the melt or vapor. We have seen a similar absorption band located at approximately the same wavelength in the other three $LnF_3$ [Ln=Sm,Tm,Yb] when deposited with IAD. Only the $SmF_3$ IAD curves are shown here in Figures 6.25 and 6.26 and one can see the band centered around 3000 Å. $SmF_3$ also showed the small peaks like the ones in $ErF_3$ and $HoF_3$ in the non-IAD trace but they disappeared in the IAD traces. Figures 6.12 and 6.16 correspond to the $LnF_3$ [Ln=Pr,Tb], the tetra- and trivalent materials in our study. $LnF_3$ instead of $LnF_4$, although they are stable compounds, show a fluorine deficiency in the spectrum at approximately 2000 Å.

Two examples of films made at 200°C deposition temperature are shown in Figures 6.23 and 6.24. The behavior of $GdF_3$, Figure 6.23, is typical of the rest of the series, the high temperature deposition results in an inhomogeneous film. Inhomogeneity in the growth direction is a variation in refractive index within a single layer and it shows itself as a half-wave point which does not coincide with the substrate line. It is believed to be a structural effect caused by higher packing density closer to the substrate. This is consistant with the XRD results from chapter four which show more crystallinity and larger crystallites for higher

temperature deposited films and with the results of Klinger and Carniglia (1984). (This inhomogeneity is the only detectable affect that crystal structure has on optical properties.) Notice that the inhomogeneity changes direction with respect to the substrate index as the wavelength changes. The half-wave point is higher than the substrate in the longer wavelength region and lower than the substrate at shorter wavelengths. This holds even in the VUV for $MgF_2$ substrates. (We are convinced that this is not UV absorption because for this group of high temperature films, there was good stoichiometry and no more oxygen than in ambient temperature films. We know of no other common causes of UV absorption in films.) Figure 6.24 shows the transmittance of a $LuF_3$ film deposited at 200°C. It is interesting because the index seems to have been evenly raised to equal that of the substrate since the fringes surround the substrate trace. At the same time the interface is not negligible since if it was we would see no fringes at all. Elevated temperature deposition also decreases absorption caused by oxygen and water inclusion. This composition effect is believed to be an artifact of the bake-out and is not shown in any of the UV and visible figures but was shown and discussed in the VUV section.

The next five figures show the optical effects of IAD on $SmF_3$ thin films. They are measurements made on the same films used in chapter five for the crystal structure study. Figure 6.25 demonstrates the effect of current density on transmittance by comparing four films deposited under otherwise identical conditions. We see that the fluorine sputtering result shown in chapter five is corroborated here by the absorption peak in the UV. We also see that the oxygen inclusion as a cause for absorption result from chapter five is corroborated here by the decrease in the hump at 2300 Å as current density increases. We can see that as the current

density increases the effects of IAD become more pronounced. The minimum threshold for seeing the effects of IAD with the Cary traces was 50 eV and 10 $\frac{\mu A}{cm^2}$. The films did not appear pink or orange until about 250 eV and 20 $\frac{\mu A}{cm^2}$ and the XRD could not detect fluorine deficiency until 750 eV and 10 $\frac{\mu A}{cm^2}$. RBS could detect it sometimes and not others. The increase of ion energy does not have the same effects, see Figure 6.26. IAD increases index, this effect is both structural (packing density) and compositional (oxygen addition). IAD increases absorption by adding oxygen and by creating $LnF_x$ with particular bands in the UV and visible.

Figure 6.27 shows the reflectance and transmittance of two ambient temperature $SmF_3$ films, one IAD and one non-IAD. It is the first figure we have shown so far containing reflectance data and the only one we need for the VUV through visible data. Reflectance is less than 10% all through these wavelength regions for all of the materials. It is offered in figure 6.27 as proof that when the transmittance decreases it is really due to absorption and not an increase in reflectance.

The crystal structure and composition results of the annealing study were shown in chapter five. Figures 6.28 and 6.29 contain the optical results. The non-IAD $SmF_3$ film had a typical transmittance profile before anneal and after anneal we see that it becomes heavily absorbing. The IAD film looses its $SmF_2$ character after anneal and looks just like the non-IAD film. We know from both RBS and XRD that this is the transmittance profile of SmOF.

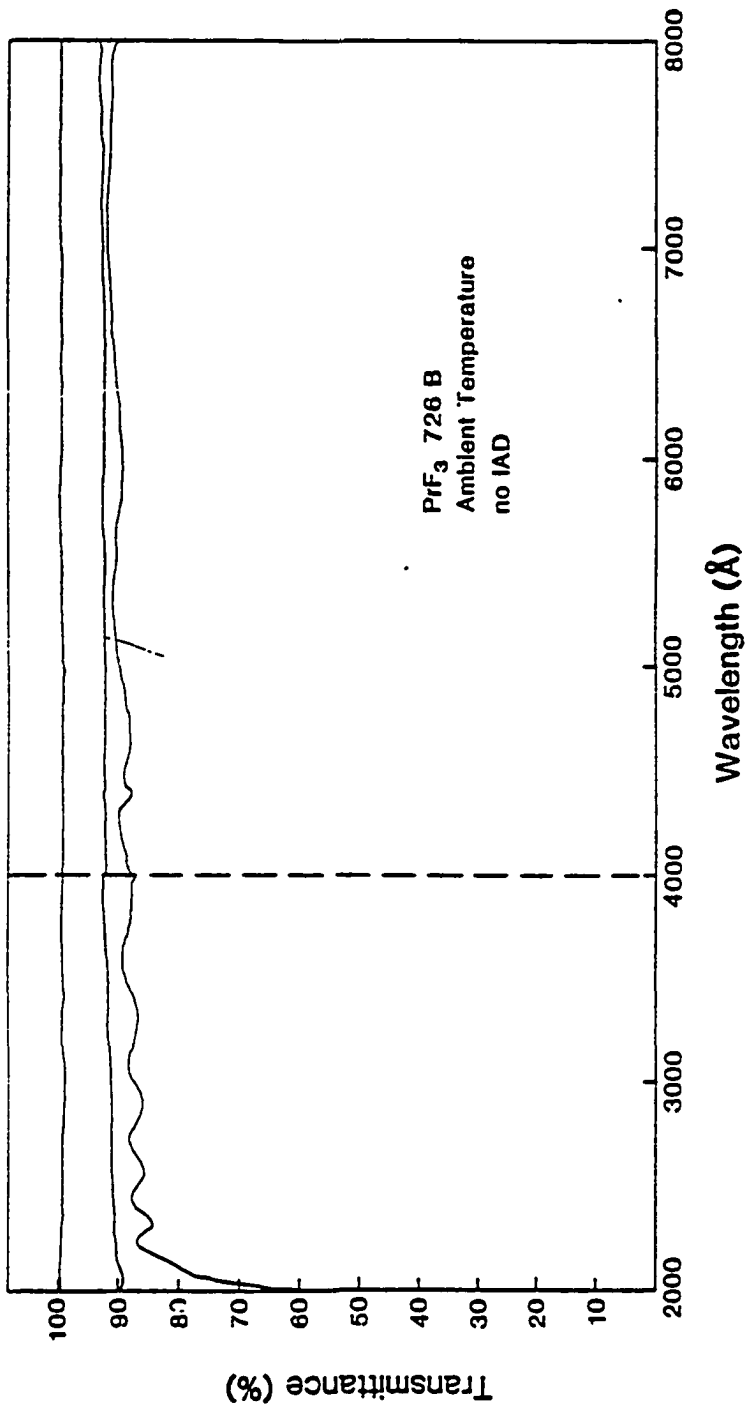


Figure 6.12. UV and visible transmittance of Praseodymium Trifluoride.

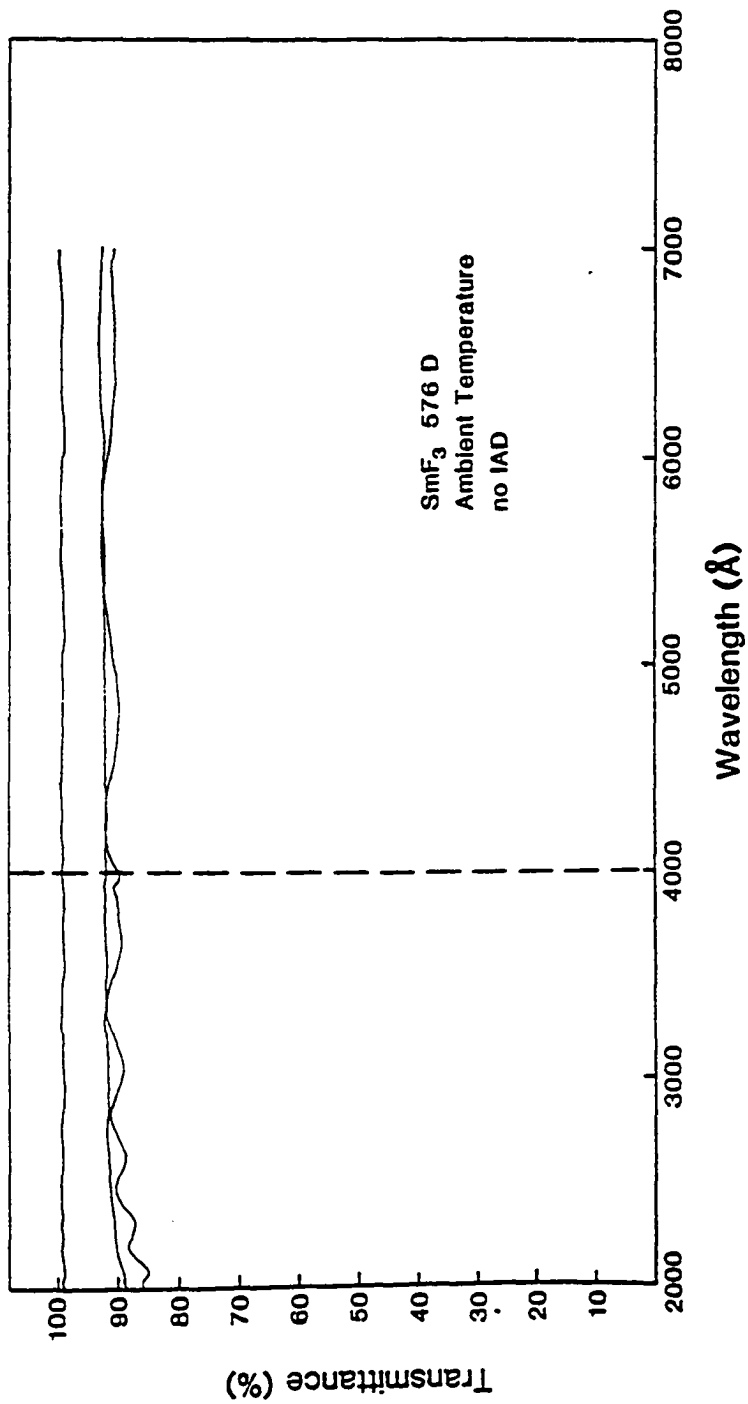


Figure 6.13. UV and visible transmittance of Samarium Trifluoride.

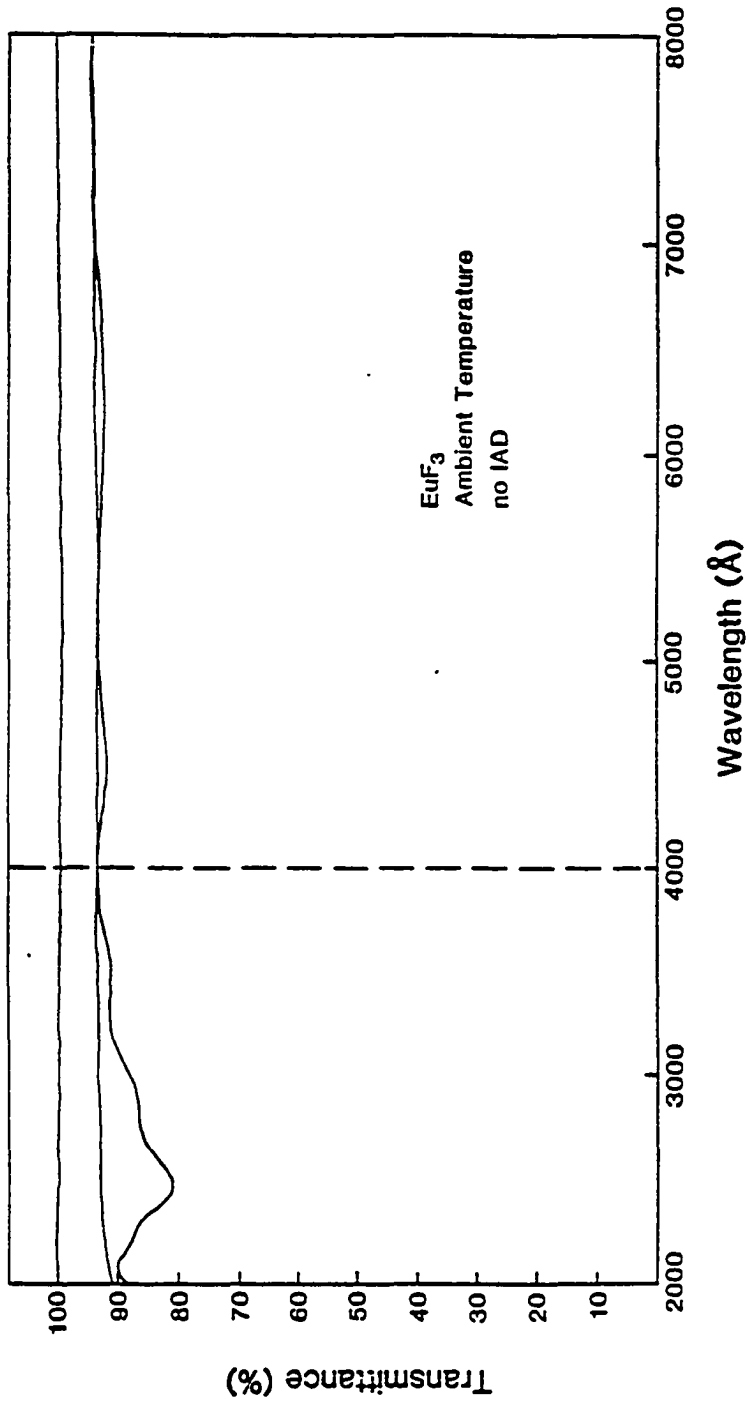


Figure 6.14. UV and visible transmittance of Europium Trifluoride.

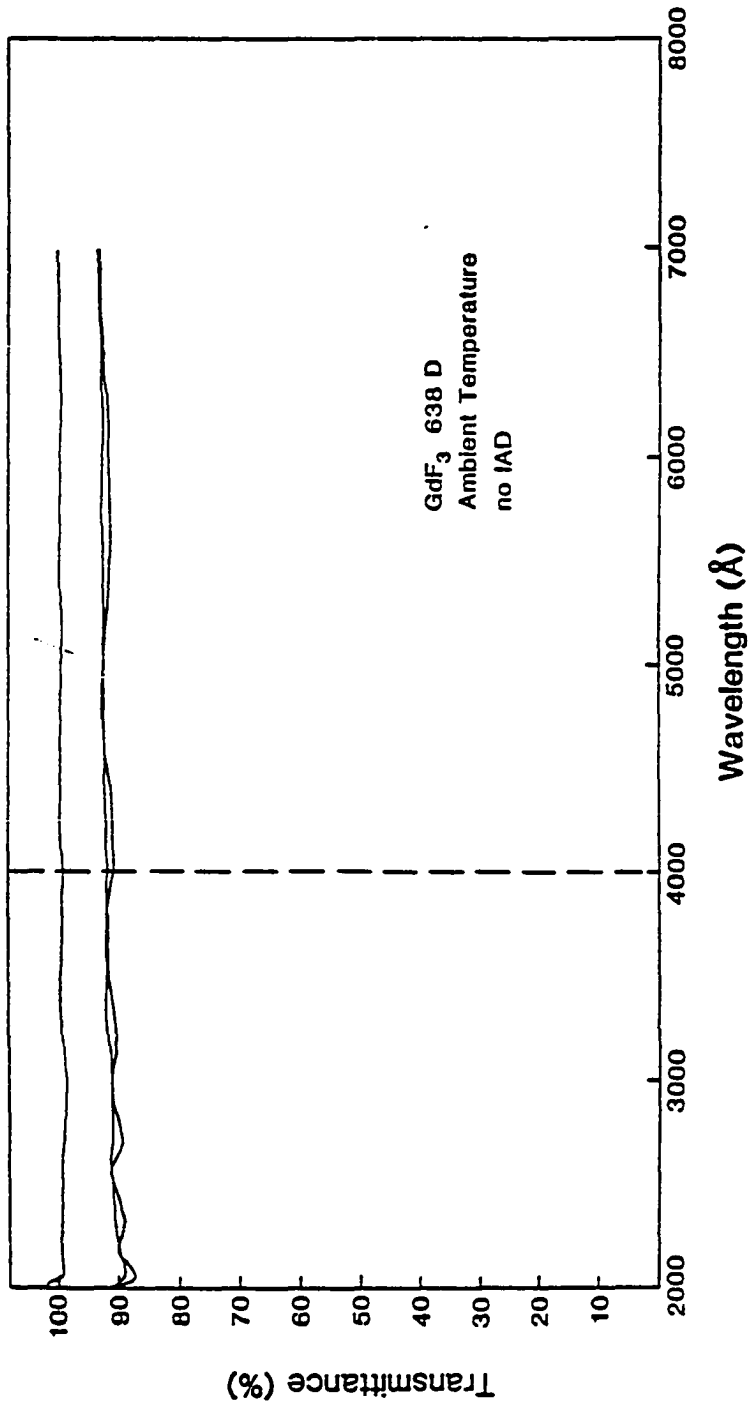


Figure 6.15. UV and visible transmittance of Gadolinium Trifluoride.

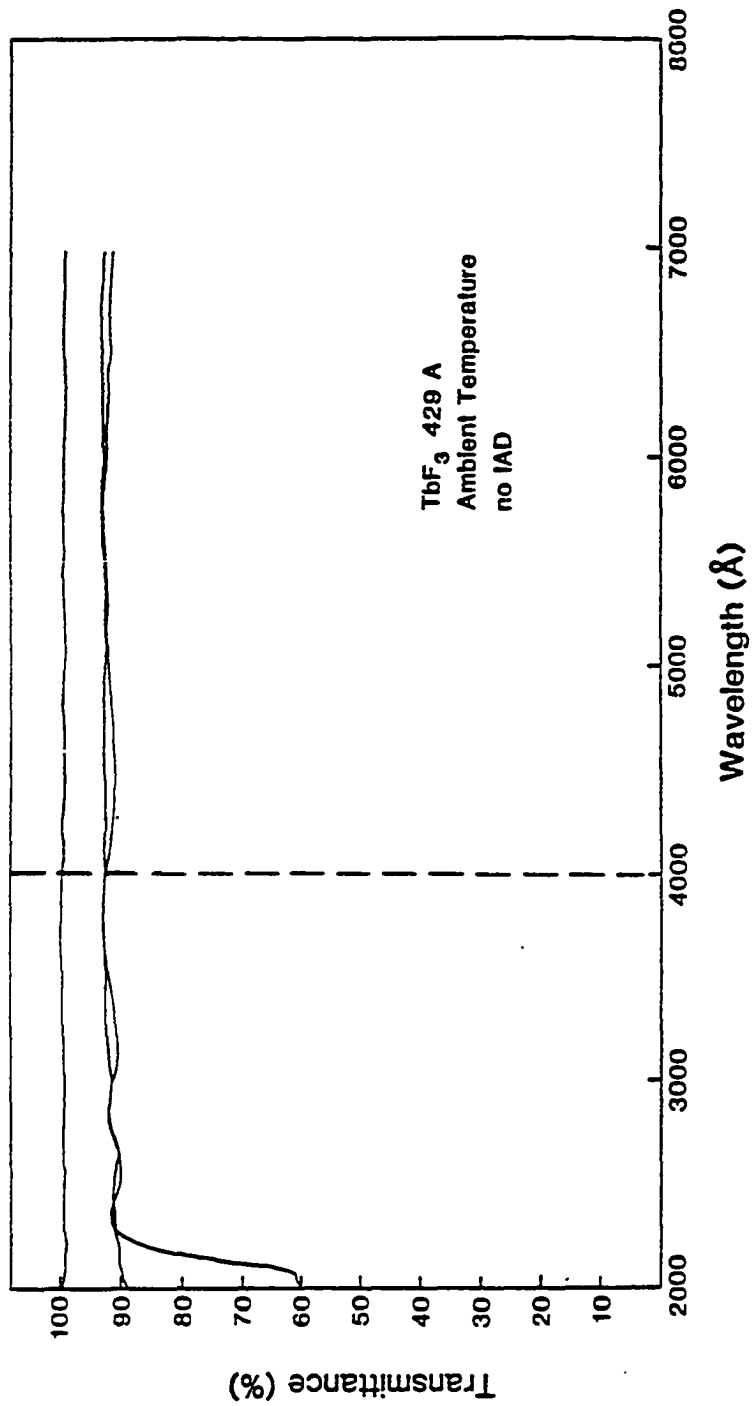


Figure 6.16. UV and visible transmittance of Terbium Trifluoride.

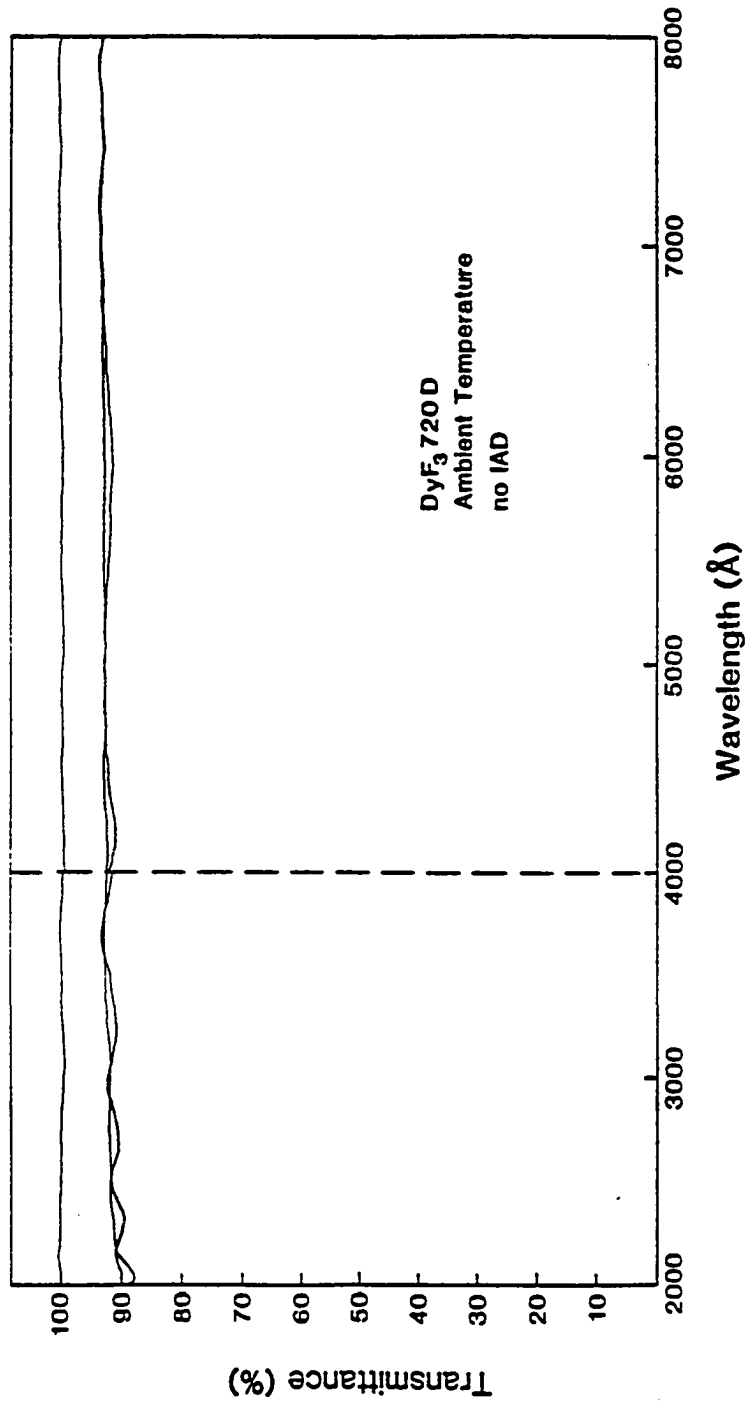


Figure 6.17. UV and visible transmittance of Dysprosium Trifluoride.

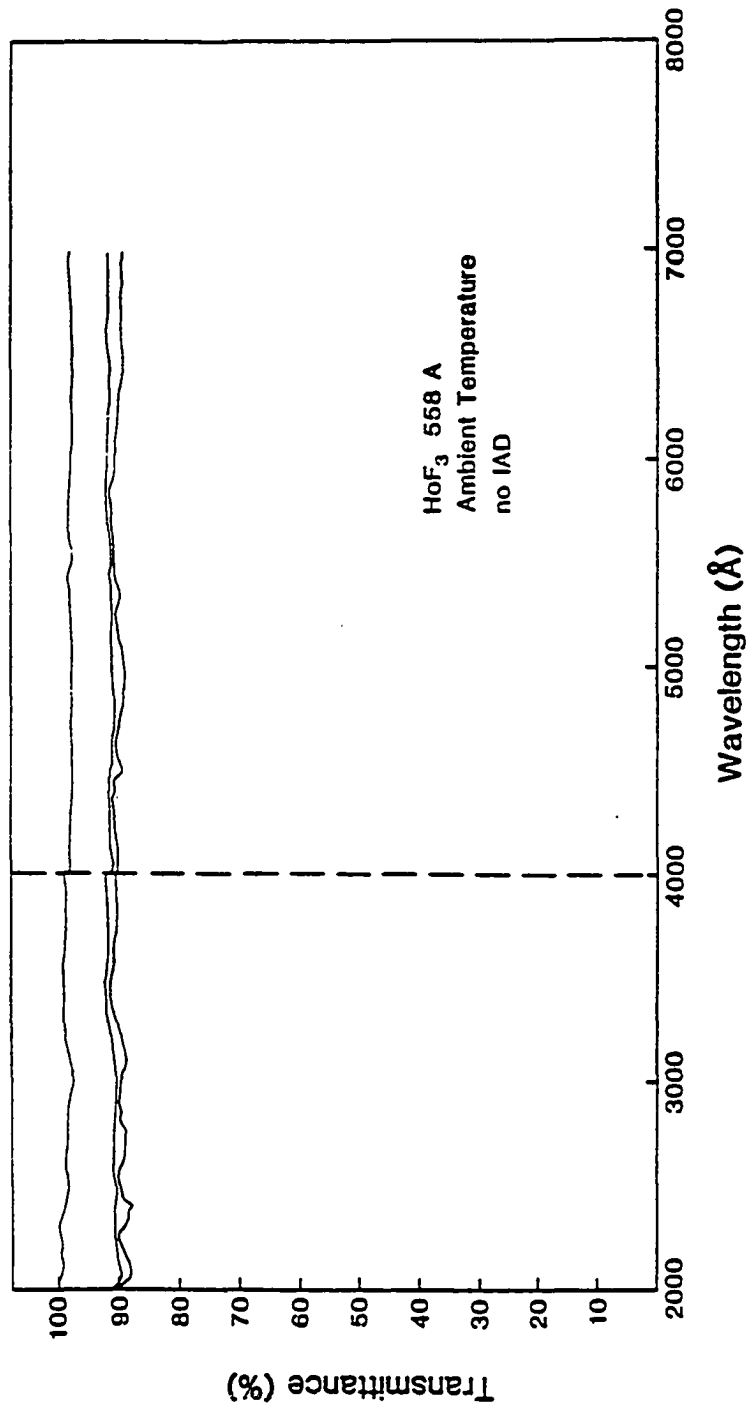


Figure 6.18. UV and visible transmittance of Holmium Trifluoride.

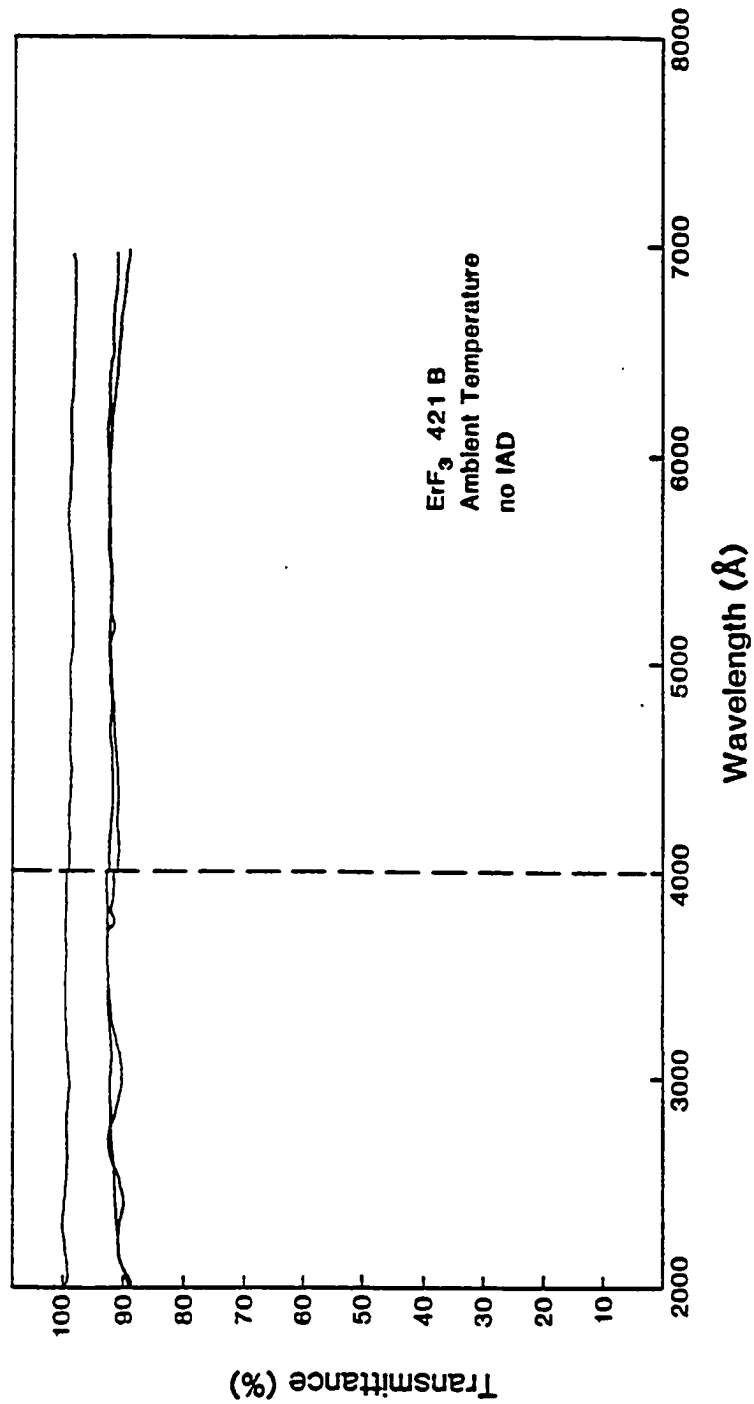


Figure 6.19. UV and visible transmittance of Erbium Trifluoride.

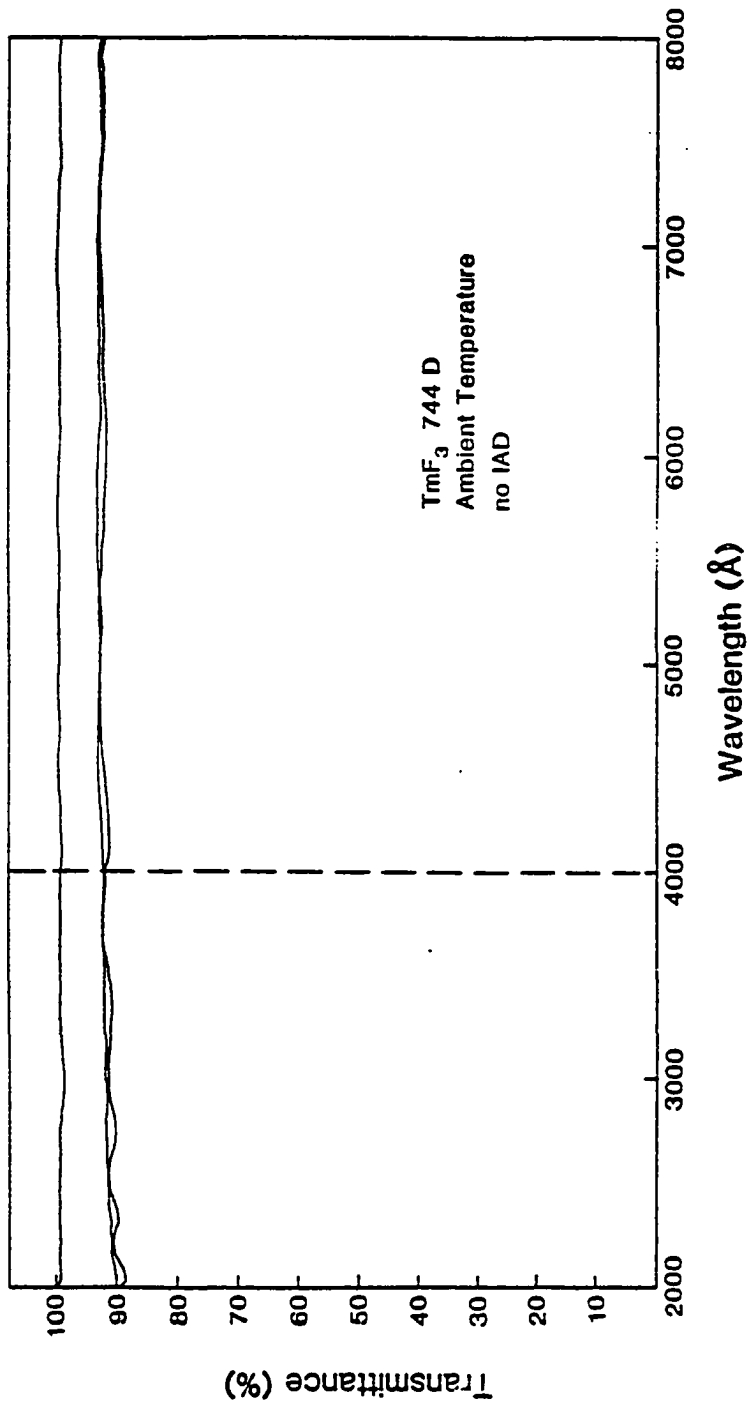


Figure 6.20. UV and visible transmittance of Thulium Trifluoride.

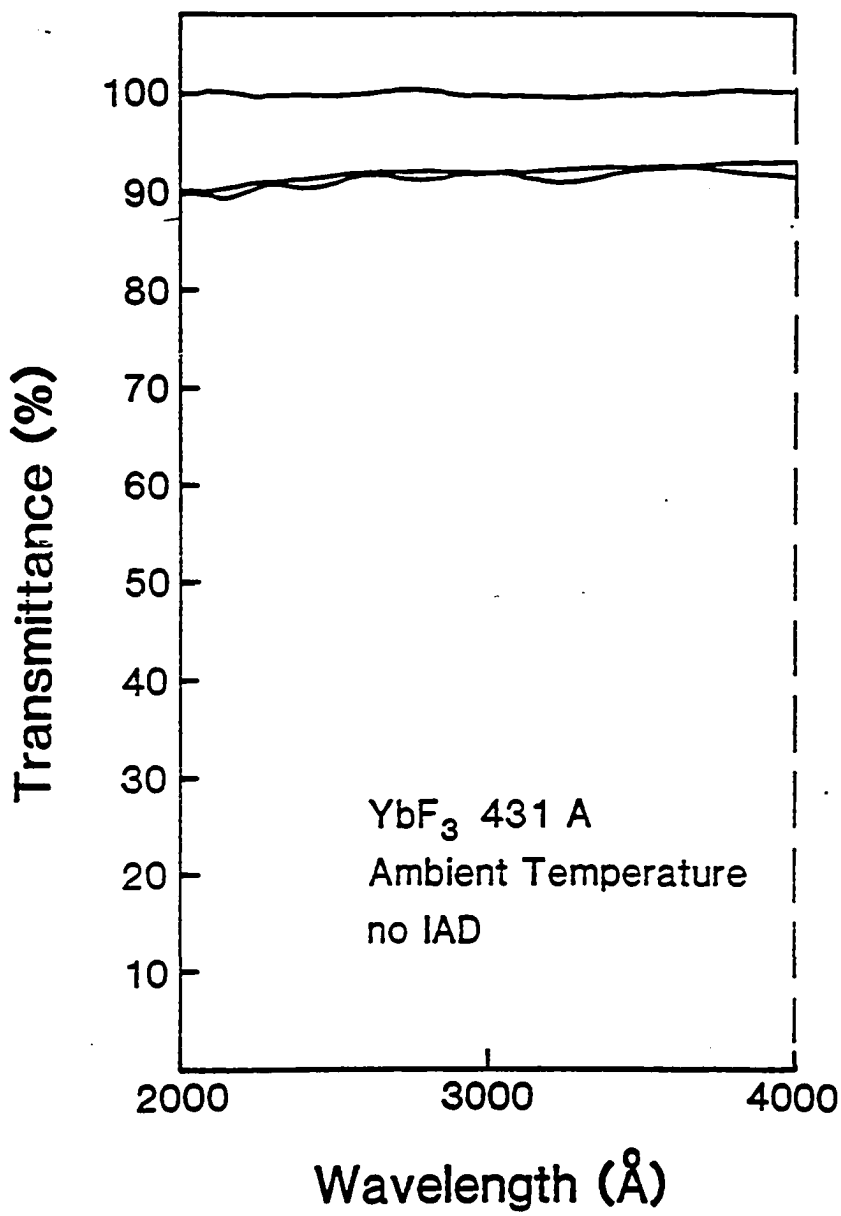


Figure 6.21. UV and visible transmittance of Ytterbium Trifluoride.

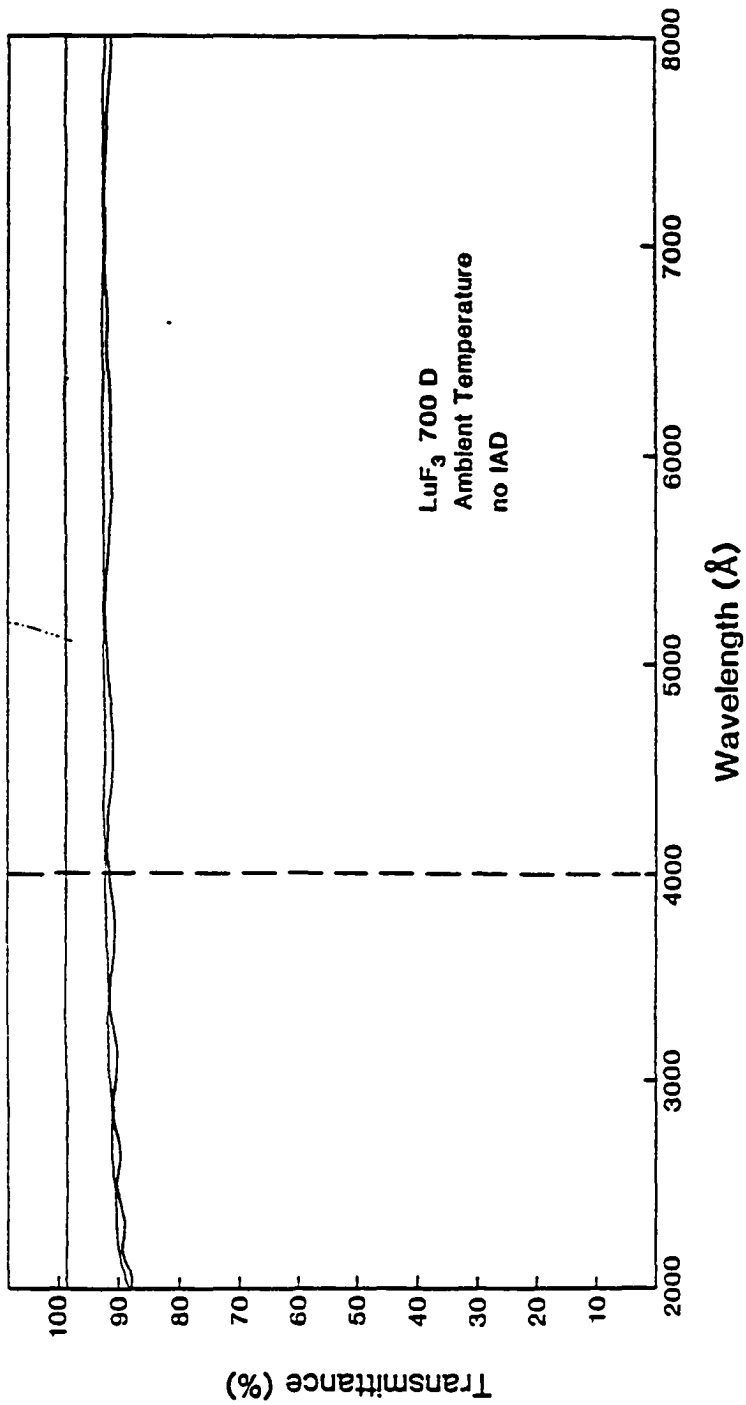


Figure 6.22. UV and visible transmittance of Lutetium Trifluoride.

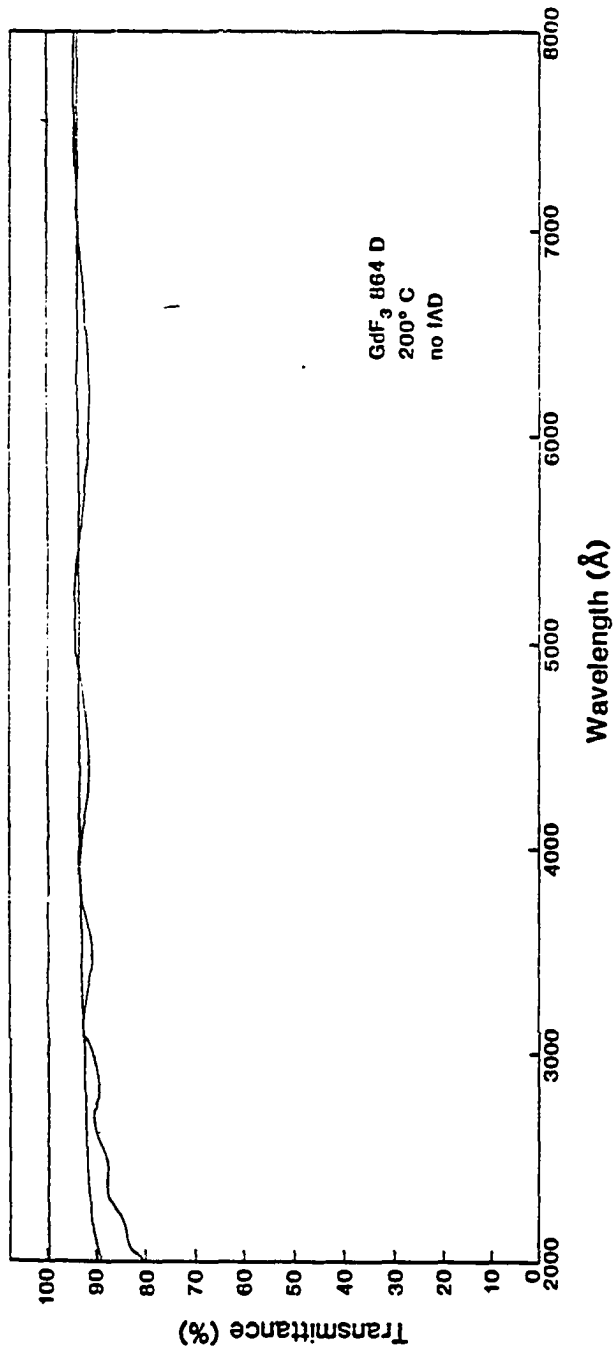


Figure 6.23. UV and visible transmittance of $GdF_3$ thin film deposited at 200°C.

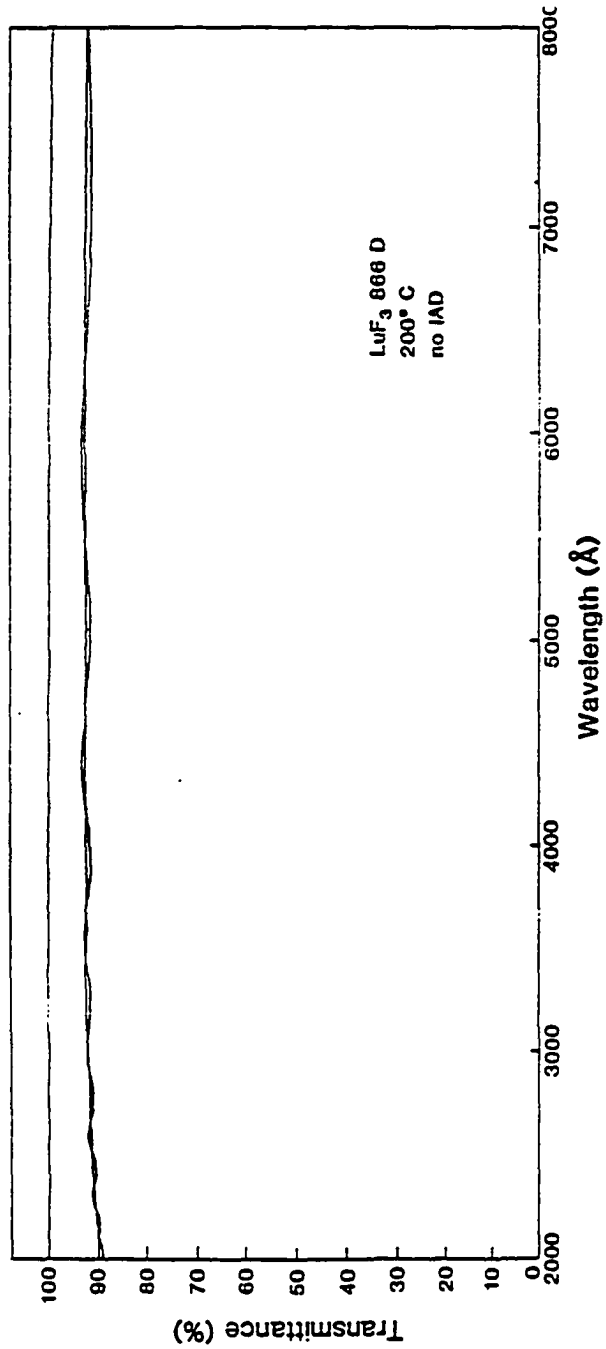


Figure 6.24. UV and visible transmittance of $LuF_3$ thin film deposited at 200°C.

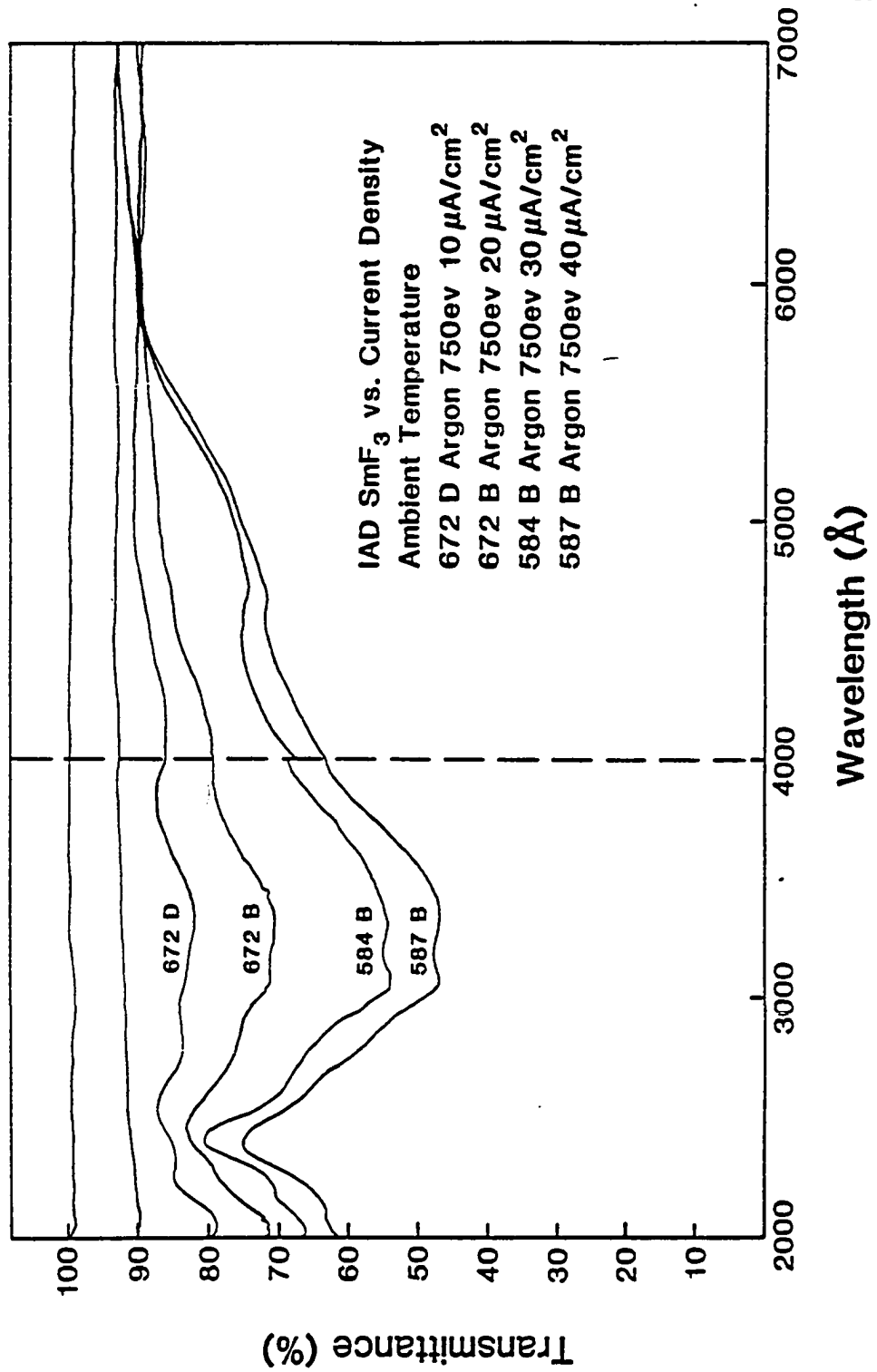


Figure 6.25. UV and visible transmittance of IAD $SmF_3$ thin films showing the effect of increasing ion current density.

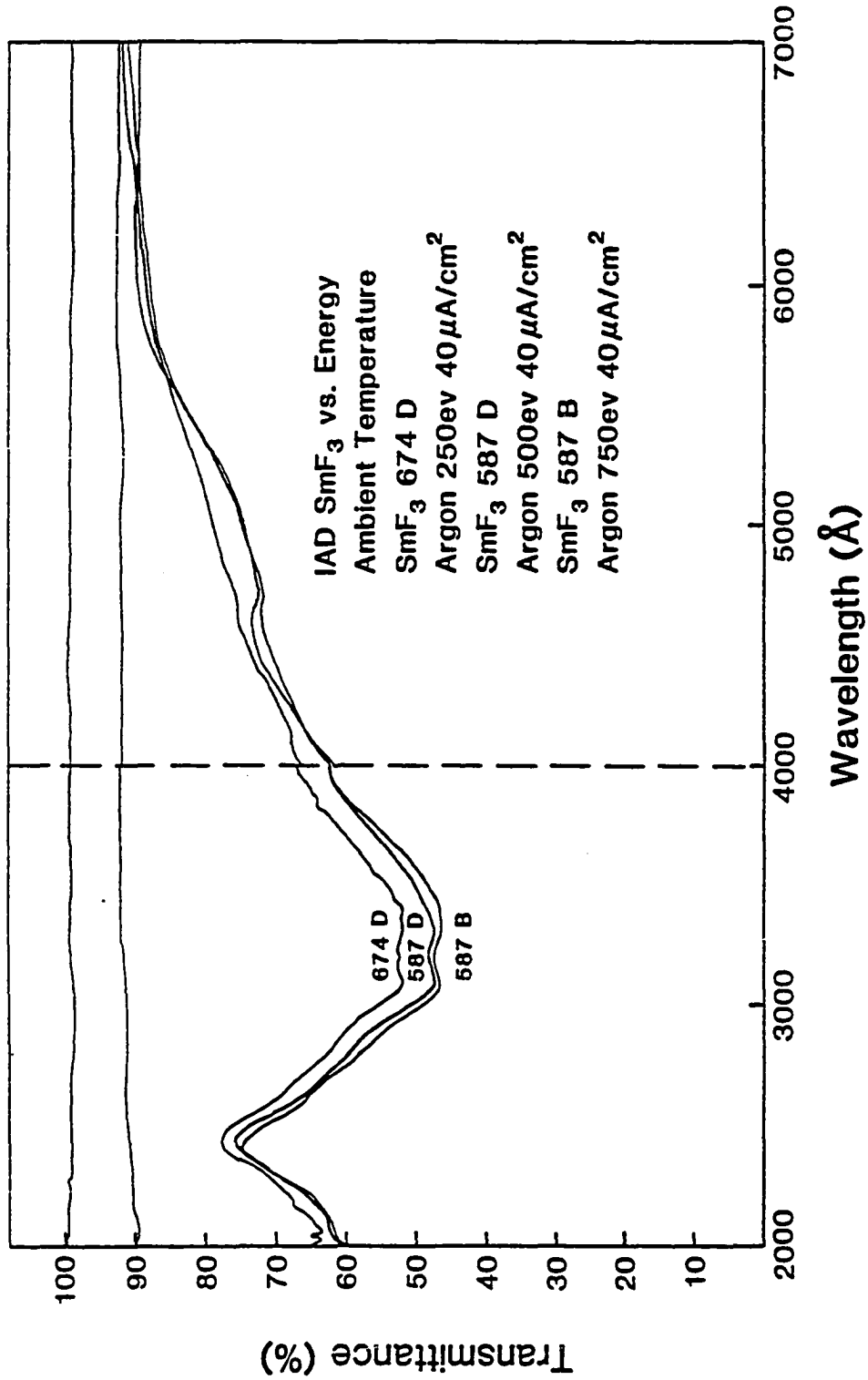


Figure 6.26. UV and visible transmittance of IAD $SmF_3$ thin films showing the effect of increasing ion energy.

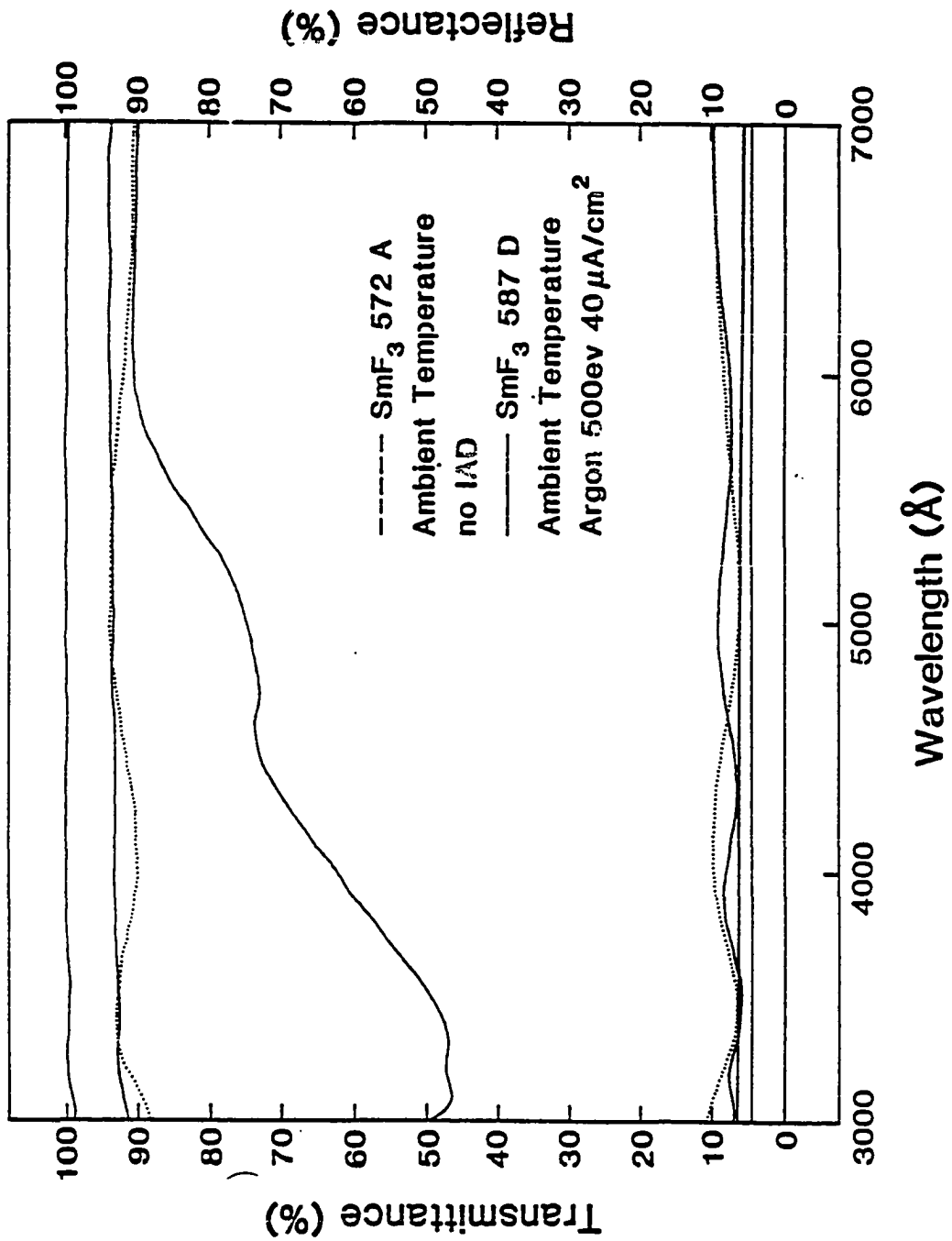


Figure 6.27. UV and visible transmittance and reflectance of ambient temperature, non-IAD and IAD $SmF_3$ films.

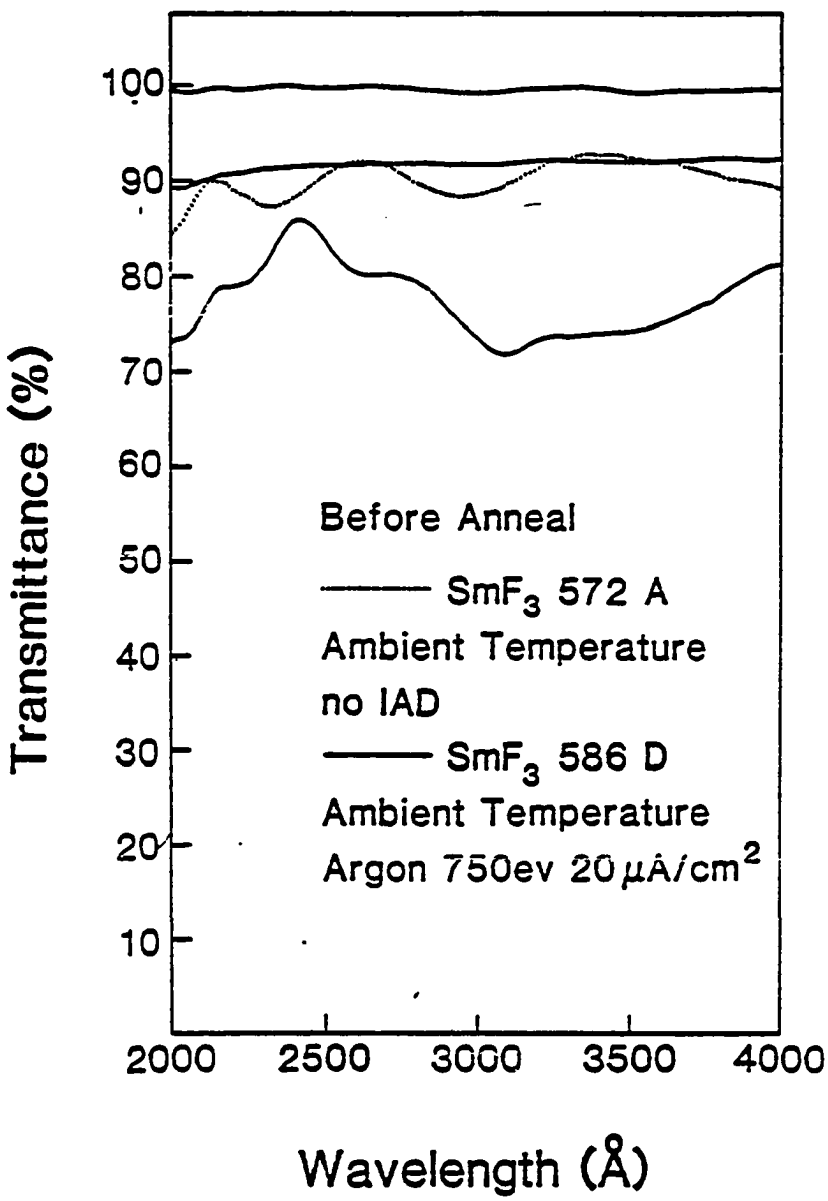


Figure 6.28. UV and visible transmittance of $SmF_3$ thin films before anneal.

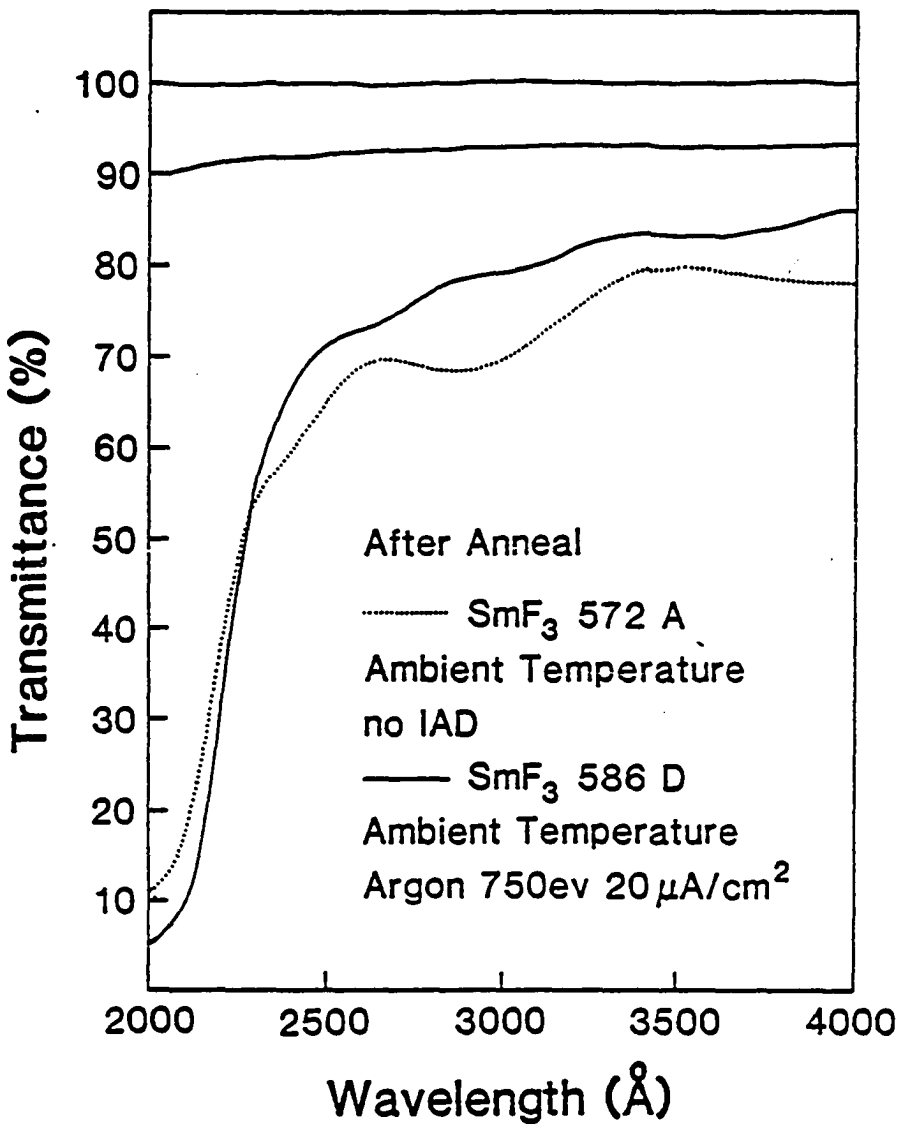


Figure 6.29. UV and visible transmittance of $SmF_3$ thin films after anneal.

Infrared Transmittance

We deposited films approximately 5000 Å thick onto silicon substrates and the transmittance measurements are shown in Figures 6.30 through 6.39 for $LnF_3$ [Ln=Sm-Lu]. The trace for a given film will have several features. Around 3630 and 3400 $cm^{-1}$ are the free and bonded $OH^-$ stretching absorption bands, respectively, and around 2400 $cm^{-1}$ the $CO_2H$. At 1700 $cm^{-1}$ the CO double bond strech appears and at 1100 the CO single bond stretch (Streitwieser and Heathcock 1976). Around 1000 $cm^{-1}$ and below are absorption bands ue to the substrate. We see no features from the materials themselves in the IR spectrum. This agrees with the bulk results of Rast (1968) and Lowndes (1969) who found that the optical phonons begin absorbing after 20 $\mu$m. (Recall the NIR contains some 4f-4f bands but they are not shown here.)

By looking at the various figures we see that both high temperature (Figure 6.39) and IAD (Figures 6.31, 6.33, 6.38) can make the bonded $OH^-$ band disappear. This is thought to be a structural effect, increased packing density, for the IAD films. For the high temperature films it is thought to be both increased packing density and bake-out. Just as heavy ion bombardment caused absorption in other regions of the spectrum it can cause it in the IR, as seen in Figure 6.31 and 6.33. The other water and carbon dioxide bands represent these species in the air and probably not in the sample. They are random with respect to deposition conditions as they should be since we had no nitrogen purge.

Figure 6.40 shows a set of our reflectance and transmittance measurements on $TbF_3$ which were made at OCLI. Comparison of R and T at any given wavelength shows very little absorption unless one is at the absorption band of an impurity or contaminant. The fact that these films show so little absorptance in the IR makes

the $LnF_3$ an attractive substitute for $ThF_4$ since the Ln are not radioactive.

In fact, an extinction coefficient of less than $4\times10^{-6}$ at 1.06 $\mu$m, as measured by laser calorimetry (also at OCLI), was found for both bombarded and unbombarded $GdF_3$ films.

In order to simulate more closely a typical IR coating, we deposited two $GdF_3$ films which were 1.5 $\mu$m thick, both at 100°C but one with argon ion-assist and one without. The transmittance measurements are shown in figure 6.32 (the dips at 3500 are not half-wave points but $OH^-$ absorption). Neither film showed signs of stress, even after storage in air for several months but both films showed tensile stress after humidity testing.

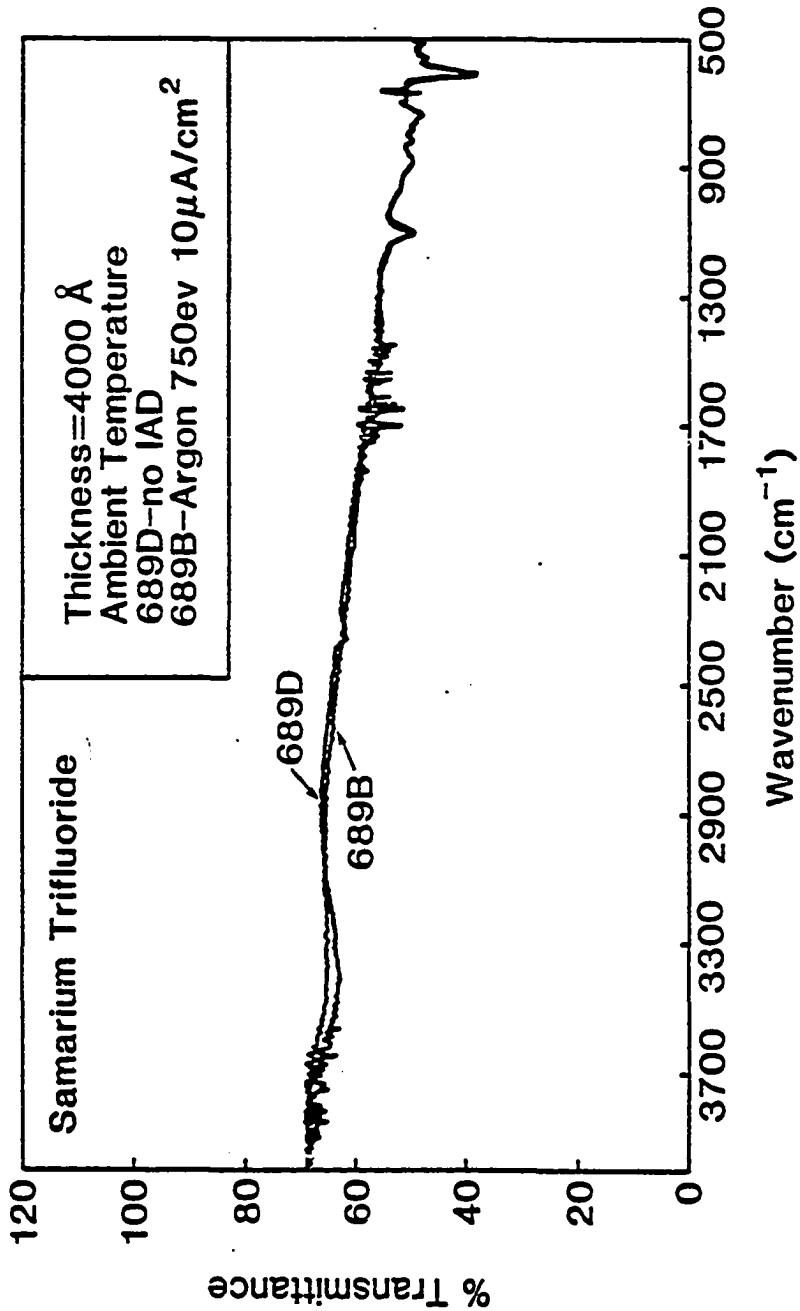


Figure 6.30. Infrared transmittance of Samarium Trifluoride.

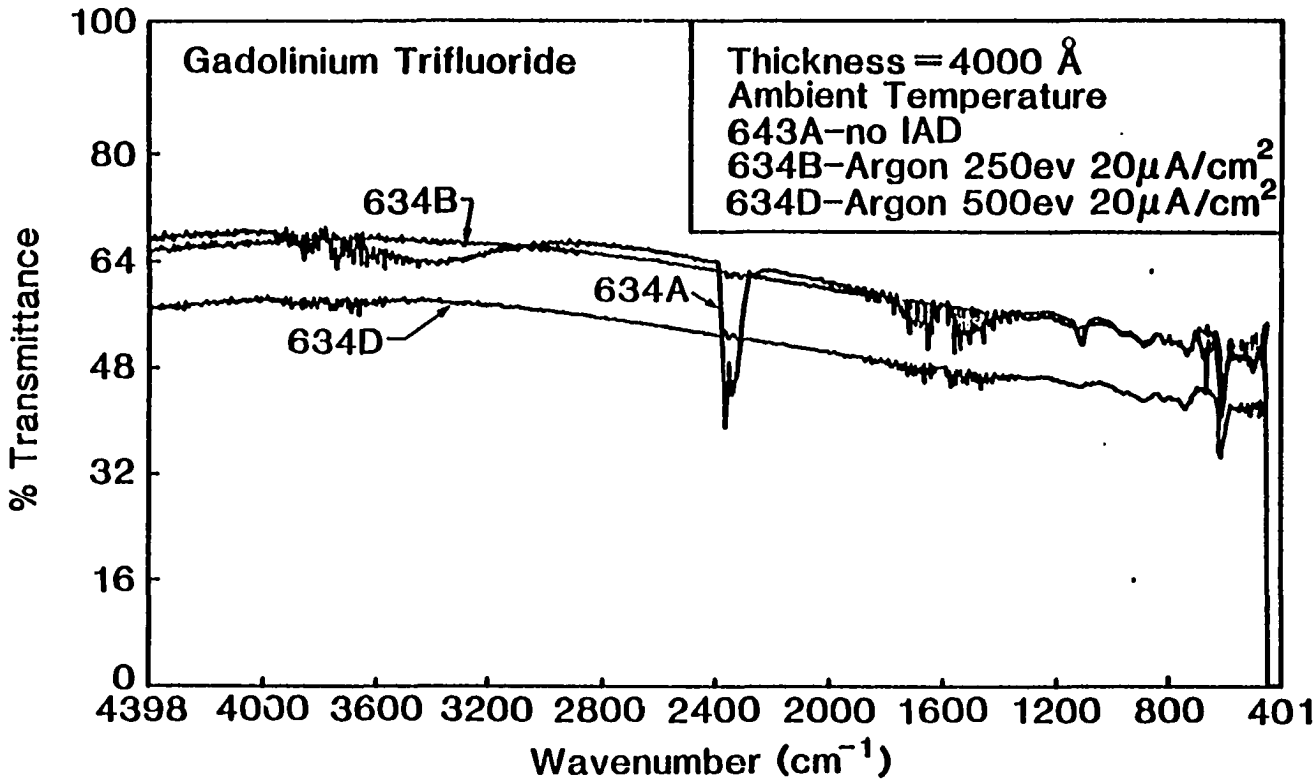


Figure 6.31. Infrared transmittance of Gadolinium Trifluoride.

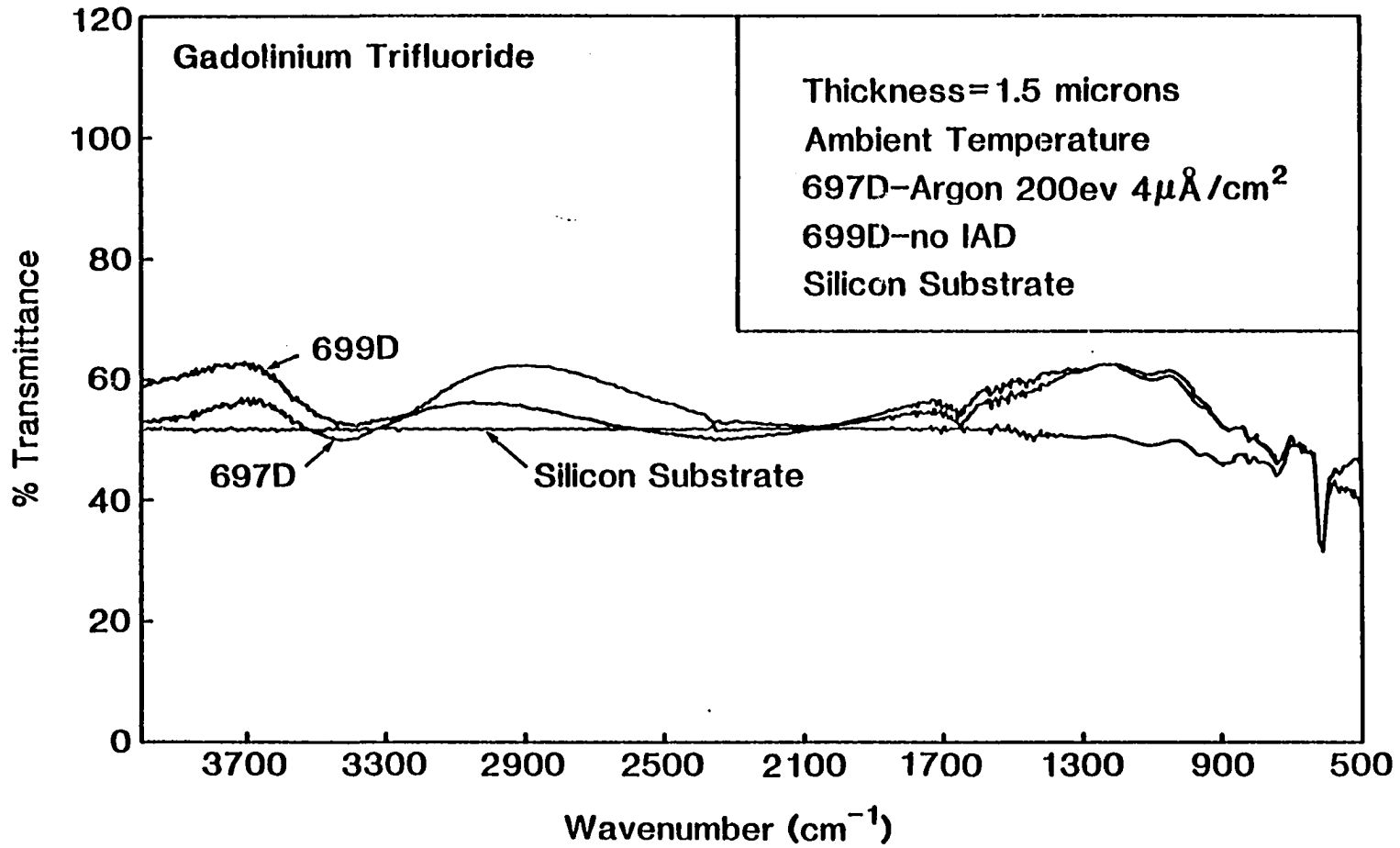


Figure 6.32. Infrared transmittance of Gadolinium Trifluoride.

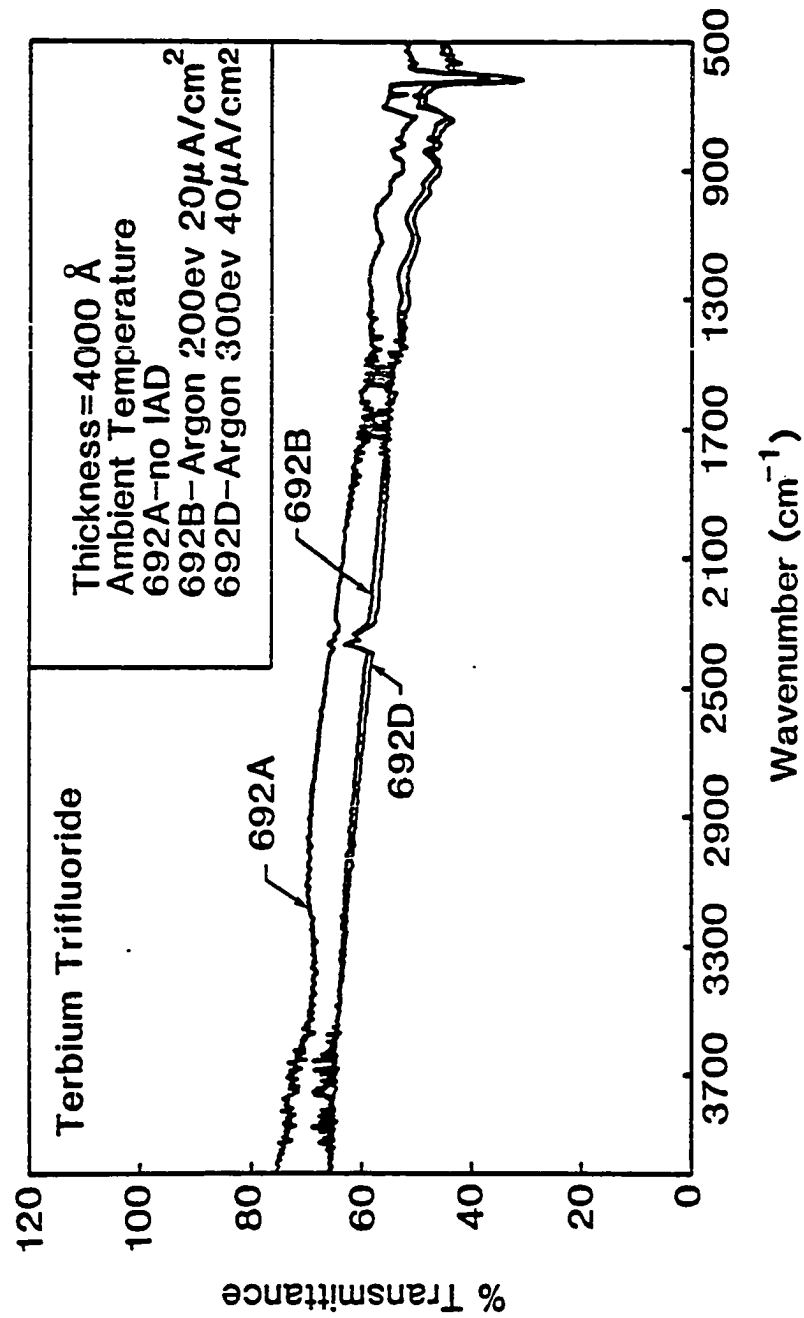


Figure 6.33. Infrared transmittance of Terbium Trifluoride.

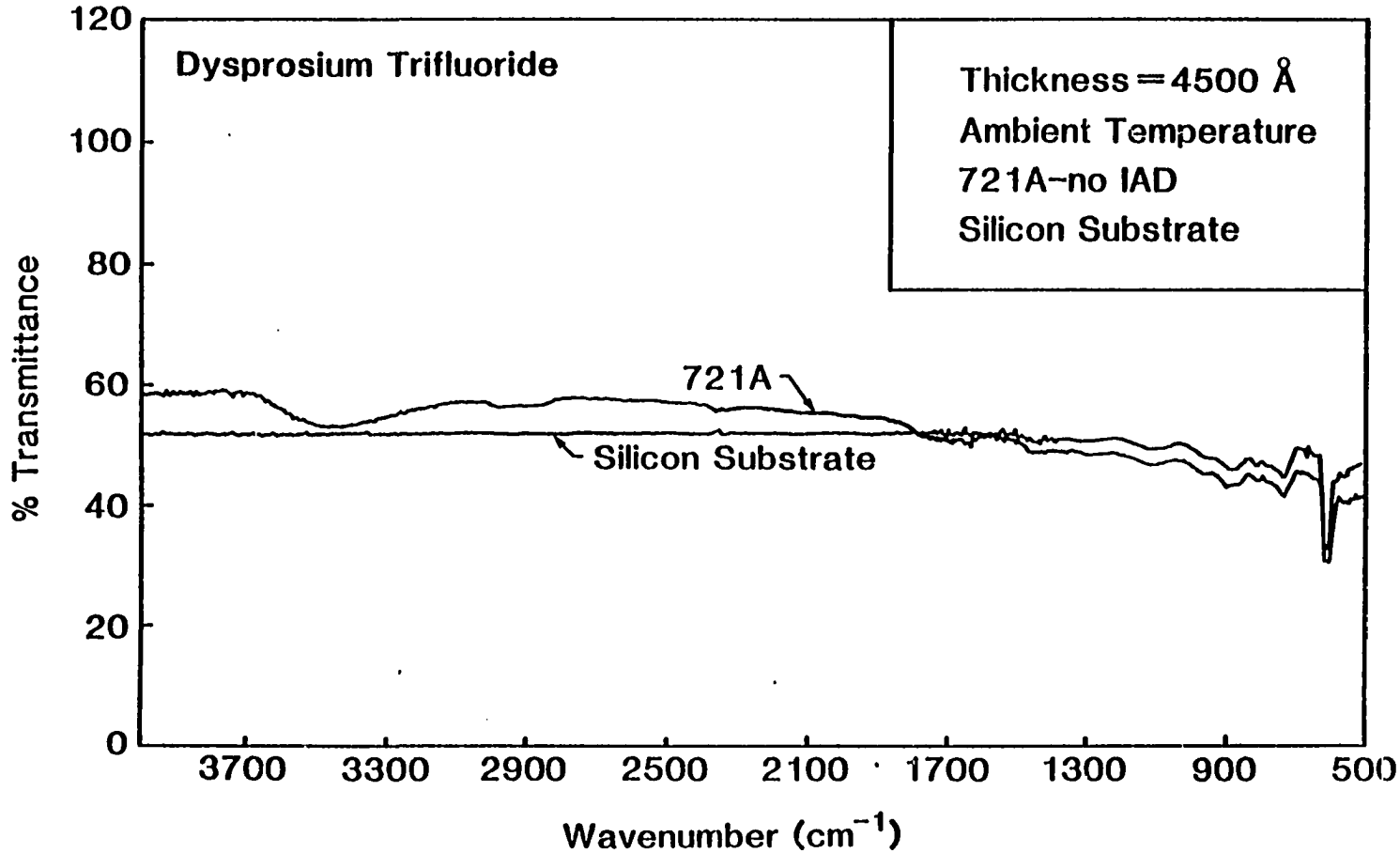


Figure 6.34. Infrared transmittance of Dysprosium Trifluoride.

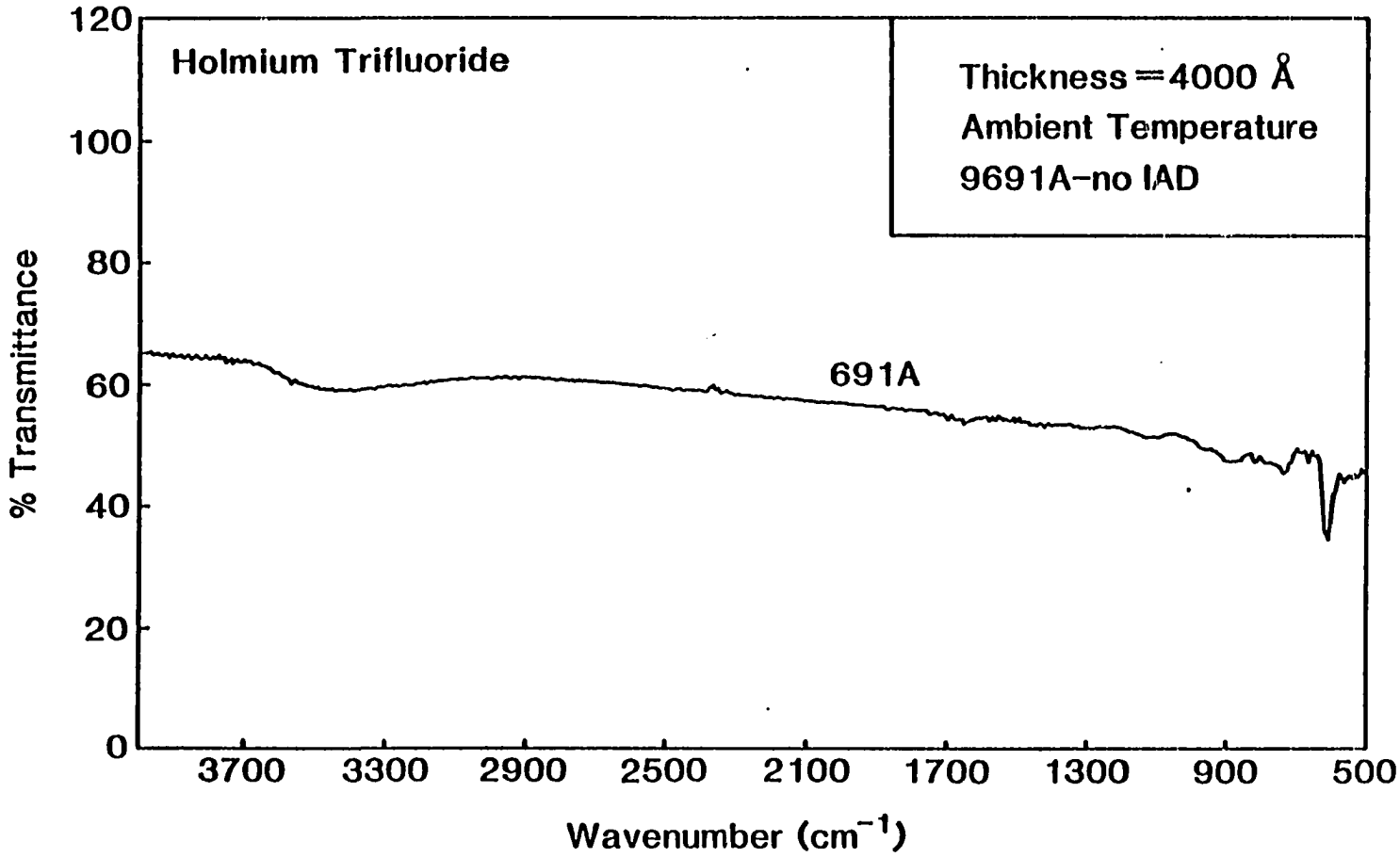


Figure 6.35. Infrared transmittance of Holmium Trifluoride.

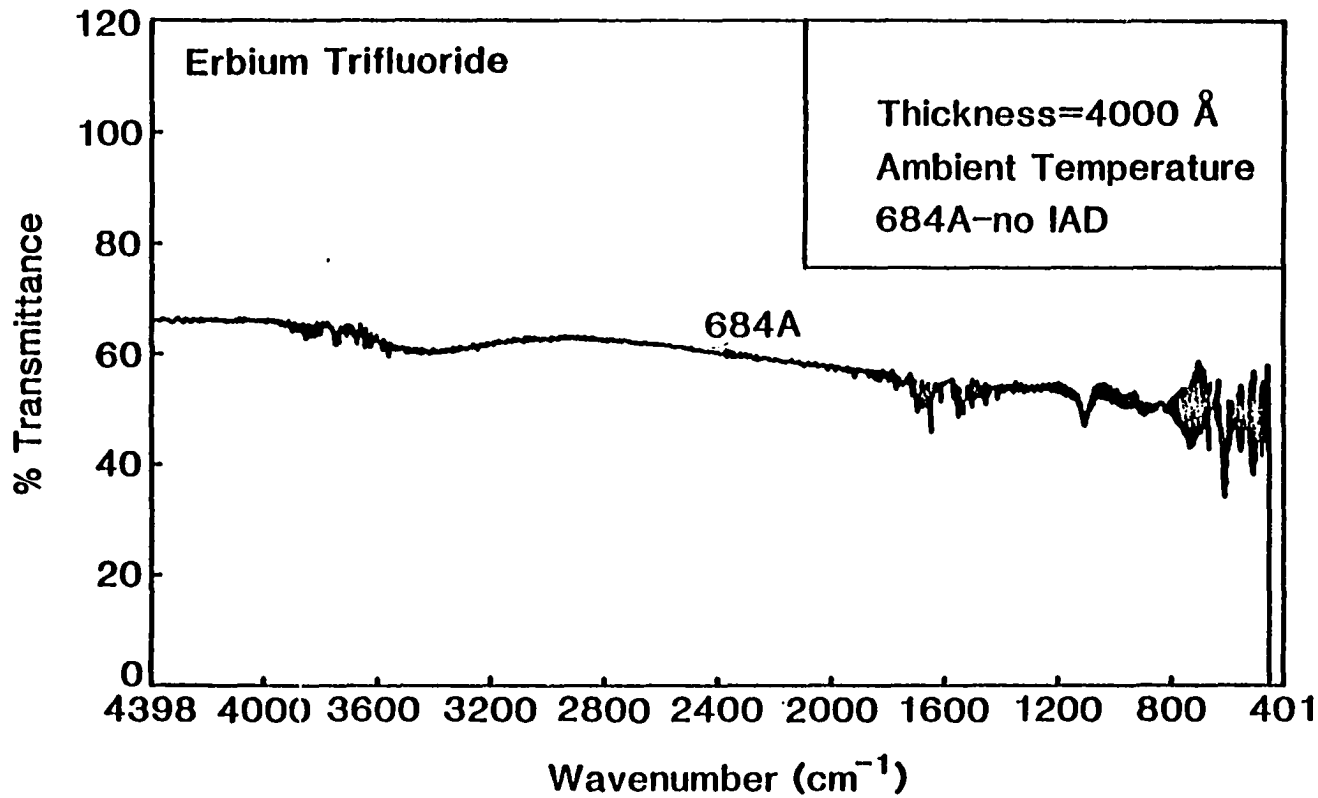


Figure 6.36. Infrared transmittance of Erbium Trifluoride.

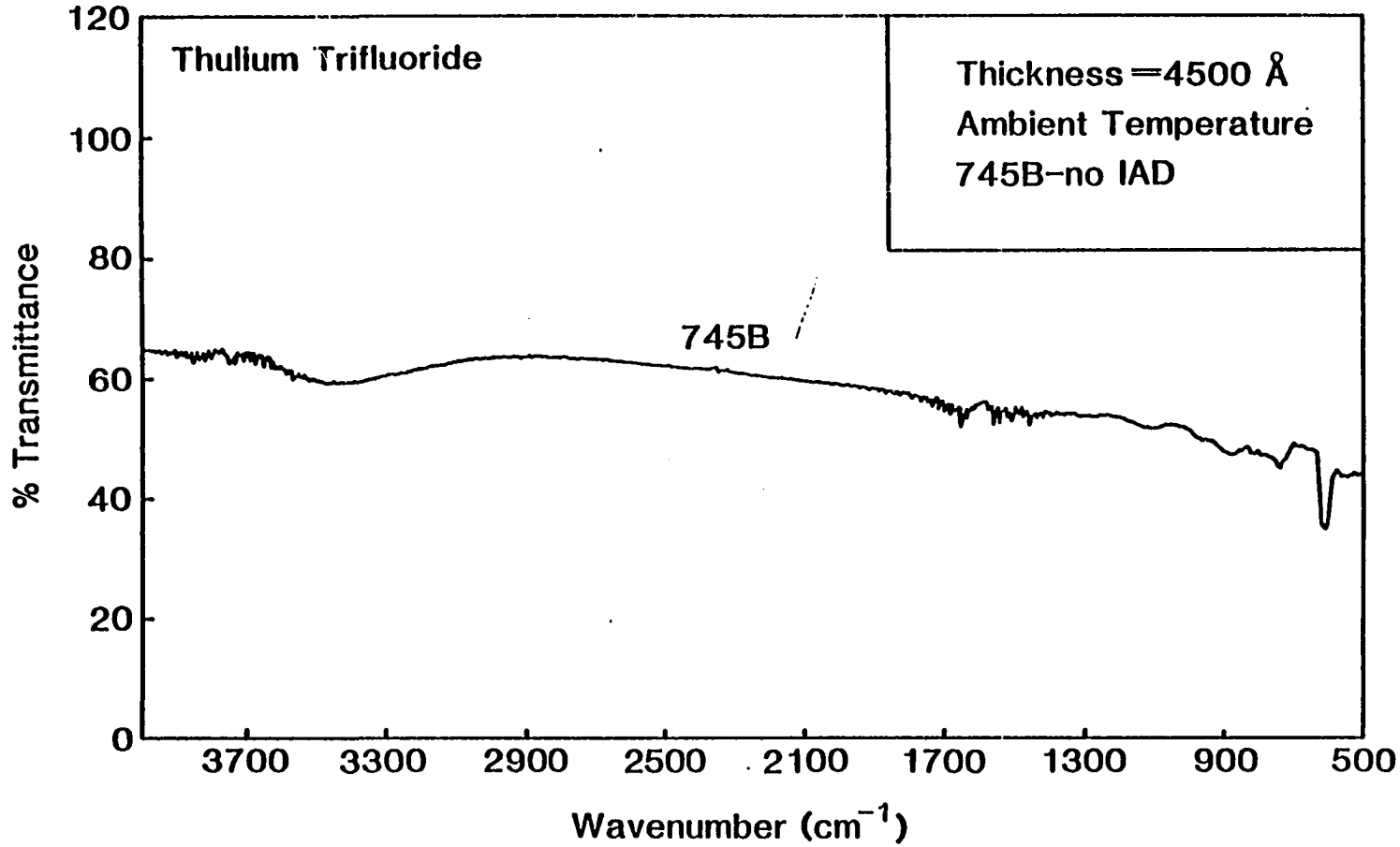


Figure 6.37. Infrared transmittance of Thulium Trifluoride.

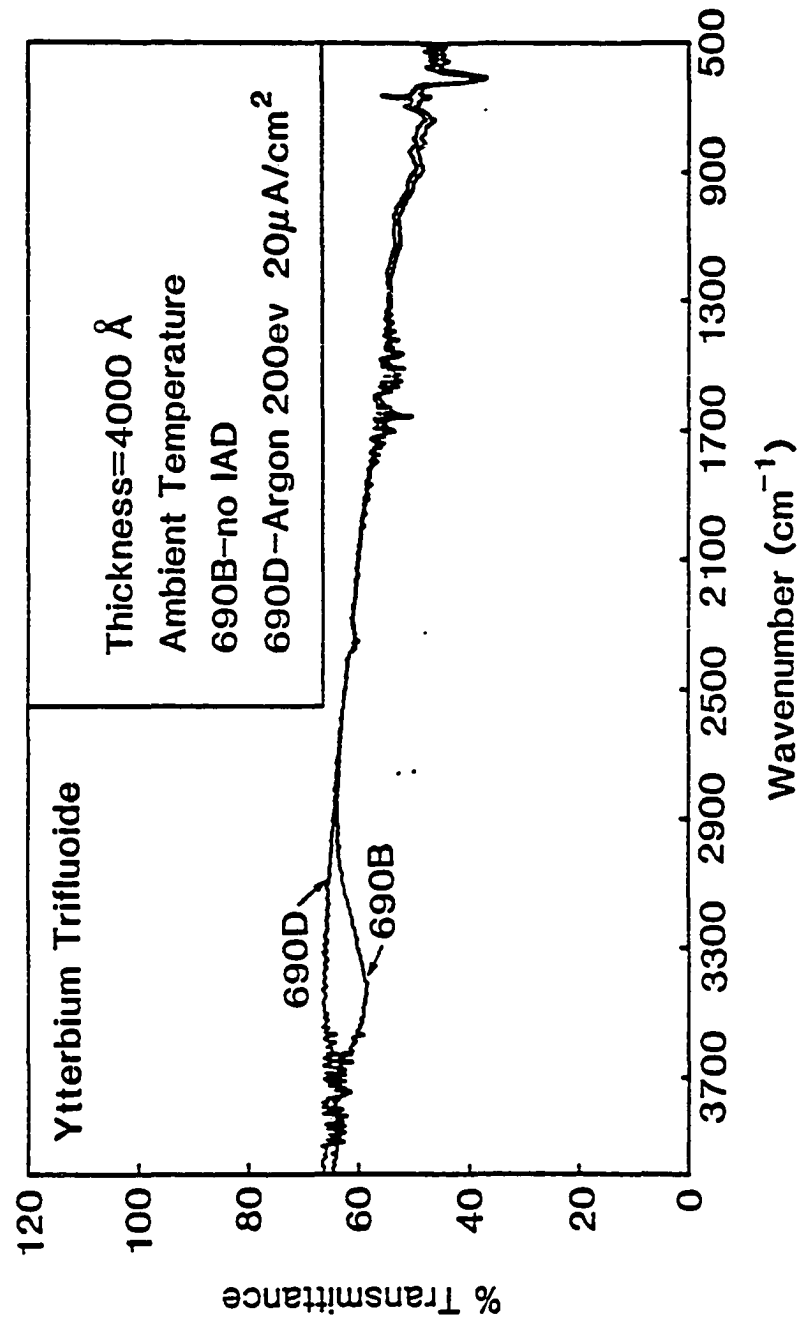


Figure 6.38. Infrared transmittance of Ytterbium Trifluoride.

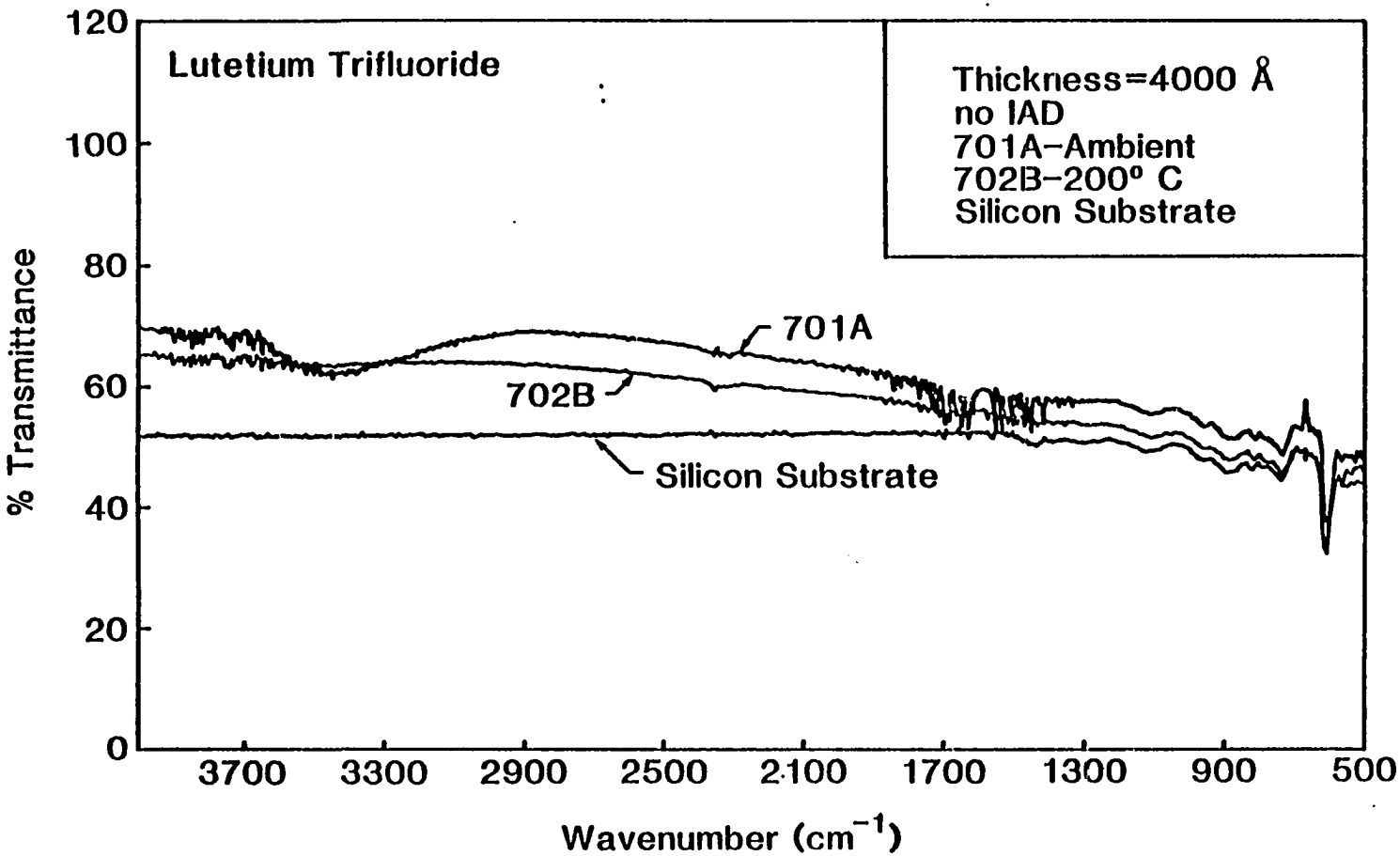


Figure 6.39. Infrared transmittance of Lutetium Trifluoride.

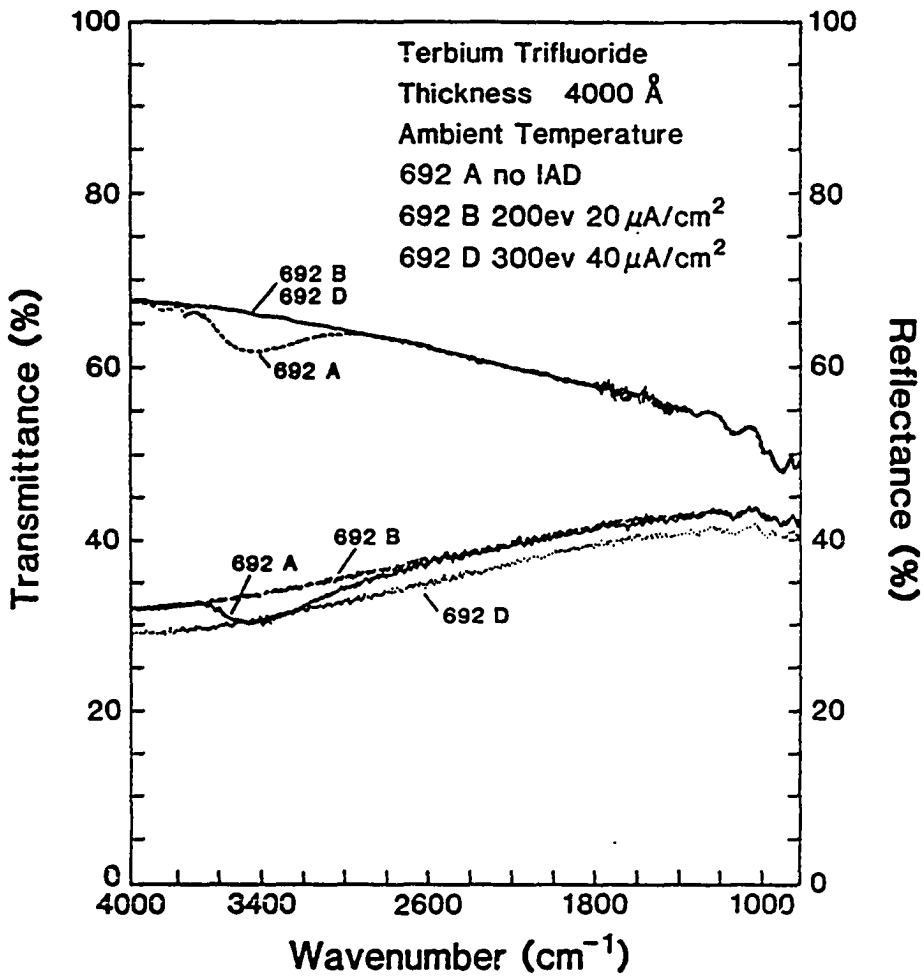


Figure 6.40. Infrared transmittance and reflectance of Terbium Trifluoride.

Refractive Index

Refractive indices were calculated from visible and near-UV transmittance curves Figures 6.12 through 6.22 using the Manifacier envelope method described in chapter three (Manifacier et al. 1976). The visible and near-UV indices of all of the lanthanide trifluorides are around 1.5. $LuF_3$ has the lowest average index (1.50) over the range 2000 Å to 6000 Å. $SmF_3$ has the highest average index (1.58) over the same range. Figure 6.44 illustrates that ion bombardment increases the refractive index of a coating. This the result of two processes, increased packing density (structural) and oxygen inclusion (compositional). These materials are of index values such that they would be a high index compliment to $MgF_2$ (n=1.38, Pulker 1984) in the VUV and UV. They could also be the low index of a pair in the longer wavelength regions (Lingg 1987).

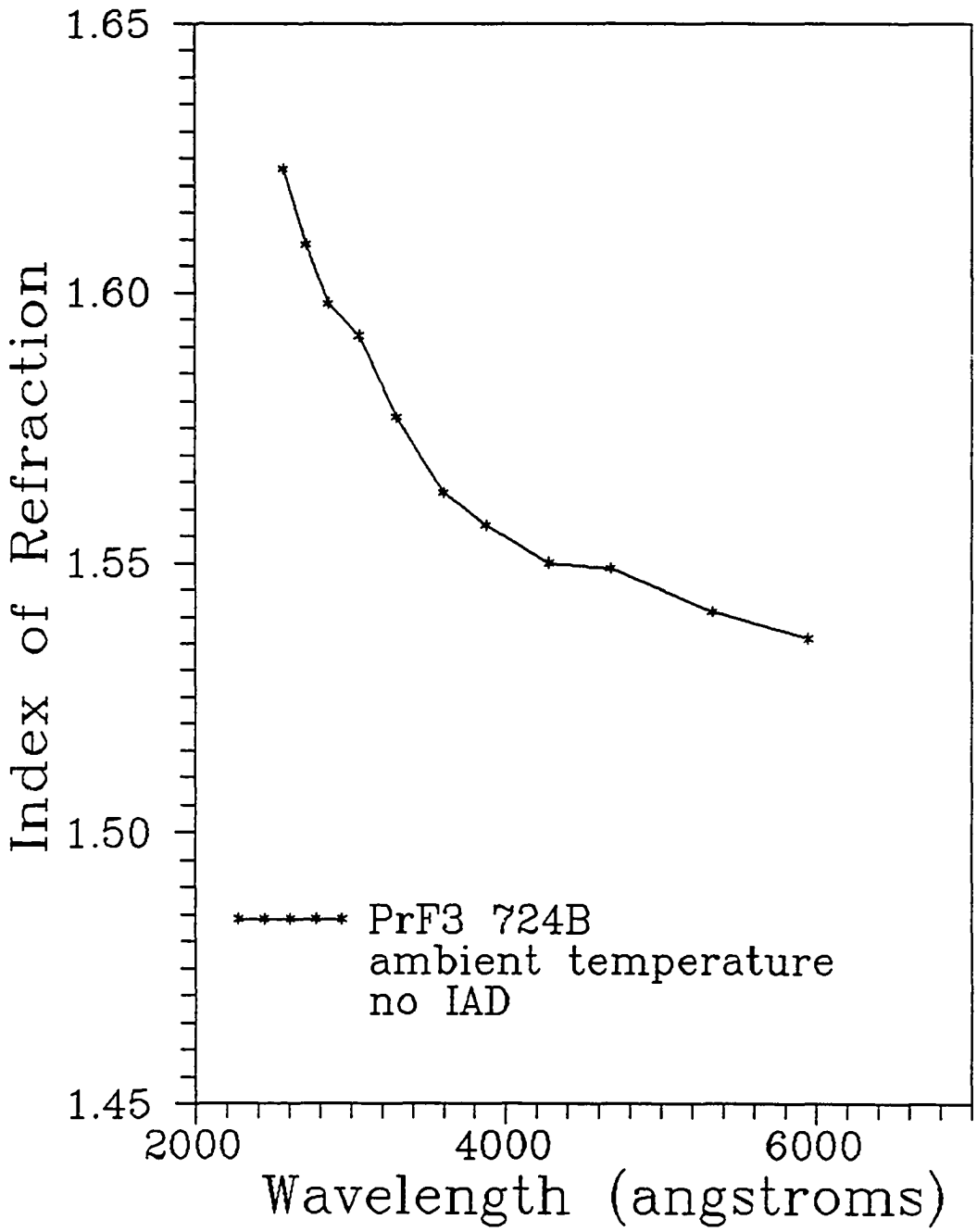


Figure 6.41. Praseodymium Trifluorid. refractive index.

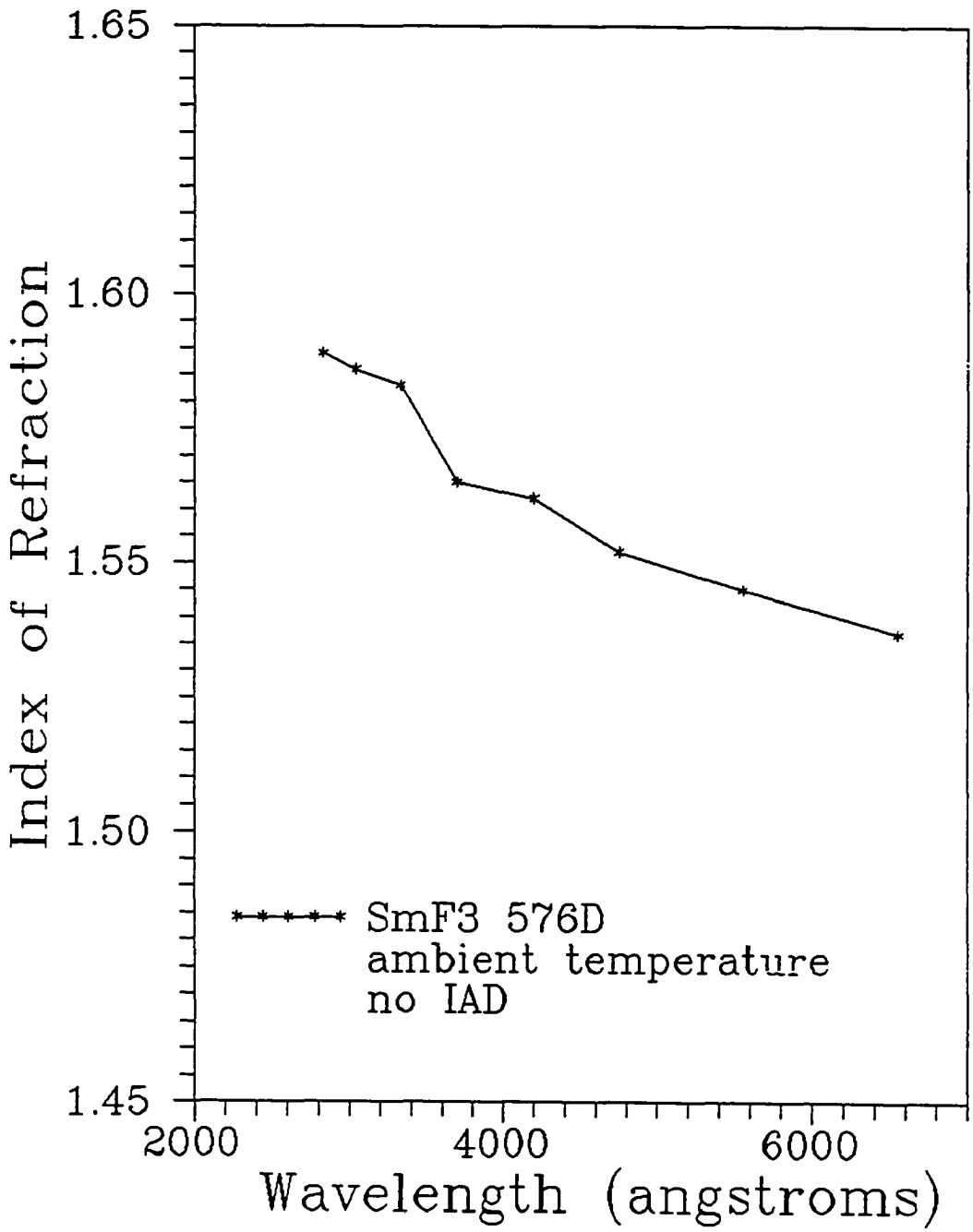


Figure 6.42. Samarium Trifluoride refractive index.

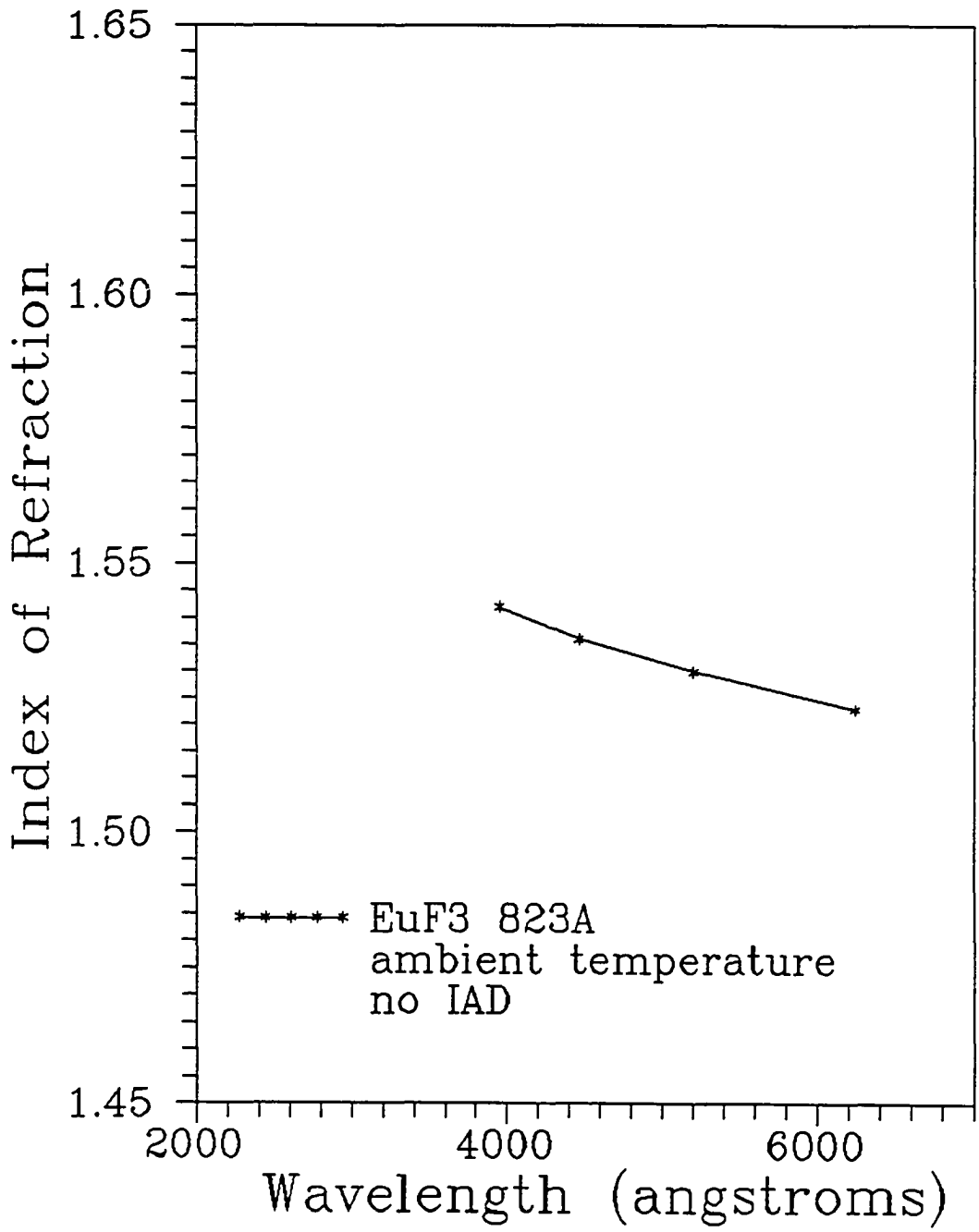


Figure 6.43. Europium Trifluoride refractive index.

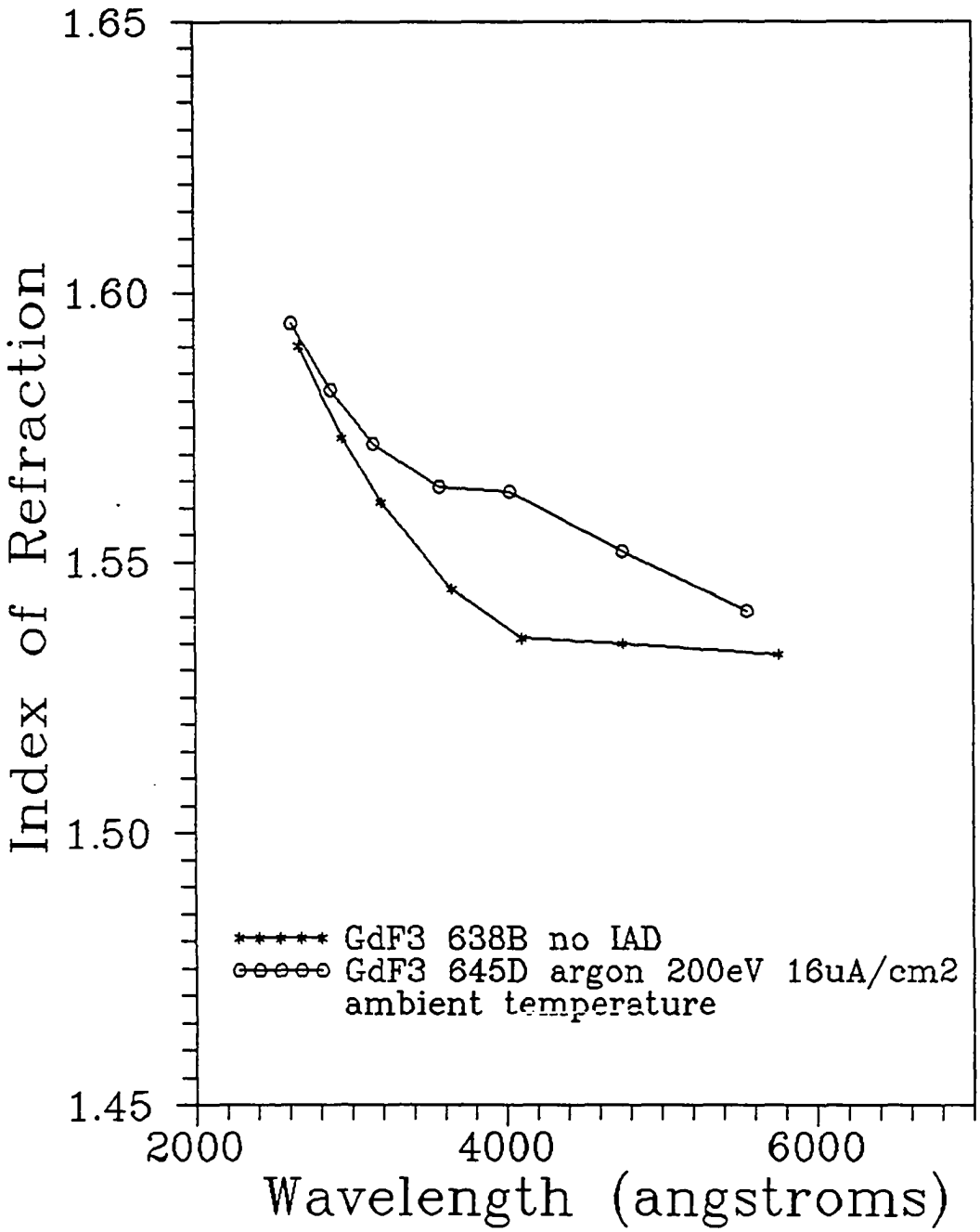


Figure 6.44. Gadolinium Trifluoride refractive index.

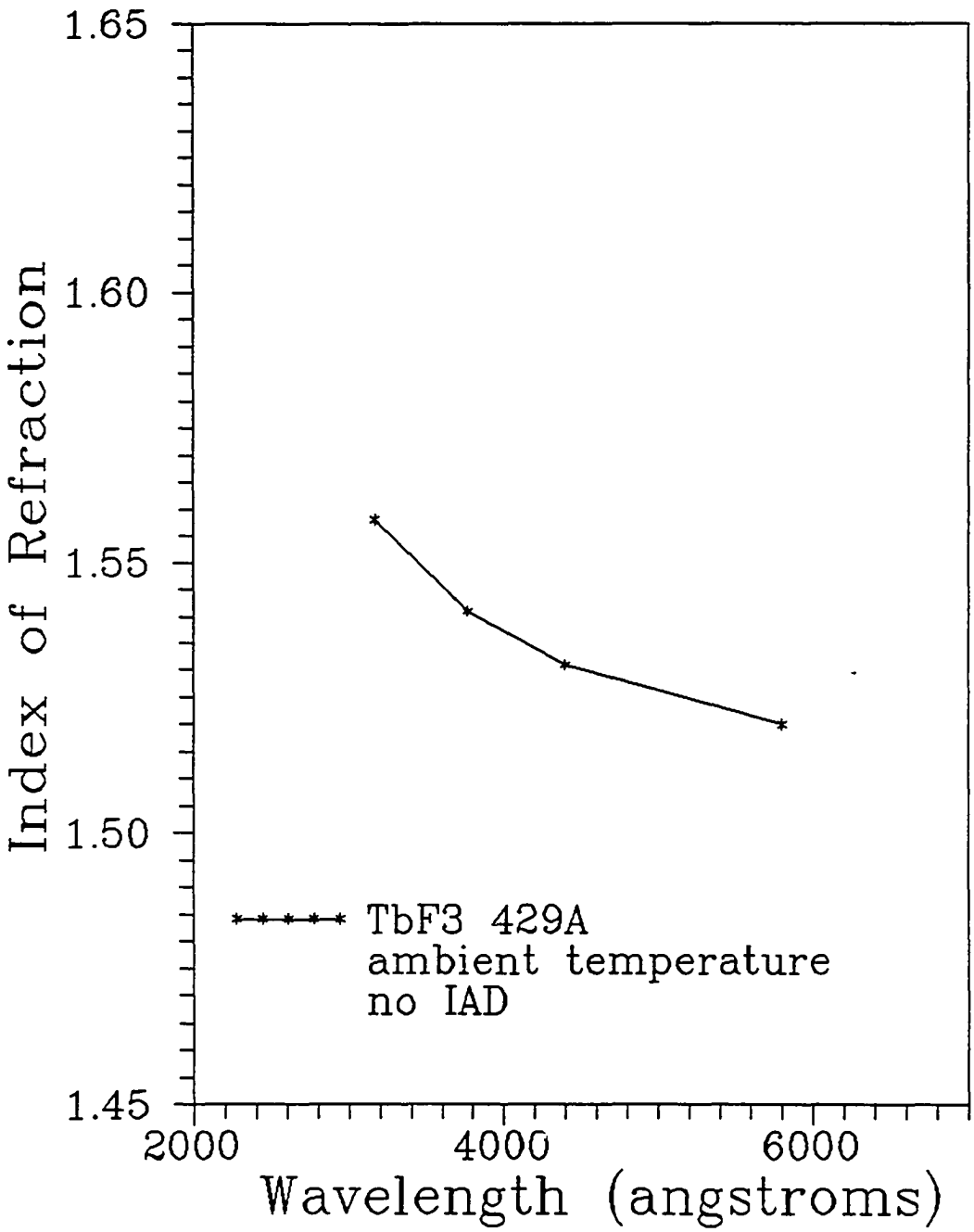


Figure 6.45. Terbium Trifluoride refractive index.

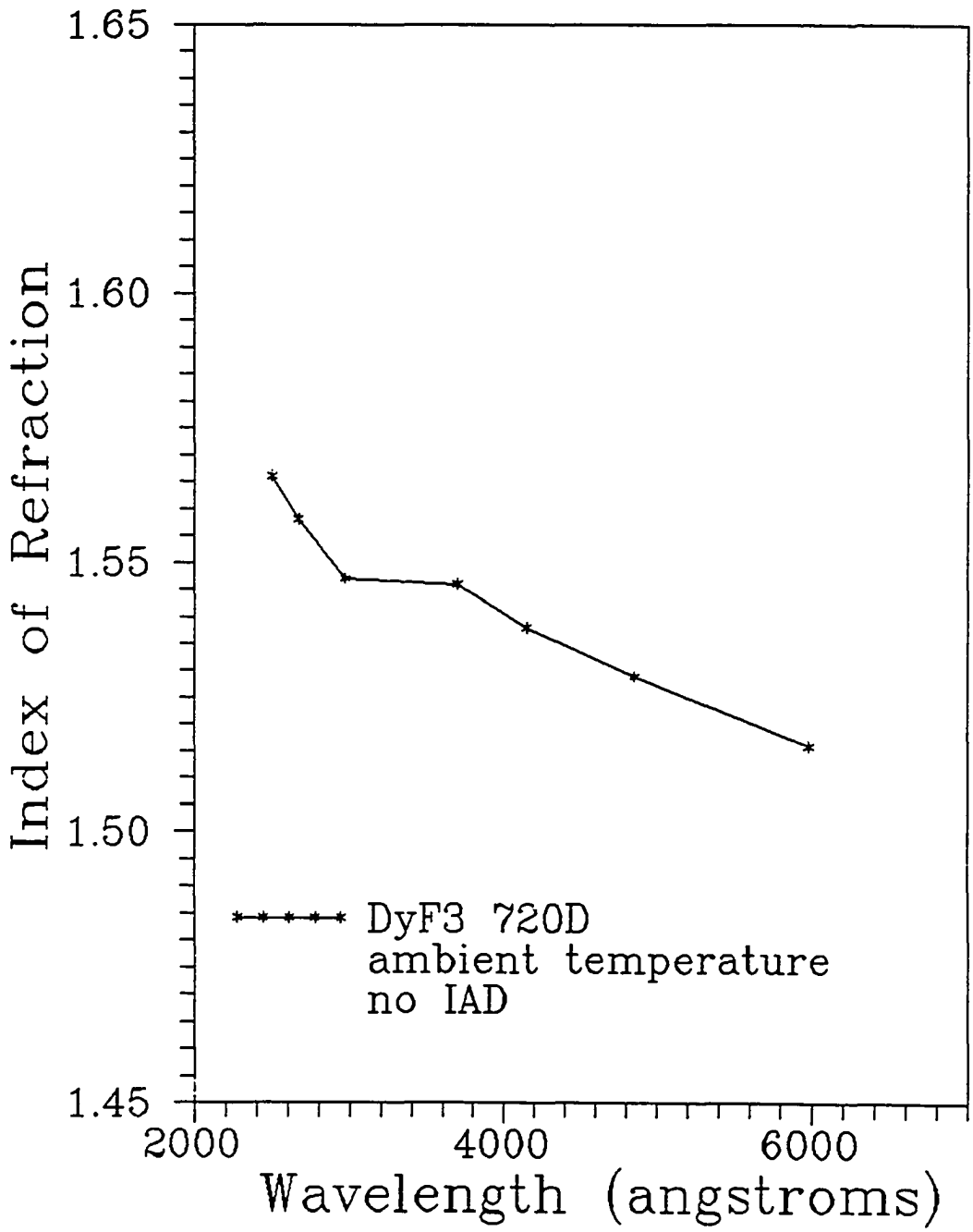


Figure 6.46. Dysprosium Trifluoride refractive index.

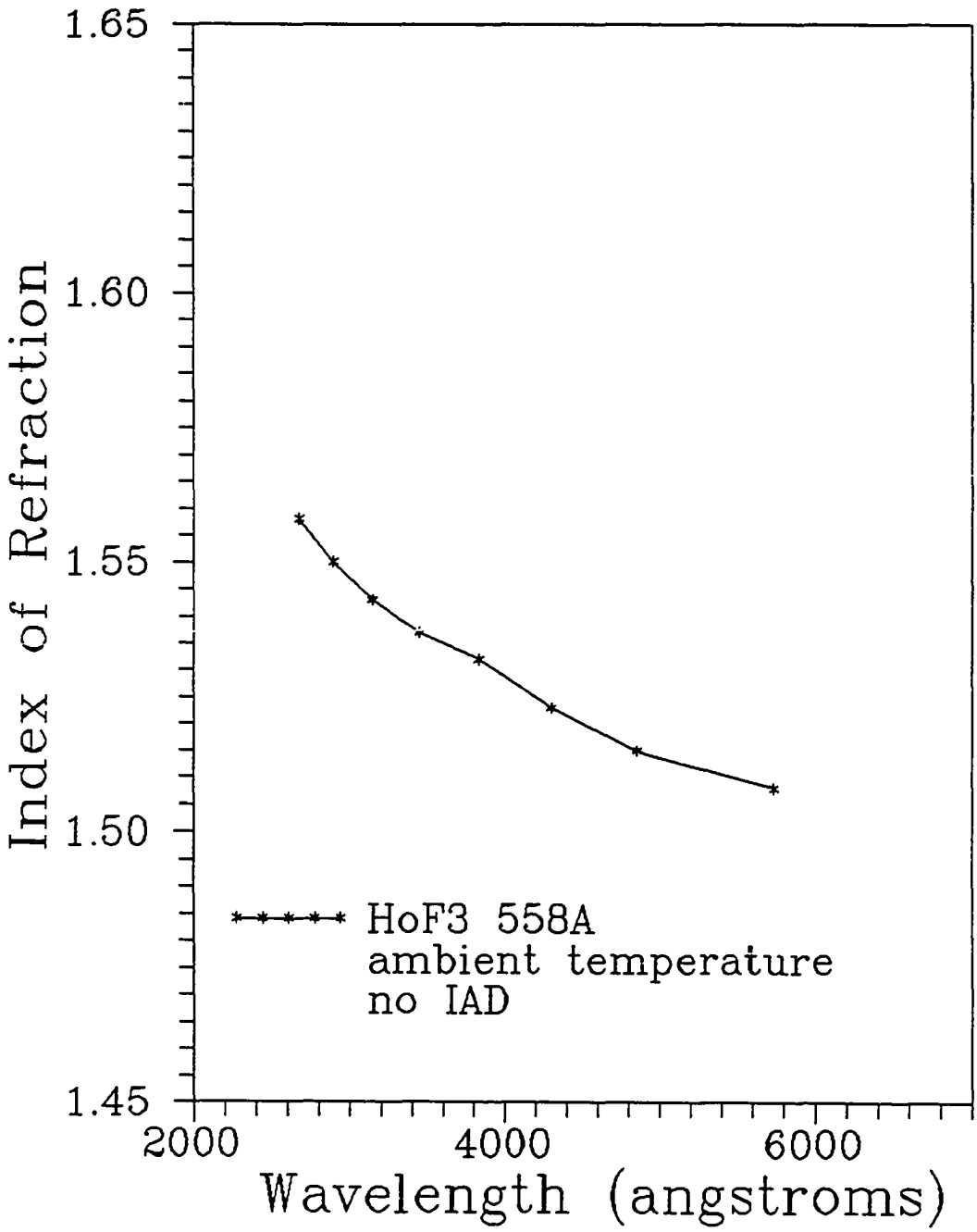


Figure 6.47. Holmium Trifluoride refractive index.

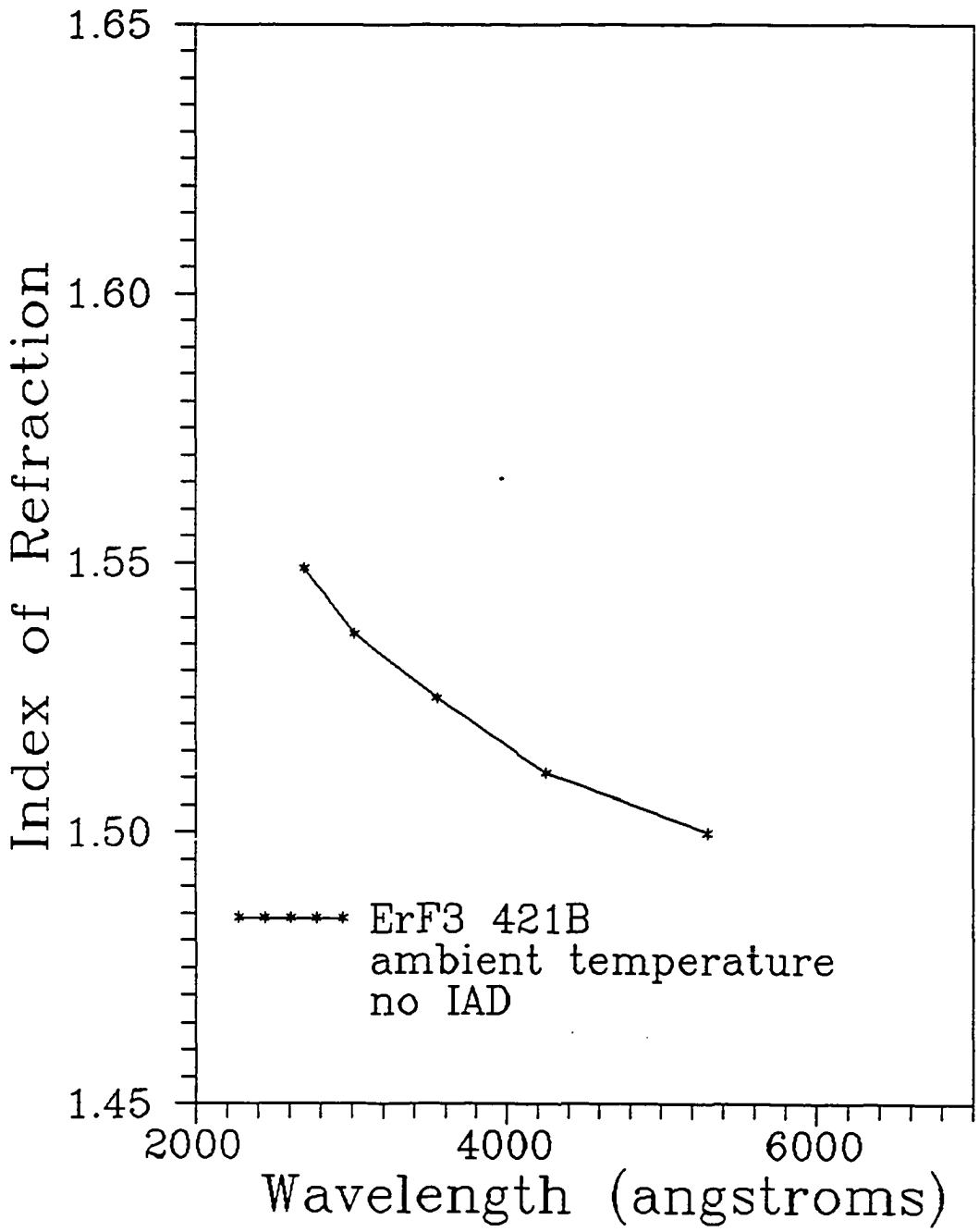


Figure 6.48. Erbium Trifluoride refractive index.

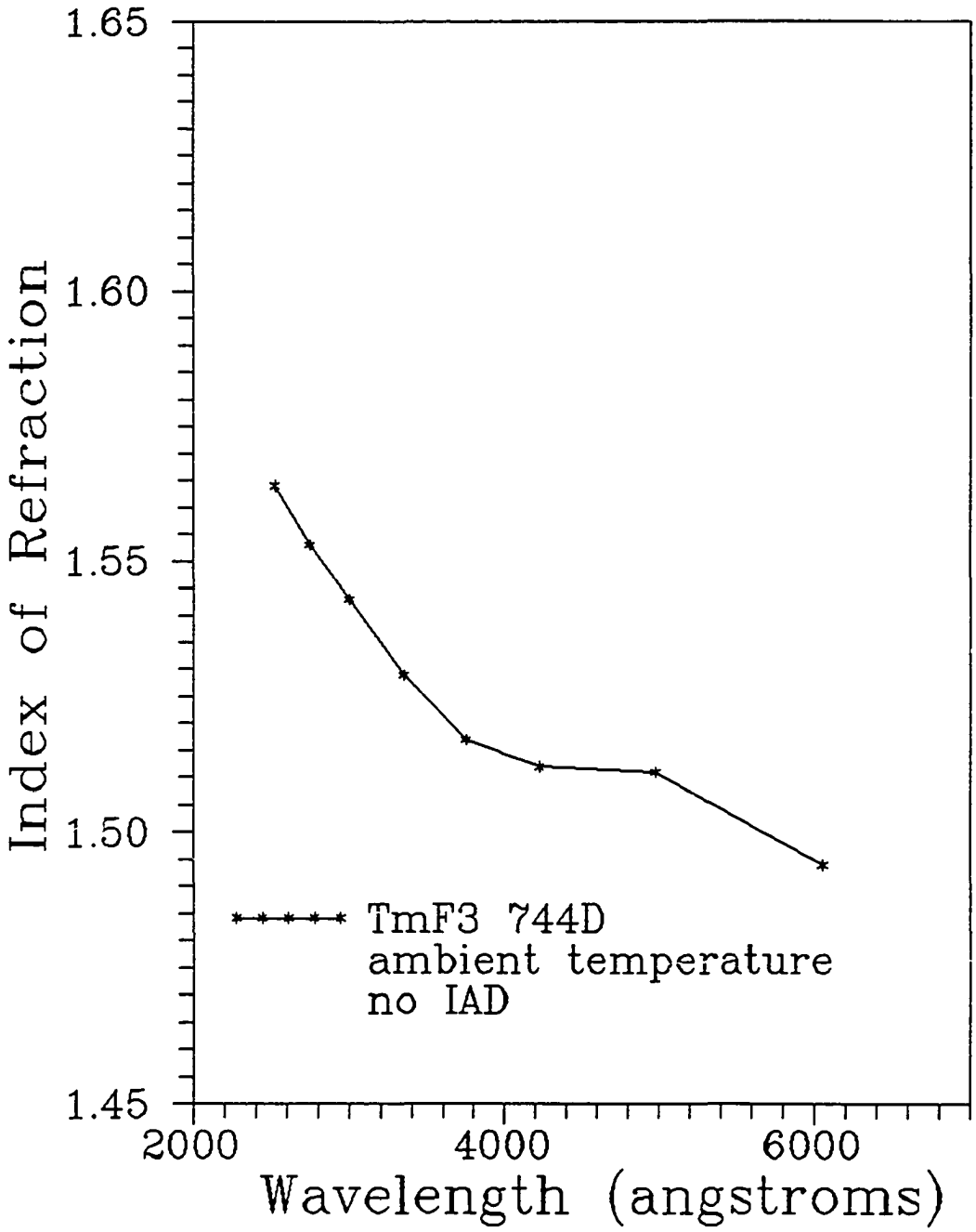


Figure 6.49. Thulium Trifluoride refractive index.

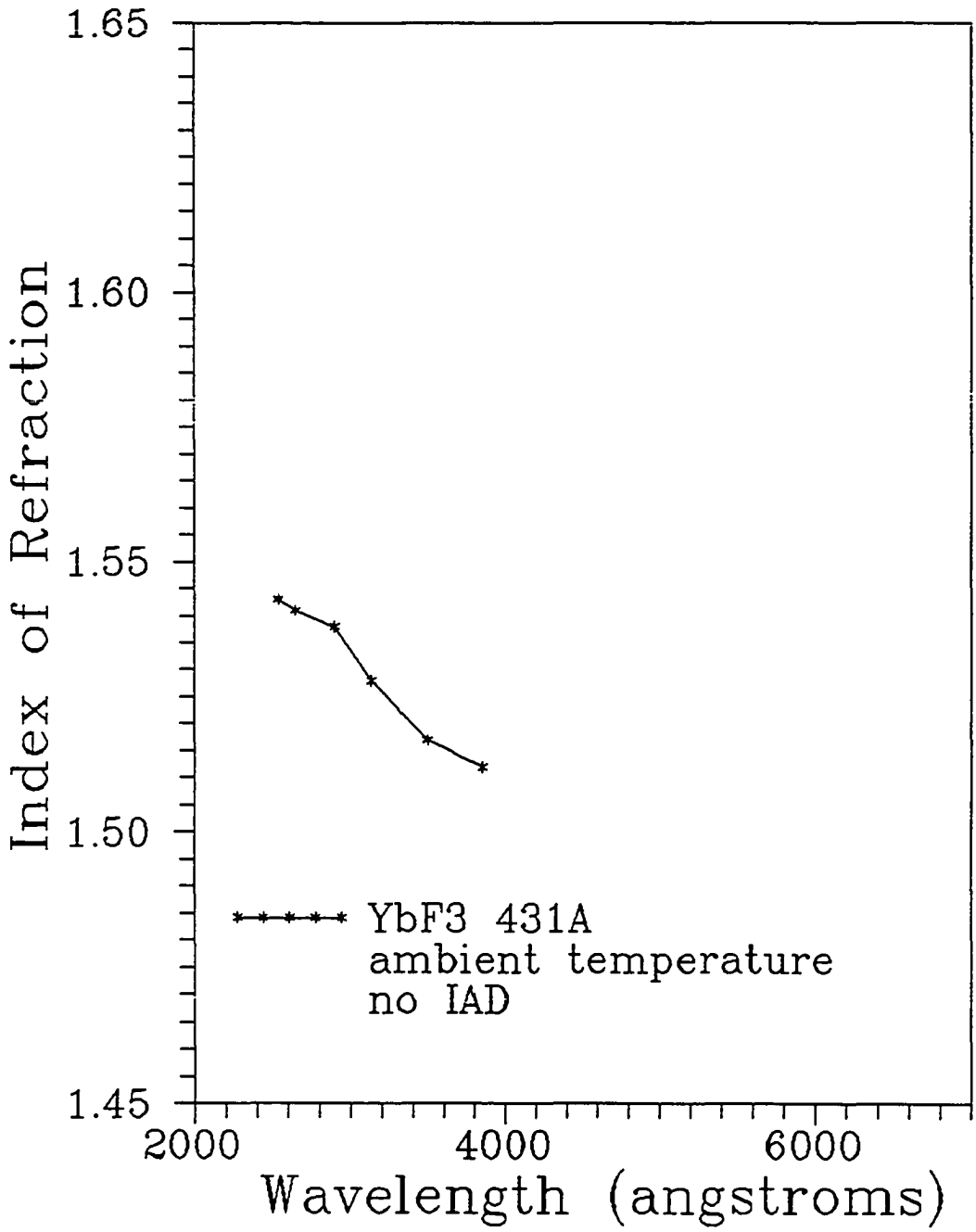


Figure 6.50. Ytterbium Trifluoride refractive index.

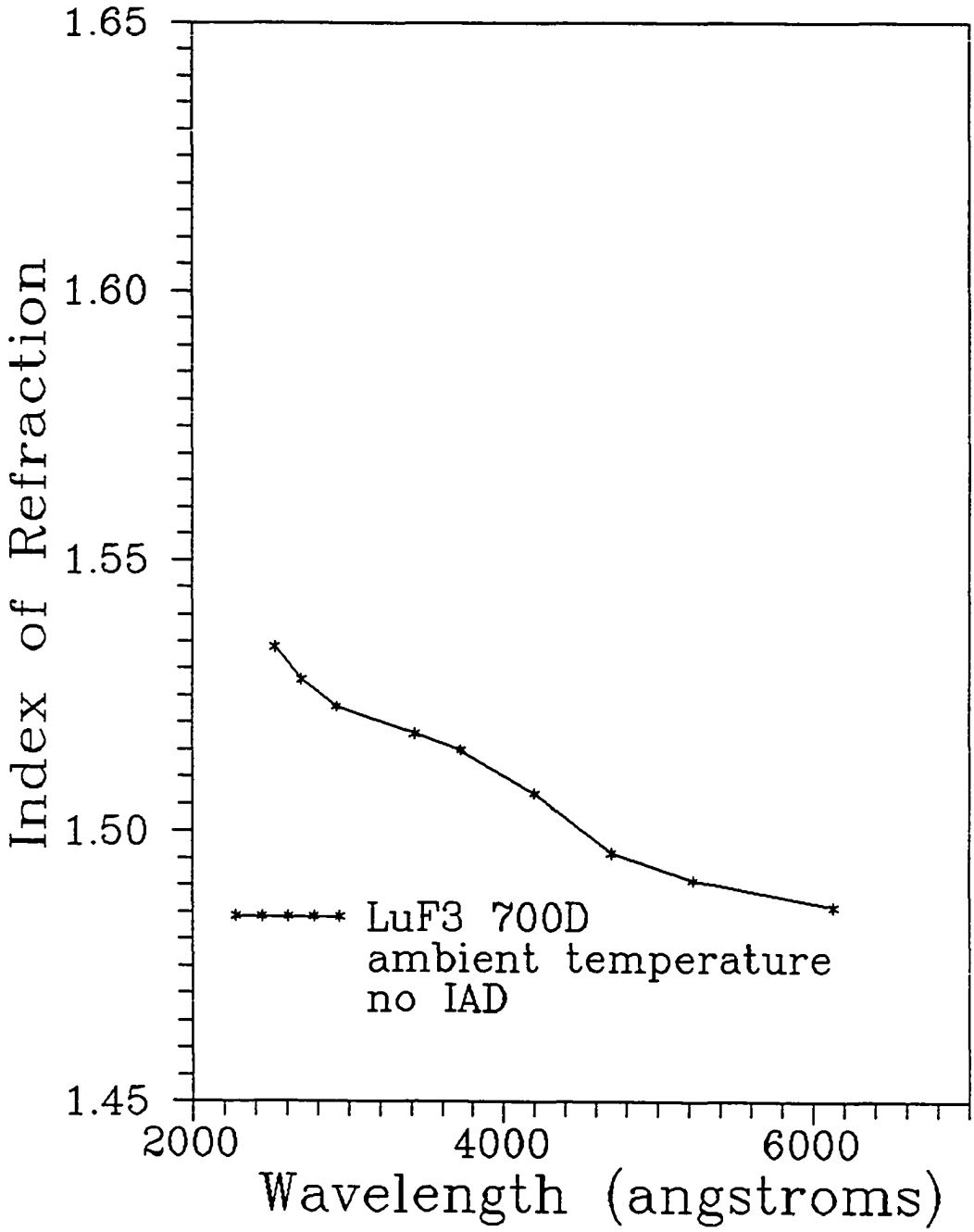


Figure 6.51. Lutetium Trifluoride refractive index.

Durability

All of the coatings, conventional and IAD, of all the materials except $TbF_3$, passed the Mil-Spec-M-13508C test; that is, 24 hours at 95% humidity and 45°C without deterioration.

Discussion

We have measured the optical transmittance, and by inference the reflectance, of thin films of $LnF_3$. High transmittance over an extremely large wavelength range makes these materials viable as optical coatings in regions of the spectrum where there are not many choices. We have correlated the optical properties with some of the measured thin film physical properties, e.g., the influence of the lanthanide contraction on the fundamental absorption edge. We were able to catagorize absorption bands by grouping Ln's according to their valencies.

The $LnF_3$ have the widest transmission range of any optical coating material (Pulker 1984) presently in use. We have shown that the $LnF_3$ can be evaporated sucessfully with conventional techniques and equipment. The resulting coatings are durable and exhibit desirable optical transmittance and refractive index. While $GdF_3$ and $LuF_3$ are optically the best materials, $LuF_3$ is the most expensive. This work has increased the choices for components of multilayer optical coatings and in some cases (VUV and IR) doubled the choices.

We have used the $LnF_3$ to explore the effects of different deposition processes on ionic fluoride compounds. The effect of high temperature deposition on optical properties is to cause inhomogeneity. Using our results from chapter four, we explained this as a structural effect. Using our composition results from chapter four we explained the increase in VUV transmittance with temperature as an

artifact of a cleaner vacuum system.

We found that the most sensitive technique of the ones used here for detection of fluorine deficiency was optical transmittance, although proof that preferential fluorine sputtering was occuring in $SmF_3$ was provided by RBS and XRD. We found the onset of fluorine deficiency occured at an incident ion energy of 50 eV and a current density of $\frac{10\mu A}{cm^2}$. We obtained optical corroboration for our previous results on the effect of current density and ion energy on thin films. Again the current density is the dominant variable.

From our IR data, we ascertained that the amount of $OH^-$ in the films decreased when IAD was used. It also decreased when films were deposited at high temperature. This is similar to the effect Targove explained as an increase in packing density. We got an increase in refractive index with IAD but also an increase in UV absorption. The UV absorption can be split into two parts, fluorine deficiency and oxygen inclusion. Using the multivalent metal Sm for the cation, we were able to separate the phenomena of oxygen inclusion from fluorine deficiency; an advantage which is not possible for trivalent metals such as Gd (results not shown here) or La (Targove 1987). The optical transmittance of a slightly fluorine deficient film will show the typical absorption bands in the UV but the shortest wavelength fringe will go back up to the substrate line. When oxygen is included in the film, that fringe will also begin to dip in transmittance. That is the first example we have seen of the separation of the two effects. It is the basis of our reasoning that increasing refractive index is not solely due to packing density. This conclusion is supported by the annealing results showing the different transmittance profiles of the SmOF and $SmF_2$ and $SmF_3$.

# CHAPTER 7

# CONCLUSIONS

We have already discussed many specific conclusions about our experiments in the previous chapters. Here I will attempt to draw general conclusions about the whole body of work presented in this document. I will also present suggestions for experiments which naturally follow from our work, which we do not have the resources to complete ourselves.

The first contribution we have made was to systematically tie together the principles of physics and materials science and the technology of optical coatings. We used the series of $LnF_3$ to clearly illustrate and separate the effects of electronic structure, ionic radius, and deposition processes on thin films of $LnF_3$. We have showed how to use bulk phase diagrams to predict thin film structure. We have demonstrated that the series of $LnF_3$ thin films derive their structure from obeying Ostwald's rule.

We are the first to evaluate the performance of these eleven $LnF_3$ as optical coating materials. We demonstrate that these materials have desirable optical coating properties and thus have increased the materials options for coating engineers. In fact we have doubled the choices for coating materials in the VUV and IR.

We have performed an in-depth study of the effects of IAD on $LnF_3$ thin film structure, composition, and optical properties and a comparison with temperature

effects. We have evidence to back up the statement that oxygen in these films has little effect on structure but quite a large effect on optical properties. We conclude that packing density within columns reaches a constant value with regard to IAD and leaves the material in a metastable state.

An experiment we would like to try is to study the effect of IAD on stoichiometry as a function of atomic number. The study might be more useful for people intending to sputter these materials since the main effect of IAD would be to preferentially sputter fluorine. Two effects relevant to the final stoichiometry are the masses of the cation and anion and the tendency of some Ln's in the series toward divalency.

Perhaps the most interesting and challenging problem is a continuation of the growth study relating preferred orientation of crystallites to resulting stress in the films. The most obvious difficulty being the relation of crystal structure to microstructure. It is particularly desirable since the study can be done with x-ray diffraction, a simple technique and accessable for many.

Research into the behavior of the materials is interesting in itself. But for some investigators the potential application of these materials to multilayer coatings of various design and to other optical devices such as $LnF_3$-LnOF rugate filters, waveguides including nonlinear and doped ones, is the most exciting thing about them. There is also the open area of $Ln_a$ -$Ln_b$ -$Ln_c$-$F_3$ films. These are analagous to the multi-component glasses developed to have tailored optical and mechanical properties. One might solve the problem of stress in the fluorides without getting the phase separation that restricts materials such as ZBLAN which are made up of incompatible fluorides.

## LIST OF REFERENCES

Afanasiev, M. L., S. P. Habuda, and A. G. Lundin, "The symmetry and basic structures of $LaF_3$, $CeF_3$, $PrF_3$, and $NdF_3$," Acta. Crystallog. B 28 (1972) 2903.

Allen, T. H., "Properties of ion assisted deposited silica and titania films," Proc. SPIE 325 *Optical Thin Films* (1982) 93.

Amra, C., P. Roche, and E. Pelletier, "Interface roughness cross-correlation laws deduced from scattering diagram measurements on optical multilayers: effect of the material grain size," J. Opt. Soc. Am. B 4 (1987) 1087.

Anderson, J. S., "Current Problems in Nonstoichiometry" in *Advances in Chemistry Series Number 39: Nonstoichiometric Compounds*, ACS, Wash., DC, 1963, page 1.

Baer, Y. and G. Busch, "X-ray photoemission study of the outermost levels of the rare earth metals," J. Elec. Spect. Rel. Phen. 5 (1974) 611.

Baldini, G. and L. Rigaldi, "Thin films in vacuum ultraviolet spectroscopy," Thin Solid Films 13 (1972) 143.

Barninghausen, H., "Kristallchemische studien an seltenerd-dihalogeniden die Kristallstruktur von Europium (II)-Chlorid," Revue de Chimie Minerale 10 (1973) 77.

Baumeister, P. and O. Arnon, "Use of hafnium dioxide in multilayer dielectric reflectors for the near uv," Appl. Opt. 16 (1977) 439.

Becher, J., R. L. Kernell and C. S. Reft, "Proton-induced F-centers in LiF and $MgF_2$," J. Phys. Chem. Solids 44 (1983) 759.

Bedford, R. G. and E. Catalano, "A study of the binary systems $SmF_2$-$SmF_3$, $EuF_2$-$EuF_3$, and $YbF_2$-$YbF_3$ and their equilibria with corresponding Ln-Pt systems," Proc. Eighth Rare Earth Res. Conf., Reno, Volume 1, page 388.

Bennett, H. E. and J. M. Bennett, "Precision measurements in thin film optics", *Physics of Thin Films*, G. Hass and R. E. Thun, eds., Academic Press, New York, 1967, p.12.

Black, P. W. and J. Wales, "Materials for use in the fabrication of infrared interference filters," Infrared Physics 8 (1968) 209.

Blodgett, A. J. Jr., W. E. Spicer, and A. Y.-C. Yu, "The band structure of gadolinium: Photoemission and optical studies," *Optical Properties and Electronic Structure of Metals and Alloys*, Proc. Int. Colloq., F. Abeles,ed. Paris 13-16 Sept. 1965 p.246 North Holland, Amsterdam, Wiley, New York (1966).

Briggs, D., *Handbook of X-ray and ultraviolet photoelectron spectroscopy*, Heyden and Son Ltd., London, 1977, page 1.

Brinkman, J. A., "Production of atomic displacements by high-energy particles," Am. J. Phys. 24 (1956) 246.

Brinkman, J. A., "On the nature of radiation damage in metals," J. Appl. Phys. 25 (1954) 961.

Brown, D., *Halides of the Transition Elements: Halides of the Lanthanides and Actinides*, Wiley-Interscience, London, 1968.

Brown, F. C. "Ultraviolet spectroscopy of solids with the use of synchrotron radiation" from *Solid State Physics*, 29 (1974) 1.

Buckel, W., "Internal stresses," J. Vac. Sci. Technol. 6 (1969) 606.

Campagna, M., G. K. Wertheim and Y. Baer, "4. Unfilled Inner Shells: Rare Earths and Their Compounds," in *Topics In Applied Physics* 27 Photoemission in Solids II Case Studies, eds. Ley and Cardona, Springer-Verlag, New York, 1979.

Catalano, E., R. G. Bedford, V. G. Silveira, and H. H. Wickman, "Nonstoichiometry in rare-earth fluorides," J. Phys. Chem. Solids 30 (1969) 1613.

Christian, J. W., *An Advanced Textbook in Physical Metallurgy*, Oxford, NY, 1965.

Chu, W. K., J. W. Mayer, M. A. Nicolet, *Backscattering Spectrometry*, Academic Press, New York, 1978.

Cohen, R. L., G. K. Wertheim, A. Rosencwaig, H. J. Guggenheim, "Multiplet splitting of the 4s and 5s electrons of the rare earths," Phys. Rev. B 5 (1972) 1037.

Cotton F. A. and G. Wilkinson, *Advanced Inorganic Chemistry*, Wiley Interscience, 1972.

Crosswhite H. M. and H. W. Moos, eds., *Optical Properties of Ions in Crystals*, Wiley-Interscience, New York, 1967.

Daniels and Alberty, *Physical Chemistry*, Wiley, New York, 1972.

Dharmadhikari, V. S., "Conduction and dielectric polarization in neodymium fluoride thin films," J. Appl. Phys. 54 (1983) 4087.

Dickson, C. R. and R. N. Zare, "Beam-gas chemiluminescent reactions of Eu and Sm with $O_3$, $N_2O$, $NO_2$ and $F_2$," Chemical Physics 7 (1975) 361.

Dieke, G. H., H. M. Crosswhite, and B. Dunn, "Emission spectra of the doubly and triply ionized rare earths," J. Opt. Soc. Amer. 51 (1961) 820.

Dieke G. H. and H. M. Crosswhite, "The spectra of the doubly and triply ionized rare earths," Appl. Opt. 2 (1963) 675.

Dieke, G. H., *Spectra and Energy Levels of Rare Earth Ions in Crystals*, H. M. Crosswhite and H. Crosswhite, eds., Wiley-Interscience, New York, 1968.

Dimmock, J. O., A. J. Freeman, and R. E. Watson, "Electronic band structure and optical properties of rare-earth metals," *Optical Properties and Electronic Structure of Metals and Alloys*, Proc. Int. Colloq., F. Abeles, ed., Paris 13-16 Sept. 1965 p.237, North Holland, Amsterdam, Wiley, New York (1966).

Dzioba, S. and R. Kelly, "On the kinetic energies of sputtered excited particles II. Theory and applications to group IIA fluorides," Surface Science 100 (1980) 119.

Edgett, L. B. and Suzanne C. Stotlar, "Study of possible solarization-related impurities in $CaF_2$ and other fluorides," Proc. SPIE 540 Southwest Conference on Optics (1985) 134.

Eyring, L. and B. Holmberg, "Ordered Phases and Nonstoichiometry in the Rare Earth Oxide System," in *Advances in Chemistry Series Number 39: Nonstoichiometric Compounds*, ACS, Wash., DC, 1963, p.46.

French R. H., and R. L. Coble, "Temperature dependence of the VUV optical spectra and band structure of $Al_2O_3$," SP657.

Fritzsche, H., "What are Non-Crystalline Semiconductors," *Fundamental Physics of Amorphous Semiconductors*, F. Yonezawa,ed., Springer Series in Solid State Sciences 25, Springer-Verlag, Berlin 1981, p.1.

Gee, J. R., I. J. Hodgkinson, and H. A. Macleod, "Moisture-dependent anisotropic effects in optical coatings," Appl. Opt. 24 (1985) 3188.

Gibson, U. J. "Ion beam processing of optical thin films," *Physics of Thin Films* 13, M. H. Francombe, J. L. Vossen, Eds., Academic Press, New York, 1987.

Gloede, C., N. Kaiser, R. Mattheis, and H. Muller, "Ultraviolet losses in MgF2 thin films induced by the evaporation boat," Thin Solid Films 152 (1987) L139.

Gregson, D., C. R. A. Catlow, A. V. Chadwick, G. H. Lander, A. N. Cormack, and B. E. F. Fender, "The Structure of $LaF_3$ - A Single-Crystal Neutron Diffraction Study at Room Temperature," Acta Cryst.B 39 (1983) 687.

Greis O., and D. J. M. Bevan, "Electron Diffraction from $LaF_3$ Single Crystals," J. Solid State Chem. 24 (1978) 113.

Greis, O., "Uber neue Verbindungen im System $SmF_2$-$SmF_3$," J. Solid State Chemistry 24 (1978) 227.

Greis, O. and M. R. S. Cader, "Polymorphism of high-purity rare earth trifluorides," Thermochimica Acta 87 (1985) 145.

Greis O., and M. S. R. Cader, "Preparation and Characterization of Fluorite-Related Superstructure Phases $Sr_2RF_7$ with R=Sm-Lu and Y," J. Less-Common Metals 118 (1986) 21.

Grigorov G. I. and I. N. Martev, "Inert gas entrapment in films produced by ion-

assisted physical vapour deposition processes," Thin Solid Films **156** (1988) 265.

Gschneider, K. A. Jr., "On the nature of 4f bonding in the lanthanide elements and their compounds." J. Less-Common Metals **25** (1971) 405.

Gschneider, K. A. Jr., and L. Eyring, *Handbook on the Physics and Chemistry of Rare Earths*, North Holland, Amsterdam, 1982.

Hagstrom, S. B. M. "X-ray photoemission studies of valence electronic levels in solids," *Electron spectroscopy*, ed. D. A. Shirley, Worth, Amsterdam, 1972, p.515.

Hammamatsu Corporation, private commumication.

Hanak, J. J. and J. P. Pellicane, "Effect of secondary electrons and negative ions on sputtering of films," J. Vac. Sci. Technol. **13** (1976) 406.

Harper, J. M. E., J. J. Cuomo, and H. T. G. Hentzell, "Quantitative ion beam process for the deposition of compound thin films," Appl. Phys. Lett. 43 (1983) 547.

Harper, J. M. E., J. J. Cuomo, R. J. Gambino, and H. R. Kaufman, "Modification of thin film properties by ion bombardment during deposition," in *Beam Modification of Solids, 1: Ion Bombardment Modification of Surfaces Fundamentals and Applications*, Auciello and Kelly, eds., Elsevier, New York, 1984, p.127.

Harper, J. M. E., J. J. Cuomo, R. J. Gambino, H. R. Kaufman, "Modification of thin film properties by ion bombardment during deposition," Nuclear Instruments and Methods in Physics Research **B7/8** (1985) 886.

Hass, G., J. B. Ramsey, and R. Thun, "Optical properties and structure of cerium dioxide films," J. Opt. Soc. Amer. **48** (1958) 324.

Hass, G., J. B. Ramsey, and R. Thun, "Optical properties of various evaporated rare earth oxides and fluorides," J. Opt. Soc. Amer. **49** (1959) 116.

Hass, G. and W. R. Hunter, "New developments in vacuum-ultraviolet reflecting

coatings for space astronomy," in *Space Optics*, Thompson and Shannon, eds., National Academy of Science (1974) 525.

Heaps, W. S., L. R. Elias, and W. M. Yen, "Vacuum-ultraviolet absorption bands of trivalent lanthanides in $LaF_3$," Phys. Rev. B 13 (1976) 94.

Heden, P. O., H. Lofgren, and S. B. M. Hagstrom, "4f electronic states in the metals Nd, Sm, Dy, and Er studied by x-ray photoemission," Phys. Rev. Lett. 26 (1971) 432.

Herman, P. R., P. E. Larocque, R. H. Lipson, W. Jamroz, and B. P. Stoicheff, "Vacuum ultraviolet laser spectroscopy III: laboratory sources of coherent radiation tunable from 105 to 175 nm using Mg, Zn, and Hg vapors," Can. J. Phys. 63 (1985) 1581.

Herzig, H., B. K. Flint, and C. M. Fleetwood, Jr., "Broadband reflectance coatings for vacuum ultraviolet application," Appl. Opt. 26 (1987) 605.

Hildenbrand, D. L., "Mass-spectrometric studies of bonding in the group IIA fluorides," J. Chem. Phys. 48 (1968) 3657.

Hilsch R., and R. W. Pohl, "Einige Dispersionsfrequenzen der Alkalihalogenid-kristalle im Schumanngebiet," Z. Physik 59 (1930) 812.

Hippel, A. V. "Einege Prinzipielle Gesichtspunkte zur Spektroskopie der Ionenkristalle und ihre Anwendung auf die Alkalihalogenide," Z. Physik 60 (1931) 680.

Hirsch, E. H. and I. K. Varga, "The effect of ion irradiation on the adherence of germanium films," Thin Solid Films 52 (1978) 445.

Hirsch, E. H. and I. K. Varga, "Thin film annealing by ion bombardment," Thin Solid Films 69 (1980) 99.

Holloway P. H., and G. E. McGuire, "Chemical characterization of coatings by analytical techniques sensitive to the surface and near-surface," Thin Solid Films 53 (1978) 3.

Hunter, W. R. and S. A. Malo, "The temperature dependence of the short

wavelength transmittance limit of vacuum ultraviolet window materials-I. experiment," J. Phys. Chem. Solids **30** (1969) 2739.

Hunter, W. R., "The preparation and use of unbacked metal films as filters in the extreme ultraviolet," in Physics of Thin Films Volume 7, Academic Press, NY, 1973, p.43.

Hunter, W. R. "A review of vacuum ultraviolet optics," Proc. SPIE **140** *Optical Coatings - applications and Utilization II* (1978) 122.

Hunter, W. R., D. W. Angel, and G. Hass, "Optical properties of evaporated platinum films in the vacuum ultraviolet from 220 Å to 150 Å," J. Opt. Soc. Amer. **69** (1979) 1695.

Hunter, W. R. "Measurement of optical properties of materials in the vacuum ultraviolet spectral region," Appl. Opt. **21** (1982) 2103.

Hunter, W. R., "Measurement of optical constants in the vacuum ultraviolet spectral region," *Handbook of Optical Constants of Solids*, Academic Press, Inc., 1985, p. 69.

Hwangbo, C. K., L. J. Lingg, J. P. Lehan, H. A. Macleod, and F. Suits, "Reactive ion assisted deposition of aluminum oxynitride thin films" Appl. Opt. 28 (1989) 2779.

Ikeda, H., H. Akasaka, and Z. Wakimoto, "Multilayer antireflection coatings for ultraviolet (200-400 nm) and application," in *Space Optics* Thompson and Shannon, eds., National Academy of Sciences (1974) 554.

*International Tables for X-ray Crystallography, Vol.I, Symmetry Groups, Vol.II, Mathematical Tables, Vol.III, Physical and Chemical Tables*, Kynoch Press, Birmingham, England, Vol.I, 1952, Vol.II, 1959, Vol.III, 1962.

Jamroz, W., P. E. LaRocque, and B. P. Stoicheff, "Generation of continuously tunable coherent vacuum-ultraviolet radiation (140 to 106) in zinc vapor," Opt. Lett. 7 (1982) 617.

Joint Committee on Powder Diffraction Standards, Plates 5-517, 12-792, 27-1399, 27-581, 24-846, 17-281, 32-981, 34-1059, 34-1067, 34-1095, 34-1166, 11-412, 15-813, 15-244, 9-201.

Kato, R., K. Nakamura, A. Matsui, and Y. Uchida, "Reflection and absorption spectra of LiF in the extreme ultraviolet region," J. Phys. Soc. Japan 15 (1960) 2105.

Kato, R., S. Nakashima, K. Nakamura, and Y. Uchida, "Optical properties of irradiated LiF crystals in the extreme ultraviolet region," J. Phys. Soc. Japan 15 (1960) 2111.

Kelly, R., "The varieties of surface alteration: structural, topographical, electronic, and compositional," in *Beam Modification of Solids, 1: Ion Bombardment Modification of Surfaces Fundamentals and Applications*, Auciello and Kelly, eds., Elsevier, New York, 1984, p.79.

Kelly, R., "On the problem of whether mass or chemical bonding is more important to bombardment-induced compositional changes in alloys and oxides," Surface Science **100** (1980) 85.

Kingery, W. D., H. K. Bowen, D. R. Uhlmann, *Introduction to Ceramics*, Wiley, New York, 1976.

Kittel, C., *Introduction to Solid State Physics*, Wiley, New York, 1976.

Klinger, R. E. and C. K. Carniglia, "Crystalline phase inhomogeneity in thin zirconia films," (A) JOSA A 1 (1984) 1289.

Klug, H. P. and L. E. Alexander, *X-ray Diffrqction Procedures for Pclycrystalline and Amorphous Materials*, Wiley, New York, 1954.

Knyazev, Y. V. and M. M. Noskov, "The optical properties of rare earth metals," Phys. Stat. Sol. (b) **80** (1977) 11.

Kolopus, J. L., J. T. Lewis, W. P. Unruh, and L. G. Nelson, "The F centre in $MgF_2$. II: Optical absorption and epr," J. Phys. C: Solid St. Phys. **4** (1971) 3007.

Kondratyuk, I. P., A. A. Loshmanov, L. A. Murdyan, B. A. Maksimov, M. I. Sirota, E. A. Krivandina, and B. P. Sobolev, "Neutron-diffraction study on $NdF_3$," Sov. Phys. Crystallogr. **33** (1988) 57.

Kowalczyk, S. P., N. Edelstein, F. R. McFeely, L. Ley, and D. A. Shirley, "X-ray photoemission spectra of the 4d levels in rare-earth metals," Chem. Phys. Lett. 29 (1974) 491.

Krill, G., J. P. Senateur, and A. Amamov, "Valence Changes of Sm ions in SmS1-xPx, XPS and UPS Study," J. Phys. F 10 (1980) 1889.

Kunzmann, P. and L. Eyring, "On the crystal structures of the fluorite-related intermediate rare-earth oxides," J. Solid State Chem. 14 (1975) 229.

Laiho, R., M. Lakkisto, and T. Levola, "Brillouin Scattering Investigation of the Elastic Properties of $LaF_3$, $CeF_3$, $PrF_3$, and $NdF_3$," Phil. Mag. A 47 (1983) 235.

Laiho, R. and M. Lakkisto, "Investigation of the refractive indices of $LaF_3$, $CeF_3$, $PrF_3$, and $NdF_3$," Phil. Mag. B 48 (1983) 203.

Lammers, M. J. J. and G. Blasse, "Luminescence properties of rare-earth-activated gadolinium fluoride ($GdF_3$) and Oxyfluorides (GdOF)," Phys. Stat. Sol. (b) 127 (1985) 663.

Lang, W. C., B. D. Padalia, L. M. Watson, D. J. Fabian, and P. R. Norris, "Multiplet structure in x-ray photoelectron spectra of rare earth elements and their surface oxides," *Electron Spectroscopy of Solids and Surfaces*, Faraday Discussions of the Chemical Society 60 (1975) 37.

Laporte, P., J. L. Subtil, M. Courbon, M. Bon, and L. Vincent, "Vacuum-ultraviolet refractive index of LiF and $MgF_2$ in the temperature range 80-300K," J. Opt. Soc. Am. 73 (1983) 1062.

Leavitt, J. A., L. C. McIntyre, M. D. Ashbaugh, B. Dezfouly-Arjomandy, and J. G. Oder, "Characterization of optical coatings with backscattering spectrometry," Appl. Opt. 28 (1989) 2762.

Lingg, L. J., J. D. Targove, J. P. Lehan, and H. A. Macleod, "Ion-assisted deposition of lanthanide trifluorides for VUV applications," Proc. SPIE 818 *Current Developments in Optical Engineering II*, (1987) page 86.

Lingg, L. J., C. K. Hwangbo, B. G. Bovard, J. P. Lehan, H. A. Macleod, "Effect of ion-assisted deposition on the crystallinity of samarium fluoride films," in Optical Society of America 1988 Technical Digest Series Vol. 6, *Optical*

*Interference Coatings*, p.276.

Lowdermilk, W. H. and D. Milam, "Review of ultraviolet damage threshold measurements at Lawrence Livermore National Laboratory," Proc. SPIE 476 *Excimer Lasers, Their Applications, and New Frontiers in Lasers* (1984) 143.

Lowndes, R. P., J. F. Parrish, and C. H. Perry, "Optical phonons and symmetry of tysonite lanthainde fluorides," Phys. Rev., 182 (1969) 913.

Macleod, H. A., "Structure-related optical properties of thin films," J. Vac. Sci. Technol. A 4 (1985) 418.

Macleod, H. A., " Thin-film optical coatings," *Applied Optics and Optical Engineering*, Vol. X, Academic Press, Inc., New York, 1987, p.1.

Madden, R. P. "Preparation and measurement of reflecting coatings for the vacuum ultraviolet," *Physics of Thin Films* 1, G. Hass, ed., Academic Press (1963) p.123.

Mann, A. W., "Structural relationships and mechanisms for the stoichiometry change from $MX_3$ ($YF_3$-type) through $MX_2$ (fluorite-type) to $M_2X_3$ (C-type sesquioxide)," J. Solid State Chem. 11 (1974) 94.

Mansmann, M., "Die kristallstrukture von lanthantrifluorid," Z. fur Kristallographie 122 (1965) 375.

Marcinow, T., and K. Truszkowska, "Rare earth oxide films: their preparation and optical properties, " Appl. Opt. 20 (1981) 1755.

Markham, J. J., *F-Centers in Alkali Halides, Solid State Physics Advances in Research and Applications Supplement 8*, F. Seitz and D. Turnbull, eds., Academic Press, New York, 1966, page 3.

Martin, P. J., "Review of ion-based methods for optical thin film deposition," J. Materials Science 21 (1986) 1.

Martin, P. J., H. A. Macleod, R. P. Netterfield, C. G. Pacey, and W. G. Sainty, "Ion-beam-assisted deposition of thin films," Appl. Opt. 22 (1983) 178.

Martin, P. J., W. G. Sainty, R. P. Netterfield, D. R. McKenzie, D. J. H. Cockayne, S. H. Sie, O. R. Wood, H. G. Craighead, "Influence of ion assistance on the optical properties of $MgF_2$," Appl. Opt. 26 (1987) 1235.

Martin, P. J. and R. P. Netterfield, "Optical films produced by ion-based techniques," *Progress in Optics* 23, E. Wolf, ed., Elsevier Science Publishers B. V., 1986, p.115.

Martin, P. J., R. P. Netterfield, W. G. Sainty, G. J. Clark, W. A. Lanford, S. H. Sie, "Ion-assisted deposition of bulklike ZrO2 films," Appl. Phys. Lett. 43 (1983) 711.

Martin, P. J., R. P. Netterfield, W. G. Sainty, "Modification of the optical and structural properties of dielectric ZrO2 films by ion-assisted deposition," J. Appl. Phys. 55 (1984) 235.

McCarthy, D. E., "Transmittance of optical materials from 0.17 $\mu$ to 3.0 $\mu$," Appl. Opt. 6 (1967) 1896.

Messerly, M. J., Ph. D. dissertation, University of Arizona, 1987.

Messier, R., A. P. Giri, and R. A. Roy, "Revised structure zone model for thin film physical structure," J. Vac. Sci. Technol. A 2 (1984) 500.

Movchan, B. A. and A. V. Demchishin, "Study of the structure and properties of thick vacuum condensates of nickel, titanium, tungsten, aluminum oxide and zirconium dioxide," Fiz. Met. Metalloved. 28 (1969) 653.

Muller, K. H., "Model for ion-assisted thin-film densification," J. Appl. Phys. 59 (1986) 2803.

Muller, K. H., "Role of incident kinetic energy of adatoms in thin film growth," submitted to Surface Science Letters.

Muller, K. H., "Ion-beam-induced epitaxial vapor-phase growth: a molecular-dynamics study," Phys. Rev. B, 35 (1987).

Muller, K. H., R. P. Netterfield, and P. J. Martin, "Dynamics of zirconium oxide thin-film growth and ion-beam etching," Phys. Rev. B, 35 (1987) 103.

Naguib and R. Kelly, "Criteria for bombardment-induced structural changes in non-metallic solids," Radiation Effects 25 (1975) 1.

Netterfield, R. P., "Ion-assisted processes in optical thin film deposition," Proc. SPIE 678 *Optical Thin Films II: New Developments* (1986) 14.

Nisar, M., A. Roth, G. Stephan, and S. Robin, "Far ultraviolet reflectance spectra of $CeF_3$, $PrF_3$, and $NdF_3$," Opt. Comm. 8 (1973) 254.

Nowick, A. S. and S. Mader, "Effect of Substrate Temperature on Structure of Evaporated Alloy Thin Films," in International Symposium on Basic Problems in Thin Film Physics, R. Niedermayer and H. Mayer, eds., Gottingen, Vandenhoeck, and Ruprecht, Gottingen, 1966, p.212.

O'Keeffe, M. and B. G. Hyde, "Relationships between the structures of the rare earth fluorides and high chalcocite $Cu_2S$. Implications for solid electrolyte Behavior," J. Solid State Chem. 13 (1975) 172.

Olson, C. G., M. Piacentini, and D. W. Lynch, "Optical properties of single crystals of some rare-earth trifluorides, 5-34 eV," Phys. Rev. B 18 (1978) 5740.

Padalia, B. D. and D. J. Fabian, "On the location of unoccupied 4f states in rare earth metals," J. Phys. F: Metal Phys. 4 (1974) L179.

Page, L. J. and E. H. Hygh, "Calculation of energy bands in alkali halides," Phys. Rev. B 1 (1970) 3472.

Palik, E. D., "Status of optical constants of solids from x-ray to mm-wave region," SP.657.

Pauling, L., *Nature of the Chemical Bond*, Cornell Univ. Press, Ithica, 1960.

Pawlewicz, W. T., "Optical coating materials for the ultraviolet - selection and characterization," Proc. SPIE 476 *Excimer Lasers, Their Applications, and New Frontiers in Lasers* (1984) 163.

Pouey, M. and A. Malherbe, "Set up for filter and mirror efficiencies measurements in the UV and VUV spectral range," Proc. SPIE 652 *Thin Film Technologies*

*II* (1986) 113.

Pulker, H. K., "Characterization of optical thin films," Appl. Opt. 18 (1979) 1969.

Pulker, H. K., *Coatings on Glass*, Elsevier, Amsterdam, 1984, page 96.

Quemerais, A., B. Loisel, G. Jezequel, J. Thomas, and J. C. Lemonnier, "Optical spectra of gadolinium and dysprosium: study of the 5p thresholds," J. Phys. F: Metal Phys. 11 (1981) 293.

Raine, K. W.,"Anomalous optical absorption in dielectric thin films deposited by electron bombardment," Thin Solid Films 38 (1976) 323.

Rainer, F., W. H. Lowdermilk, D. Milam, C. K. Carniglia, T. Tuttle Hart, and T. L. Lichtenstein, "Materials for optical coatings in the ultraviolet," Appl. Opt. 24 (1985) 496.

Rast, H. E., H. H. Caspers, S. A. Miller, and R. A. Buchanan, "Infrared dispersion and lattice vibrations of $LaF_3$," Phys. Rev. 71 (1968) 1051.

Ritter, E. "Optical film materials and their applications," Appl. Opt. 15 (1976) 2316.

Sachtler, W. M. H., G. J. H. Dorgelo, and R. Jongepier, "Alloy Phases in Copper-Nickel Films Experimental Results and Thermodynamic Calculations," in International Symposium on Basic Problems in Thin Film Physics, R. Niedermayer and H. Mayer, eds., Gottingen, Vandenhoeck, and Ruprecht, Gottingen, 1966, p.218.

Sainty, W. G., R. P. Netterfield, and P. J. Martin, "Protective dielectric coatings produced by ion-assisted deposition," Appl. Opt. 23 (1984) 1116.

Saxe, S. G., M. J. Messerly, B. Bovard, L. DeSandre, F. J. Van Milligen, and H. A. Macleod, "Ion bombardment-induced retarded moisture adsorption in optical thin films," Appl. Opt. 23 (1984) 3633.

Schlesinger, M. and T. Szczurek, "Vacuum ultraviolet spectra of $CaF_2$:$Eu^{+3}$ and $CaF_2$:$Sm^{+3}$," J. Opt. Soc. Am. 70 (1980) 1025.

Schneider, E. G. and H. M. O'Bryan, "The absorption of ionic crystals in the ultraviolet," Phys. Rev. 51 (1937) 293.

Schuler, C. C. "Recent studies on the optical properties of rare-earth metals," *Optical Properties and Electronic Structure of Metals and Alloys*, Proc. Int. Colloq., F. Abeles,ed., Paris 13-16 Sept. 1965 p.221, North Holland, Amsterdam, Wiley, NY (1966).

Scott, M. L., "A review of UV coating material properties," in *Laser Induced Damage in Optical Materials: 1983 NBS Special Publication 688.*

Segmuller, A. and M. Murakami, "Characterization of Thin Films by X-Ray Diffraction," in *Thin Films from Free Atoms and Particles*, Kenneth J. Klabunde, ed., Academic Press, New York, 1985, p.325.

Seitz, F. and J. S. Koehler, "Displacment of Atoms during Irradiation," *Solid State Physics* 4, Seitz and Turnbull, eds., Academic Press, New York, p.305.

Sibley, W. A. and O. E. Facey, "Color centers in $MgF_2$," Phys. Rev. 174 (1968) 1076.

Signorelli, A. J. and R. G. Hayes, "X-ray spectroscopy of various core levels of lanthanide ions: the roles of monopole excitation and electrostatic coupling," Phys. Rev. B (1973) 81.

Sinha, S. P., *Complexes of the Rare Earths*, Pergamon Press, Oxford, 1966.

Sinha, S. P., ed., Proceedings of the NATO Advanced Study Institute on "Systematics and the Properties of the Lanthanides", Braunlage, Germany July 11-25, 1982, D. Reidel Publishing, Dordrecht, 1983.

Smith, D. and P. Baumeister, "Refractive index of some oxide and fluoride coating materials," Appl. Opt. 18 (1979) 111.

Smith, P. L., W. H. Parkinson, J. E. G. Wheaton, A. P. Thorne, and C. J. Harris, "Imaging, high-resolution, vacuum ultraviolet spectrometer," Proc. SPIE 687 *Ultraviolet Technology* (1986) 81.

Smoluchowski, R., "Radiation Effects in Dielectric Solids," in *Effects of Radiation on*

*Materials*, J. J. Harwood, H. H. Hauser, J. G. Morse, and W. G. Rauch, eds. Reinhold Publishing Co., New York, 1958, p.144.

Sobolev, B. P., P. P. Fedorov, D. B. Shteynberg, B. V. Sinitsyn, and G. S. Shakhkalamian, "On the problem of polymorphism and fusion of lanthanide trifluorides. I. The influence of oxygen on phase transition temperatures," J. Solid State Chem. 17 (1976) 191.

Sobolev, B. P., P. P. Fedorov, K. B. Seiranian, and N. L. Tkachenko, "On the problem of polymorphism and fusion of lanthanide trifluorides. II.Interaction of $LnF_3$ with $MF_2$ (M=Ca,Sr,Ba), change in structural type in the $LnF_3$ series, and thermal charactreistics," J. Solid State Chem. 17 (1976) 201.

Spedding, F. H., and A. H. Daane, *The Rare Earths*, Wiley, New York, 1961.

Spedding, F. H., and D. C. Henderson, "High temperature heat contents and related thermodynamic functions of seven trifluorides of the rare earths: Y, La, Pr, Nd, Gd, Ho, and Lu," J. Chem. Phys. 54 (1971) 2476.

Spedding, F. H., B. J. Beaudry, D. C. Henderson, and J. Moorman, "High temperature enthalpies and related thermodynamic functions of the trifluorides of Sc, Ce, Sm, Eu, Gd, Tb, Dy, Er, Tm, and Yb," J. Chem. Phys. 60 (1974) 1578.

Staritzky, E. and L. B. Asprey, "Crystallographic Data: 154.Yttrium Trifluoride, $YF_3$, Orthorhombic Form; 155.Samarium Trifluoride, $SmF_3$, Orthorhombic Form; 156.Ytterbium Trifluoride, $YbF_3$, Orthorhombic Form," Anal. Chem. 29 (1957) 855.

Stern, F., "Elementary theory of the optical properties of solids," in *Solid State Physics* 15, Academic Press, New York, 1963, p.299.

Streitwieser, A. and C. H. Heathcock, *Introduction to Organic Chemistry*, Macmillan, New York, 1976.

Sugar, J., "Analysis of the spectrum of triply ionized Praseodymium (Pr IV)," J. Opt. Soc. Amer. 55 (1965) 1058.

Targove, J. D., M. J. Messerly, J. P. Lehan, C. C. Weng, R. H. Potoff, and H. A. Macleod, "Ion-assisted deposition of fluorides," Proc. SPIE 678 *Optical Thin*

*Films II: N w Developments* (1986) 115.

Targove, J. D., L. J. Lingg, J. P. Lehan, and H. A. Macleod, "Effect of oxygen incorporation on the structure of ion-beam-assisted $LaF_3$ thin films," Appl. Opt. 27 (1988) 213.

Targove, J. D., J. P. Lehan, L. J. Lingg, H. A. Macleod, J. A. Leavitt, and L. C. McIntyre, Jr., "Ion-assisted deposition of lanthanum fluoride thin films," Appl. Opt. 26 (1987) 3733.

Targove, J. D., B. G. Bovard, L. J. Lingg, an H. A. Macleod, "Densification of aluminum fluoride thin films by ion-assisted deposition," Thin Solid Films 159 (1988) L59.

Targove, J. D., L. J. Lingg, J. P. Lehan, C. K. Hwangbo, H. A. Macleod, J. A. Leavitt, and L. C. McIntyre, Jr., "Preparation of aluminum nitride and oxynitride thin films by ion-assisted deposition," Mat. Res. Soc. Symp. Proc. 93 1987 Materials Research Society, p.311.

Targove, J. D., Ph. D. dissertation, University of Arizona, 1987.

Taylor, J. W. and P. L. Hartman, "Photoelectric effects in certain of the alkali halides in the vacuum ultraviolet," Phys. Rev. 113 (1959) 1421.

Temple, P. A. "The measurement of absorption in thin films by laser calorimetry," Proc. SPIE 652 *Thin Film Technologies II* (1986) 272.

Tanguy, B., M. Vlasse, and J. Portier, "Etude de la non-stoechiometrie dans le systeme europium-oxygene-fluor," Revue de Chimie Minerale 10 (1973) 63.

Thoma, R. E., H. Insley, and G. M. Hebert, "The sodium fluoride-lanthanide trifluoride systems," Inorg. Chem. 5 (1966) 1222.

Thoma, R. E., and G. D. Brunton, "Equilibrium dimorphism of the lanthanide trifluorides," Inorganic Chemistry 5 (1966) 1937.

Thornton, J. A., "High rate thick film growth," Ann. Rev. Mater. Sci. 7 (1977) 239.

Thornton, J. A., "Influence of apparatus geometry and deposition conditions on the structure and topography of thick sputtered coatings," J. Vac. Sci. Technol. 11 (1974) 666.

Turley, R. S., R. A. McFarlane, J. Remillard, D. G. Steel, "Production of intense, coherent, tunable, narrow-band Lyman-alpha radiation," Proc. SPIE 912 OE/LASE 1988 page 17.

Turnbull, D., "Phase Changes," *Solid State Physics* 3, Seitz and Turnbull, eds., Academic Press, New York, 1956, p.225.

Unruh, W. P., L. G. Nelson, J. T. Lewis, and J. L. Kolopus, "The f centre in $MgF_2$ I: epr and endor," J. Phys. C: Solid St. Phys. 4 (1971) 2992.

Van Vechten, D., G. K. Hubler, and E. P. Donovan, "Characterization of a 3 cm Kaufman ion source with nitrogen feed gas," J. Vac. Sci. Technol. 36 (1986) 841.

Varnier, F., M. Rasigni, G. Rasigni, J. P. Palmari, and A. Llebaria, "Height and slope distributions for surfaces of rough metallic deposits," Appl. Opt. 21 (1982) 3681.

Wells, A. F., *Structural Inorganic Chemistry*, Clarendon Press, Oxford, 1962.

Wertheim, G. K., A. Rosencwaig, R. L. Cohen, and H. J. Guggenheim, "Exchange splitting in the 4f photoelectron spectra of the rare earths," Phys. Rev. Lett. 27 (1971) 505.

Wertheim, G. K., "Resource Letter ME-1 on the Mossbauer effect," Am. J. Phys. 31 (1963) 1.

Wertheim, G. K., A. Hausmann, and W. Sander, "The electronic structure of point defects as determined by mossbauer spectroscopy and by spin resonance," *Defects in Crystalline Solids Series*, S. Amelinickx, R. Gevers, and J. Nihoul, North Holland, Amsterdam 1971.

Wertheim, G. K., R. L. Cohen, A. Rosencwaig, and H. J. Guggenheim, "Multiplet splitting and two-electron excitation in the trivalent rare earths," in *Electron Spectroscopy*, D. A. Shirley, ed., North-Holland, Amsterdam, 1972, p.813.

Wirick, M. P., "The near ultraviolet optical constants of lanthanum fluoride," Appl. Opt. 5 (1966) 1966.

Wood, O. R., H. G. Craighead, J. E. Sweeney and P. J. Maloney, "Vacuum ultraviolet loss in magnesium fluoride films," Appl. Opt. 23 (1984) 3644.

Wybourne, B. G., "Theoretical studies of lanthanide and actinide spectra," J. Opt. Soc. Amer. 55 (1965) 928.

Wysocka-Lisek, J., *Spectrum Lines of Rare Earths Arranged by Wavelengths*, Lubelskie Towarzystwo Naukowe, Lodz Poland, 1970.

Yokozeki, A. and M. Menzinger, "Molecular beam chemiluminescence. VIII: pressure dependence and kinetics of Sm + ($N_2O$, $O_3$, $F_2$, $Cl_2$) and Yb + ($O_3$, $F_2$, $Cl_2$) reactions. Dissociation energies of the diatomic reaction products," Chemical Physics 14 (1976) 427.

Zalkin, A. and D. H. Templeton, "The crystal structures of $YF_3$ and related compounds," J. Am. Chem. Soc. 75 (1953) 2453.

Zalkin, A., D. H. Templeton, and T. E. Hopkins, "The atomic parameters in the lanthanum trifluoride structure," Inorganic Chemistry 5 (1966) 1466.

Zallen, R., *The Physics of Amorphous Solids*, Wiley Interscience, New York, 1983.

Zmbov, K. F. and J. L. Margrave, "Mass-spectrometric studies at high temperatures. XI. The sublimation pressure of $NdF_3$ and the stabilities of gaseous $NdF_2$ and NdF," J. Chem. Phys. 45 (1966) 3167.

Zmbov, K. F. and J. L. Margrave, "Mass spectrometric studies at high temperatures - XIII: stabilities of samarium, europium and gadolinium mono- and difluorides," J. Inorg. Nucl. Chem. 29 (1967) 59.